ACCEPTED MANUSCRIPT

# Petrogenesis of Early Cretaceous intermediate-felsic dikes in the Jiaodong Peninsula, south-eastern North China Craton: Constraints from geochronology, geochemistry and Sr-Nd-Pb-Hf isotopes

Xuefei Liu[1], Jun Deng[1]*, Yayun Liang[1], Qingfei Wang[1], Ruiguang Pan [2], Cheng Qin[1], Yi Yang[1]

[1]State Key Laboratory of Geological Processes and Mineral Resources, China University of Geosciences, Beijing 100083, China

[2]Department of Earth Sciences, Indiana University–Purdue University Indianapolis, Indianapolis 46202, USA

***Corresponding author**:

Telephone: +86-10-82324016

Fax: +86-10-82324016

E-mail: djun@cugb.edu.cn

ACCEPTED MANUSCRIPT

---

This is the author's manuscript of the article published in final edited form as:

Liu, X., Deng, J., Liang, Y., Wang, Q., Pan, R., Qin, C., & Yang, Y. (2018). Petrogenesis of Early Cretaceous intermediate-felsic dikes in the Jiaodong Peninsula, south-eastern North China Craton: Constraints from geochronology, geochemistry and Sr-Nd-Pb-Hf isotopes. Gondwana Research. https://doi.org/10.1016/j.gr.2018.04.005

ACCEPTED MANUSCRIPT


## ABSTRACT

Early Cretaceous dike swarms are widely developed in the Jiaodong Peninsula, NE China. In this study, we newly investigated the spatial-temporal distribution, petrography, geochronology and whole-rock geochemistry of the intermediate-felsic dikes from the Jiaobei terrain and the Sulu orogenic belt in the Jiadong Peninsula. The zircon U-Pb dating has constrained the timing of the emplacement of intermediate-felsic dikes to 128–108 Ma. The quartz diorite dikes in Jiaobei show adakitic geochemical features, including high $SiO_2$ (66.3–67.5 wt.%) contents and high Sr/Y (76–149) and La/Yb (41–91) ratios. The combination of a series of isotopic data, including initial $^{87}Sr/^{86}Sr$ ratios (0.7098–0.7104) and negative $\varepsilon_{Nd}(t)$ (-20.1 to -14.7) and zircon $\varepsilon_{Hf}(t)$ values (-19.9 to -9.5), indicates that these quartz diorite dikes were likely derived from partial melting of thickened ancient lower crust with involvement of underplated mafic magmas. Additionally, the diorite dikes in Jiaobei and those in Sulu show similar chemical compositions, as both yield the high-Mg andesite (or andesitic rocks) (HMAs) characteristics with a high $Mg^{\#}$ value (60-72), high MgO, Cr, and Ni contents, and low $Na_2O$ (average = 3.25 wt.%) contents. They also exhibit crustal geochemical signatures, such as depletion in Nb, Ta, and Ti, but enrichment in Th and U; high initial $^{87}Sr/^{86}Sr$ ratios (0.7063–0.7094), and low $\varepsilon_{Nd}(t)$ (-16.7 to -9.6) and $\varepsilon_{Hf}(t)$ values (-29.4 to -9.8). The entire geochemical evidences imply that they derived from the partial melting of mantle wedge peridotite metasomatized by hydrous fluids from the subduction of the oceanic slab with marine sediments. In combination with the Early Cretaceous intrusions and mafic dikes at Jiaodong, the intermediate-felsic dikes represent a magmatic response to lithospheric thinning resulted from the prolonged thermo-mechanical-chemical erosion processes caused

ACCEPTED MANUSCRIPT

by slab rollback of the Paleo-Pacific plate.

***Keywords:*** Jiaodong Peninsula; adakitic quartz diorite dikes; high-Mg diorite dikes; lithospheric thinning; Paleo-Pacific plate

ACCEPTED MANUSCRIPT

ACCEPTED MANUSCRIPT

## 1. Introduction

In the Late Mesozoic, the eastern North China Craton (NCC) underwent massive lithospheric thinning and concomitant magmatic activities and metallogeny (Menzies et al., 1993; Zhai and Santosh, 2013; Deng and Wang, 2016). The Jiaodong Peninsula is located in the southeastern margin of the NCC (Fig. 1a). A series of igneous plutons, including the Late Jurassic granites, middle Early-Cretaceous granodiorites, late Early-Cretaceous granites and monzogranites, and Early Cretaceous dikes swarms, as well as plenty of gold deposits came into being during this period at Jiaodong (Goss et al., 2010; Goldfarb et al., 2014; Goldfarb and Santosh, 2014; Deng et al., 2015a; Santosh and Pirajno, 2015; Yang et al., 2015; Wang et al., 2016a; Yang et al., 2016a). Despite extensive research has been conducted on the Late Mesozoic magmatism, the nature of mantle composition, crust-mantle interaction and corresponding geodynamic setting at Jiaodong in this period are still debatable.

Dike swarms commonly occur in extensional tectonic settings and can provide insights into magmatic source compositions and regional geodynamic settings (Ernst et al., 1995; Hou et al., 2008; Deng et al., 2014). Widespread Early Cretaceous mafic-intermediate-felsic dikes at Jiaodong offer a ideal opportunity to probe the deep tectonic evolution and its driving forces (Deng et al., 2017). However, previous studies in the Jiaodong Peninsula mainly focused on the Early Cretaceous mafic dikes for revealing the nature of mantle (Liu et al., 2009; Guo et al., 2014; Ma et al., 2014, 2016; Cai et al., 2015; Deng et al., 2017; Liang et al., 2017), and only a few researches referred to the intermediate-felsic dikes (Tan et al., 2007, 2008; Cai et al., 2013, 2015). The intermediate-felsic dikes could also provide significant

ACCEPTED MANUSCRIPT

insights into mantle-crust process. For instance, the adakitic magmas are generally related to thickened continental crust (Xu et al., 2002; Gao et al., 2004; Wang et al., 2005; Gu et al., 2013; Ma et al., 2013); while the high-Mg andesitic magmas could record the information of mantle-crust interaction (Parman and Grove, 2004; Tatsumi, 2006; Zeng et al., 2016, 2017).

In this study, a series of intermediate-felsic dike samples were collected throughout Jiaodong Peninsula (within the Jiaobei terrain and the Sulu orogenic belt). High-precision geochronology (LA-ICPMS zircon U-Pb dating) indicates that they were formed during Early Cretaceous. Zircon Hf isotopic data, whole rock major and trace element geochemistry, and Sr-Nd-Pb isotopic data of representative rocks were also analysed to unveil the magma source(s) and to interpret the petrogenesis of these intermediate-felsic dikes. Besides, the felsic dikes (e.g. quartz diorite dikes) commonly show the adakitic geochemical features and the intermediate dikes (e.g. diorite dikes) generally have the high-Mg andesite (or andesitic rocks) (HMAs) characteristics. Therefore, investigating the petrogenesis of these intermediate-felsic dikes provides new insights into the deep geodynamic process of Jiaodong Peninsula at this period.

## 2. Geological background

The NCC is one of the earth’s oldest cratons and contains crustal rocks as old as 3.8 Ga (Zhao and Zhai, 2013). The NCC comprises the Western and Eastern Blocks separated by the Trans-North China Orogen (Wang et al., 2015; Wang et al., 2016b) (Fig. 1a). It borders the Qinling-Dabie-Sulu orogenic belt to the south and the Pacific convergent system to the east.

ACCEPTED MANUSCRIPT

The Qinling-Dabie-Sulu orogenic belt was formed by the Triassic subduction of the continental crust of the Yangtze Craton (YC) beneath the NCC (e.g., Ye et al., 2000). The eastern NCC experienced considerable lithosphere thinning in the Mesozoic during the westward subduction of the Paleo-Pacific plate (Li and Li, 2007; Sun et al., 2007). In the Early Cretaceous, widespread metamorphic core complexes, pull-apart basins, A-type granites, and dike swarms developed in the eastern NCC, reflecting the dominant regional extensional tectonics. The occurrence of these features mostly accompanied with concurrent lithospheric thinning, possibly resulting from the rollback of the subducted Pacific plate along the eastern Asian margin during the Early Cretaceous (Yang et al., 2007; Deng et al., 2017).

The Jiaodong Peninsula is located in the southeastern region of the NCC and is bounded to the west by the Tan-Lu fault (Fig. 1b). This region is divided into two different terrains by the Wulian-Yantai fault, the northwestern Jiaobei terrain and the southeastern Sulu orogenic belt (Fig. 1b) (Deng et al., 2015b). The Jiaobei terrane comprises the Jiaobei uplift in the north and the Jiaolai basin in the south. Precambrian metamorphic rocks, mainly exposed in the Jiaobei terrain, include the Neoarchean Jiaodong Group (containing TTG (tonalite-trondhjemite-granodiorite) gneisses, amphibolites, and mafic granulite sequences (Yang et al., 2016b); the Paleoproterozoic Fenzishan and Jinshan groups (containing schist, paragneiss, calc-silicate rocks, marble, and minor mafic granulites and amphibolites) (Li et al., 2013); and the Meso-Neoproterozoic Penglai group (containing marble, slate, and quartzite) (Faure et al., 2004). These Precambrian basement rocks are partially overlain by the Cretaceous continental sediments and associations of volcanic rocks emplaced in the Jiaolai

ACCEPTED MANUSCRIPT

basin, which is located in the southern section of the Jiaobei terrain (Yang et al., 2016b). UHP metamorphic rocks, dominated by Neoproterozoic granitic gneisses with minor coesite-bearing eclogites, quartzite, and schist, are also present in the Sulu orogenic belt (Zhang et al., 2012). Mesozoic intrusions in the Jiaodong Peninsula can be divided into four suites: (1) the Late Triassic syenite, such as Jiazishan intrusion, which is only found in the easternmost Jiaodong Peninsula (215-209 Ma, LA-ICP-MS zircon U-Pb age, Chen et al., 2003); (2) the Late Jurassic granite plutons, namely Linglong intrusion, which are composed mainly of the Linglong and Luanjiahe granites in Jiaobei terrain (160-150 Ma, LA-ICP-MS zircon U-Pb age, Yang et al., 2012; Ma et al., 2013), and the Kunyushan granites in the Sulu orogenic belt (149-144 Ma, LA-ICP-MS zircon U-Pb age, Zhang et al., 2010); (3) the middle Early-Cretaceous granodiorite plutons, namely Guojialing intrusion, which are mainly composed of porphyritic hornblende-biotite granodiorites in the Jiaobei terrain. LA-ICP-MS and SHRIMP U-Pb zircon geochronological data show that the Guojialing intrusion were emplaced at 135–126 Ma (Yang et al., 2012; Yang et al., 2014); (4) the late Early-Cretaceous granite and monzogranite plutons are composed mainly of Aishan monzogranite and Gushan granite in Jiaobei terrain (120-113 Ma, LA-ICP-MS zircon U-Pb age, Goss et al., 2010; Li et al., 2012), and weideshan granite and Sanfoshan monzogranite in the Sulu orogenic belt (118-110 Ma, LA-ICP-MS zircon U-Pb age, Goss et al., 2010).

Numerous Early Cretaceous dike swarms occur in the Jiaodong Peninsula, and include mafic, intermediate, and felsic dikes. Most of the Jiaodong dikes have been dated (by whole-rock K-Ar, biotite Ar-Ar, and zircon U-Pb dating), yielding ages ranging from 135 Ma to 110 Ma with a peak at 125 Ma (Fig. 1b) (Tan et al., 2008; Liu et al., 2009; Cai et al., 2013,

ACCEPTED MANUSCRIPT

2015; Ma et al., 2014, 2016; Deng et al., 2017; Liang et al., 2017). Two types of mafic dike have been identified, those derived from enriched lithospheric mantle (arc-like type with enrichment in LILE and LREE but depletion in HFSE; 130–110 Ma) (Liu et al., 2009; Cai et al., 2013, 2015; Ma et al., 2014; Deng et al., 2017; Liang et al., 2017) and those derived from asthenospheric mantle (OIB-like type with no depletion in HFSE and enrichment in LREE; 123-121 Ma) (Ma et al., 2014, 2016). Those intermediate-felsic dikes studied here are mainly oriented to the N, the NNE, and the NNW in the Jiaobei terrain and to the E, the NE, and the NEE in the Sulu orogenic belt (Fig. 2).

## 3. Sampling and petrography

Samples in this study were collected from the Jiaobei terrain and the Sulu orogenic belt in the Jiaodong Peninsula. Ten intermediate-felsic dikes were sampled and analysed, including three felsic dikes and two intermediate dikes from the Jiaobei terrain and five intermediate dikes from the Sulu orogenic belt. These intermediate-felsic dikes are all classified as diorite and quartz diorite dikes based on their mineral compositions, and were sampled at a distance far from gold mineralization in order to avoid the effects of associated hydrothermal activities (Table 1, Fig. 2).

Three quartz diorite dikes were identified in the Jiaobei terrain. Quartz diorite dikes contain plagioclase (50–55%), amphibole (10–15%), quartz (10–15%), and K-feldspar (5–10%), with minor biotite and pyrite (~5%) with fine-grained panidiomorphic textures and massive structures (Fig. 2a and b). One of these three quartz diorite dikes (sample PDDZ-2) is

ACCEPTED MANUSCRIPT

classified as a quartz-diorite porphyrite, as it includes coarse plagioclase (~10%) and amphibole (~10%) phenocrysts in a groundmass of plagioclase (30–10%), amphibole (10-20%), and quartz (20–15%).

Seven diorite dikes are sampled from both the Jiaobei terrain and the Sulu orogenic belt. These diorite dikes are dominated by plagioclase (35–50%) and amphibole (10–30%), with small amounts of K-feldspar (5–10%), quartz, and pyrite, and they are characterized by euhedral or subhedral granular textures and massive structures (Fig. 2c-f). One diorite dike from the Sulu orogenic belt (sample RCYT-1) displays a porphyritic texture, featuring amphibole phenocrysts (~10%) in a groundmass of plagioclase, amphibole, biotite, quartz, and pyrite (Fig. 2g and h).

## 4. Analytical methods

A total of 26 fresh samples were collected from 10 intermediate-felsic dikes for geochemical and chronological analyses (Table 1). These samples were crushed to 200 mesh powders using an agate mortar for major, trace and rare earth element analysis as well as for Sr-Nd-Pb isotopic analysis. Samples were also crushed to 40–60 mesh powders in order to obtain zircon separates.

Zircon crystals from seven samples were separated employing conventional procedures, specifically using heavy liquids and magnetic separation, and then followed by hand-picking under a binocular microscope. Cathodoluminescence (CL) imaging is also used to select suitable positions of zircon crystals for in-situ measurements. LA-ICP-MS zircon U-Pb

ACCEPTED MANUSCRIPT

dating was conducted at the Institute of Mineral Resources, China Academy of Geological Science. The operating conditions and data reduction processes have been detailed by Hou et al. (2009). Argon and helium were used to remove common Pb remaining in the gas path. The zircon GJ-1 was used as an external standard for determining sample zircons $^{206}Pb/^{238}U$ ages (610 ± 1.7 Ma, Elhlou et al., 2006), and concentrations of U, Th, and Pb were measured based on known concentrations of the zircon standard M127 (U= 923 ppm, Th = 439 ppm, and Th/U = 0.475, Nasdala et al., 2008). ICPMS-DataCal software was used to select off-line raw data, analyse signals and quantitatively calibrate for U-Pb dating (Liu et al., 2010). Concordia diagrams and weighted mean calculations were made with Isoplot/Ex ver3. The uncertainty for each individual analysis is quoted at the 2σ level, and errors on weighted-mean ages are at the 95% confidence level.

In situ zircon Lu-Hf isotopic analyses were carried out on a Neptune Plus multi-collector ICP-MS equipped with a RESOlution M-50 laser-ablation system at the Guangzhou Institute of Geochemistry, Chinese Academy of Sciences in Guangzhou (GIG-CAS), China. Lu-Hf isotopic measurements were made on the same spots previously analysed for U-Pb ages. The laser parameters included a spot size of 45 μm, a repetition rate of 8 Hz, and with energy of 80 mJ. Helium was used as a carrier gas, and a small flow of nitrogen was added into the gas line to enhance the sample's signal. A normal single spot analysis consisted of 30 s of gas blank collection followed by 30 s of laser ablation; the overall integration time was 0.131 s, and approximately 200 cycles of data were collected in a given analysis. $^{173}Yb$ and $^{175}Lu$ were used to correct the isobaric interference of $^{176}Yb$ and $^{176}Lu$ on $^{176}Hf$. $^{176}Hf/^{177}Hf$ measurements were normalized to $^{179}Hf/^{177}Hf = 0.7325$ using an

ACCEPTED MANUSCRIPT

exponential law for mass bias correction. More details about this method have been published by Wu et al. (2006). The Penglai zircon was used as a reference standard (Li et al., 2010); analyses of this standard over the measurement period yielded $^{176}Hf/^{177}Hf = 0.282903 \pm 0.000013$ (2σ, n = 36). All analytical ratios of $^{176}Yb/^{177}Hf$, $^{176}Lu/^{177}Hf$ and $^{176}Hf/^{177}Hf$ are reported with 2σ errors.

Whole-rock chemical compositions of the intermediate-felsic dike samples were obtained in the Analytical Laboratory of the Geological Survey of China in Langfang, Hebei Province. Major elements (except for FeO and loss on ignition (LOI)) were determined by X-ray fluorescence (XRF) using a Philips Model 1480 machine equipped with an Rh tube. The analytical uncertainty of this method is better than 5%. The FeO contents and the LOI were determined using volumetric and gravimetric methods, respectively. Trace elements, including La, Ce, Pr, Nd, Sm, Eu, Gd, Tb, Dy, Ho, Er, Tm, Yb, Lu, Th, U, Nb, Ta, K, Pb, Sr, P, Hf, Ti, Y, Co and Ni, were analysed by inductively coupled plasma-mass spectrometry (ICP-MS), and all remaining elements (e.g., Ba, Cr, Rb, V, Zr) were measured using inductively coupled X-ray Fluorescence Spectroscopy. All analytical uncertainties are lower than 10%. Elemental concentrations of all measured samples were calibrated by the standards GAu9bGSR, GAu10bGSR, GAu11bGSR, and GAu12aGSR.

Whole-rock Sr, Nd, and Pb isotopic compositions of the intermediate dike samples were measured using a Micromass IsoProbe multicollector inductively coupled plasma-mass spectrometer (MC-ICP-MS) at GIG-CAS. Powdered samples, ranging from 110 to 180 mg in size, were analysed for their Sr-Nd-Pb isotope compositions. These samples were dissolved in Teflon beakers with 1 ml of $HNO_3$ and 2 ml of HF acid at 120℃ for 7 days. Pb was separated

ACCEPTED MANUSCRIPT

using the conventional anionic resin-exchange technique (using AG 1-X8 anionic resin) with HCl. Sr and REE in these solutions were separated using standard cation exchange columns with special Sr resin. Nd was separated from REE using HDEHP-coated columns. The detailed analytical procedures for Sr and Nd isotopes are described by Wei et al. (2002) and Li et al. (2004) and those for Pb isotopes are described in detail by White (2000). The sample solutions were diluted by 2% $HNO_3$ and introduced through a PFA nebulizer (at a rate of 50 μL min-1) before being buffered in a quartz cyclonic spray chamber. The integration times for Sr, Nd, and Pb were set at ~4s, and each analysis contained 100 cycles. Between each analysis, 2% $HNO_3$ was used to clear the sample uptake device. The mass fractionation corrections for $^{87}Sr/^{86}Sr$ and $^{143}Nd/^{144}Nd$ ratios were based on an $^{87}Sr/^{86}Sr$ value of 0.1194 and a $^{143}Nd/^{144}Nd$ value of 0.7219. The measured $^{87}Sr/^{86}Sr$ ratios of the NBS987 standard and $^{143}Nd/^{144}Nd$ ratios of Jndi-1 standard were 0.710267 ± 9 (2σ; n = 22) and 0.512102 ± 6 (2σ; n = 21), respectively. During Pb isotopic analyses, Tl was added to the samples as an internal standard for correcting mass-dependent isotopic fractionation. The exponential correction value of $^{205}Tl/^{203}Tl$ applied to these samples was 2.3871. Repeated analyses of the NBS981 standard yielded a $^{206}Pb/^{204}Pb$ ratio of 16.932 ± 6, a $^{207}Pb/^{204}Pb$ ratio of 15.485 ± 6, and a $^{208}Pb/^{204}Pb$ ratio of 36.678 ± 17.

## 5. Results

The LA-ICP-MS zircon U-Pb isotopic data and the in-situ zircon Hf isotopic data for intermediate-felsic dikes in the Jiaodong Peninsula are listed in Table 2 and Table 3,

ACCEPTED MANUSCRIPT

respectively. The results of the whole-rock major and trace element analyses and the Sr-Nd-Pb isotopic data for intermediate-felsic dikes in the Jiaodong Peninsula are listed in Table 4 and Table 5, respectively.

*5.1. Zircon U-Pb geochronology*

Zircons of three quartz-diorite dikes from Jiaobei (LKXDJ-1, LZYD-11 and PDDZ-2) display magmatic oscillatory zoning in CL imaging; individual crystals are subhedral to euhedral, colourless, and short to prismatic, with length range of 79-205 μm (Fig. 3a-c). Zircon grains obtained from these samples show large ranges of Th (63-983 ppm) and U (56-874 ppm) contents, with Th/U ratios varying from 0.3 to 1.8 (Table 2). These features suggest that these zircons have magmatic origins (Hoskin and Schaltegger, 2003). The samples LKXDJ-1, LZYD-11, and PDDZ-2 yield weighted mean $^{206}Pb/^{238}U$ ages of 127.4 ± 1 (2σ, MSWD=0.96), 120.7 ± 1.5 (2σ, MSWD=0.22), and 122.7 ± 1 (2σ, MSWD=0.63), respectively (Fig. 3e-g).

Zircons from one diorite dike sample in Jiaobei (PDDZ-3) display magmatic oscillatory zoning in the CL image (Fig. 3d). Most zircon grains are subhedral to euhedral, dark to light grey, and long-prismatic crystals with length ranging from 70 μm to 273 μm. Seventeen zircon separates were analysed; they show large ranges of Th (126–903 ppm) and U (340–1180 ppm) concentrations, with Th/U ratios varying from 0.17 to 0.77 (Table 2). These zircons document features of magmatic origins. These zircons yield a weighted mean $^{206}Pb/^{238}U$ age of 122.4 ± 1.4 (2σ, MSWD=0.19) (Fig. 3h).

ACCEPTED MANUSCRIPT

Zircons from two diorite dike samples in Sulu (RCYT-1 and RSZT-3) display magmatic oscillatory zonings in CL imaging; these grains form subhedral to euhedral, colourless to light grey, and short-prismatic crystals with lengths ranging from 86 μm to 179 μm (Fig. 4a-b). Zircon grains obtained from this sample record large range of Th (182-993 ppm) and U (203–667 ppm) concentrations, with Th/U ratios varying from 0.77 to 1.49 (Table 2). The samples RCYT-1 and RSZT-3 yield weighted mean $^{206}Pb/^{238}U$ ages of 116.0 ± 1.8 (2σ, MSWD=0.93) and 119.4 ± 2.2 (2σ, MSWD=0.77), respectively (Fig. 4c-d).

*5.2. Zircon Hf isotopes*

In the samples of quartz diorite dikes from Jiaobei, thirteen dated zircons from sample LKXDJ-1 were analysed for Hf isotope compositions. These crystals exhibit a narrow range of $^{176}Hf/^{177}Hf$ ratios (0.282255–0.282426), $\varepsilon_{Hf}(t)$ values (-9.5 to -15.6), and corresponding $T_{DM2}$ ages ranging from 1.79 to 2.17 Ga. Nineteen dated zircons from LZYD-11 yield $^{176}Hf/^{177}Hf$ ratios of 0.282137–0.282349, $\varepsilon_{Hf}(t)$ values of -12.5 to -19.9, and corresponding $T_{DM2}$ ages from 1.97 to 2.44 Ga. Fifteen dated zircons from PDDZ-2 yield $^{176}Hf/^{177}Hf$ ratios of 0.282146–0.282490, $\varepsilon_{Hf}(t)$ values of -11.0 to -19.5, and corresponding $T_{DM2}$ ages ranging from 1.65 to 2.41 Ga (Fig. 5a-b).

In the samples of diorite dikes from Jiaobei, seventeen dated zircons from PDDZ-3 yield $^{176}Hf/^{177}Hf$ ratios of 0.281867–0.282081, $\varepsilon_{Hf}(t)$ values of -21.8 to -29.4, and with corresponding $T_{DM1}$ ages between 1.67 and 1.96 Ga (Fig. 5c-d).

In the samples of diorite dikes from Sulu, fifteen dated zircons from RCYT-1 yield

ACCEPTED MANUSCRIPT

$^{176}Hf/^{177}Hf$ ratios of 0.282254–0.282570, $\varepsilon_{Hf}(t)$ values of -9.8 to -15.8, and corresponding $T_{DM1}$ ages ranging from 1.17 to 1.46. Five dated zircons from RSZT-3 yield $^{176}Hf/^{177}Hf$ ratios of 0.281900–0.282297, $\varepsilon_{Hf}(t)$ values of -14.3 to -28.4, and corresponding $T_{DM1}$ ages range from 1.39 Ga to 1.96 Ga (Fig. 5e-f).

*5.3. Major and trace elements*

Quartz diorite dikes in Jiaobei have high $SiO_2$ contents of 66.26–67.50 wt.% (average = 66.87 wt.%) and $Na_2O$+$K_2O$ contents of 7.38–7.93 wt.% (Fig. 6a). These dikes also record $K_2O$ contents of 3.00–4.20 wt.%, thus defining them as high-K series rocks (Fig. 6b). Furthermore, they are also characterized by high contents of $Al_2O_3$ (15.18–16.49 wt.%) and low contents of MgO (1.81–2.34 wt.%), Cr (26.3–76.6 ppm), Ni (6.03–45.5 ppm), $TiO_2$ (0.33–0.39 wt.%), and total $Fe_2O_3$ (2.69–3.16 wt.%) (Fig. 7). The quartz-diorite dikes display significant enrichment in light rare-earth elements (LREE), as well as high $(La/Yb)_N$ (29–66) and insignificant Eu anomalies (Eu/Eu*=0.8–0.9), in chondrite-normalized REE patterns (Fig. 8a). The primitive mantle-normalized spidergram (Fig. 8b) demonstrates that the Jiaobei quartz-diorite dikes are enriched in LILE (such as Ba, K, Pb, and Sr) and depleted in HFSE (such as Nb, Ta, P, and Ti).

Diorite dikes in Jiaobei have $SiO_2$ contents of 54.00–56.43 wt.% (average = 55.33 wt.%) and $Na_2O$+$K_2O$ contents of 5.02–7.20 wt.% (Fig. 6a). They record $K_2O$ contents of 2.39–4.30 wt.% and can thus be classified as high-K, shoshonitic rocks (Fig. 6b). These dikes are further characterized by high MgO (6.77–9.71 wt.%), $Mg^{\#}$ (65-72), Cr (284–506 ppm), and Ni

ACCEPTED MANUSCRIPT

(109–164 ppm), as well as by low $TiO_2$ (0.78–0.85 wt.%), $Al_2O_3$ (13.87–14.86 wt.%), $P_2O_5$ (0.38–0.75 wt.%), and total $Fe_2O_3$ (6.43–7.04 wt.%) (Fig. 7). Diorite dikes record significant LREE enrichment, with high $(La/Yb)_N$ (21–31) and slightly negative Eu anomalies (Eu/Eu*=0.8–0.9), on chondrite-normalized REE patterns (Fig. 8c). The primitive mantle-normalized spidergram (Fig. 8d) demonstrates that these diorite dikes are enriched in LILE and depleted in HFSE. While, Sulu diorite dikes record $SiO_2$ contents of 51.69–58.37 wt.% (average = 56.00 wt.%) and $Na_2O+K_2O$ contents of 5.0–5.9 wt.%; these rocks thus span a compositional range from monzodiorite to monzonite (Fig. 6a). They have $K_2O$ contents of 2.43–2.93 wt.% and can thus be classified as high-K rocks (Fig. 6b). These dikes are also characterized by high MgO (4.91–10.18 wt.%), $Mg^{\#}$ (60–72), Cr (146–386 ppm), and Ni (30–154 ppm) contents and low $TiO_2$ (0.78–0.99 wt.%), $Al_2O_3$ (13.20–16.39 wt.%), $P_2O_5$ (0.33–0.71 wt.%), and total $Fe_2O_3$ (4.29–7.22 wt.%) contents (Fig. 7). These dikes display significant LREE enrichment, with high $(La/Yb)_N$ (16–40) and unclear Eu anomalies (Eu/Eu*=0.9–1.1), on chondrite-normalized REE patterns (Fig. 8e). On a primitive mantle-normalized spidergram (Fig. 8f), Sulu intermediate dikes are enriched in LILE and depleted in HFSE.

### *5.4. Sr–Nd–Pb isotopes*

Quartz diorite dikes in Jiaobei record a narrow range of $(^{87}Sr/^{86}Sr)_i$ isotopic ratios (0.709781-0.710367) and large range of $\varepsilon_{Nd}(t)$ values (-20.1 to -14.7) (Fig. 9a). These dikes also record $(^{206}Pb/^{204}Pb)_i$ isotopic ratios of 16.906 to 17.217, $(^{207}Pb/^{204}Pb)_i$ isotopic ratios of

ACCEPTED MANUSCRIPT

15.451 to 15.507, and $(^{208}Pb/^{204}Pb)_i$ isotopic ratios of 37.373 to 37.949 (Fig. 9b and c).

Diorite dikes in Jiaobei record a narrow range of $(^{87}Sr/^{86}Sr)_i$ isotopic ratios (0.708913-0.709415) and $\varepsilon_{Nd}(t)$ values (-16.0 to -16.3) (Fig. 10a). These dikes record $(^{206}Pb/^{204}Pb)_i$ isotopic ratios of 16.665 to 17.940, $(^{207}Pb/^{204}Pb)_i$ isotopic ratios of 15.437 to 15.449, and $(^{208}Pb/^{204}Pb)_i$ isotopic ratios of 37.322 to 37.444 (Fig. 10b and c).

Sulu diorite dikes record a large range of $(^{87}Sr/^{86}Sr)_i$ isotopic ratios (0.706305-0.709089) and $\varepsilon_{Nd}(t)$ values (-9.6 to -16.7) (Fig. 10a). These dikes also record $(^{206}Pb/^{204}Pb)_i$ isotopic ratios of 16.855 to 17.191, $(^{207}Pb/^{204}Pb)_i$ isotopic ratios of 15.409 to 15.460, and $(^{208}Pb/^{204}Pb)_i$ isotopic ratios of 37.140 to 37.546 (Fig. 10b and c).

## 6. Discussion

### *6.1. Petrogenesis of high-Mg diorite dikes*

The Jiaobei and Sulu diorite dikes show similar chemical compositions, as both yield the HMAs characteristics with high values of $Mg^{\#}$ (60-72), high MgO, Cr, and Ni contents, and low $Na_2O$ (average = 3.25 wt.%), which is different from the low $Mg^{\#}$ (<44) and high $Na_2O$ (>4.3 wt.%) contents in melts produced by dehydration melting of metabasic crustal rocks (Rapp and Watson, 1995), but show the crustal signatures such as depletion in Nb, Ta, and Ti, enrichment in Th and U, high initial $^{87}Sr/^{86}Sr$ ratios (0.7063–0.7094), and low $\varepsilon_{Nd}(t)$ (-16.7 to -9.6) and $\varepsilon_{Hf}(t)$ values (-29.4 to -7.4).

ACCEPTED MANUSCRIPT

*6.1.1. Evaluation of crustal contamination and fractional crystallization*

Although the diorite dikes in Jiaobei and Sulu show the crustal signatures, such as depletion in Nb, Ta, and Ti, enrichment in Th and U, high initial $^{87}Sr/^{86}Sr$ ratios (0.7063–0.7094), and low $\varepsilon_{Nd}(t)$ (-16.7 to -9.6), significant crustal assimilation could be precluded for reasons below: (1) There are no positive correlation between $(^{87}Sr/^{86}Sr)_i$ and $SiO_2$ and negative correlation between $\varepsilon_{Nd}(t)$ and $SiO_2$ in the Jiaobei and Sulu high-Mg diorite dikes (Fig. 11); (2) these high-Mg diorite dikes record much higher concentrations of Sr (840–1282 ppm) and Ba (1400–2816 ppm) than those observed in crustal rocks of the NCC or YC (Sr = 350–254 ppm; Rb = 59–79 ppm; Ba = 688–633 ppm; Gao et al., 1998); (3) Granulite xenoliths in Quaternary basanites from Nushan, located in the southeastern region of the NCC, are considered to be suitable analogues for the Mesozoic lower crust in the southeastern NCC. These xenoliths are characterized by high Th/U, Zr/Hf, and Nb/Ta ratios, strongly negative whole rock $\varepsilon_{Nd}(t)$ values, and very low $^{87}Sr/^{86}Sr$ values (Fig. 10a) (Huang et al., 2012), all of which are different from those of the Jiaobei and Sulu high-Mg dioritic dikes. Thus, these data suggest that crustal assimilation was either impossible or unlikely to have played a significant role in the petrogenesis of the high-Mg diorite dikes in Jiaobei and Sulu.

The Jiaobei and Sulu high-Mg diorite dikes record similarly negative correlations between $SiO_2$ and MgO, total $Fe_2O_3$, $Al_2O_3$ and Ni (Fig. 7a, d and f), indicating that these dikes experienced substantial clinopyroxene and/or olivine fractionation. The decrease in total $Fe_2O_3$ and $TiO_2$ with increasing $SiO_2$ (Fig. 7b and d) may be the result of fractionation of Fe-Ti oxides. Although a positive correlation between $SiO_2$ and $Al_2O_3$ can be observed in Fig. 7c, however, the absence of observed Sr and Eu anomalies argues against significant

ACCEPTED MANUSCRIPT

plagioclase fractionation (Fig. 8c-f). Therefore, these data indicate that high-Mg diorite magmas mainly underwent fractional crystallization of olivine, clinopyroxene, and/or Fe-Ti oxides.

*6.1.2. Origin of the high-Mg diorite dikes*

The major and some trace elemental compositions of Jiaobei and Sulu diorite dikes resemble those of HMAs. Four models have been proposed to account for the origin of HMAs: (1) partial melting of subducted oceanic crust with/or overlying sediments, followed by interaction with the overlying mantle wedge (Tatsumi, 2001; Hanyu et al., 2006; Wang et al., 2011; Zeng et al., 2016); (2) partial melting of delaminated lower continental crust, followed by interaction with overlying mantle materials (Gao et al., 2004); (3) magma mixing between ultramafic-mafic magmas and felsic magmas (Streck et al., 2007; Yang et al., 2015); (4) partial melting of mantle wedge peridotite metasomatized by fluids or melts liberated from the subducting slab (e.g., Parman and Grove, 2004; Tatsumi, 2006).

Firstly, the typical melts derived from partial melting of subducted oceanic crust, followed by interaction with the overlying mantle wedge have high $SiO_2$ contents (> 60 wt.%; Tatsumi, 2001; Martin et al., 2005; Zeng et al., 2016), which is higher than those of the high-Mg diorite dikes ($SiO_2$ = 51.7-58.4 wt.%) in this study. Additionally, melts of oceanic crust are inconsistent with the high Th contents and Th/La ratios (Fig. 12a), the enriched isotopic features (Fig. 10), and lack of adakitic feature of the high-Mg diorite dikes in this study (Fig. 13) (Tatsumi, 2001; Zeng et al., 2016). Hence, the model of partial melting of subducted oceanic crust followed by interaction with the overlying mantle wedge could be

ACCEPTED MANUSCRIPT

eliminated.

Secondly, an eclogitic thickened lower continental crust is a prerequisite for the model of delamination, and this process generally produces adakitic magmas (Xu et al., 2002; Gao et al., 2004). The eclogitized lower crust foundered into the convecting mantle and subsequently melted and interacted with peridotite, which would produce high $Mg^{\#}$, Ni and Cr contents, and adakitic features (high Sr/Y = 36–135) and $(La/Yb)_N$ = 17-19 (Gao et al., 2004). However, the high-Mg diorite dikes in this study don't show the adakitic features (Fig. 13). Thus, the model of partial melting of delaminated lower continental crust, followed by interaction with overlying mantle materials is also not acceptable here.

Thirdly, the model of magma mixing between ultramafic-mafic magmas and felsic magmas is also not suitable for the high-Mg diorite dikes based on the following observation. Candidates for ultramafic-mafic magmas and crust-derived felsic magmas are most plausibly represented by the Cretaceous mantle-derived arc-like mafic dikes (130-110 Ma) (Liu et al., 2009; Cai et al., 2013, 2015; Ma et al., 2014; Liang et al., 2016) and the late Early-Cretaceous crust-derived granites and monzogranites (120-110 Ma) at Jiaodong (Goss et al., 2010; Li et al., 2012), respectively. However, the Cretaceous arc-like mafic dikes at Jiaodong have similar $(^{87}Sr/^{86}Sr)_i$ ratios (average value= 0. 0.7094) and $\varepsilon_{Nd}(t)$ (average value = -15.8) to those of high-Mg diorite dikes in this study, and don't show the tendency of magma mixing (Fig. 10). Moreover, the highest contents of $Mg^{\#}$, Ni and Cr of these Cretaceous arc-like mafic dikes, equivalent to those of high-Mg diorite dikes in Jiaobei and Sulu, could not produce basaltic magma as a potential source for the high-Mg diorite dikes (e.g. Frey et al., 1978; Xu et al., 2004). In this study, the absence of felsic enclaves in the high-Mg diorite

ACCEPTED MANUSCRIPT

dikes further against the magma mixing model.

Therefore, the model of partial melting of mantle wedge peridotite metasomatized by fluids or melts liberated from the subducting slab would be suitable for explaining the genesis of high-Mg diorite dikes from Jiaobei and Sulu. The high-Mg diorite dikes are both characterized by high MgO and compatible element (Cr and Ni) contents, and high $Mg^{\#}$ value, which indicate that they were derived from a mantle source. The trace element and Sr-Nd isotopic data of the high-Mg diorite dikes differ from those of mid-ocean ridge basalts (MORBs) or ocean-island basalts (OIBs) (Figs. 8c-f and 10a), both of which are derived from the sub-lithosphere (Zhang et al., 2002). However, characteristics observed in the high-Mg diorite dikes, such as LILE and LREE enrichment, and HFSE depletion are similar to the Aleutian arc basalts derived from partial melting of the mantle wedge peridotite metasomatized by fluids liberated from the subducting slab (Kelemen et al., 2003) (Fig. 8c-f). The high-Mg diorite dikes with high initial $^{87}Sr/^{86}Sr$ values, and low $\varepsilon_{Nd}(t)$ and $\varepsilon_{Hf}(t)$ values also display similar characteristics to those seen in contemporaneous arc-like mafic dikes at Jiaodong, which are believed to have originated from an enriched lithospheric mantle modified by slab-derived hydrous fluids (Ma et al., 2014; Deng et al., 2017) (Figs. 8c-f and 10). In this study, the negative Nb-Ta and Zr-Hf anomalies observed within the Jiaobei and Sulu high-Mg diorite dikes likely indicate the presence of subduction-related metasomatism in the source region (e.g., Elliott et al., 1997; Ma et al., 2014; Dai et al., 2017). The Jiaobei and Sulu high-Mg diorite dikes record high Rb/Y ratios, and low Nb/Zr, Th/Yb and Hf/Sm ratios (Fig. 14), indicating that lithospheric mantle has been modified by hydrous fluids derived from the subducting oceanic slab. The diorite dikes have much higher $^{87}Sr/^{86}Sr$ ratios

ACCEPTED MANUSCRIPT

than those of normal slab fluid ($^{87}Sr/^{86}Sr$ = 0.70410, Sr = 13530 ppm; Tatsumi, 2000). The aqueous fluids from the seawater-altered oceanic crust ($^{87}Sr/^{86}Sr$ = 0.7092; Tatsumi, 2000) and/or marine sediments ($^{87}Sr/^{86}Sr$ = 0.7053-0.7312; Plank and Langmuir, 1998) are likely the appropriate end member for Sr isotope. Combined with the study of whole rocks Sr-Nd-Hf isotopic compositions, the oceanic crust has higher $\varepsilon_{Nd}(t)$ and $\varepsilon_{Hf}(t)$ values (e.g. MORB ＞ 0, Hofmann, 2003) than those of diorite dikes, (Fig. 10). Therefore, the metasomatic agent containing only oceanic crust cannot explain that low $\varepsilon_{Nd}(t)$ and $\varepsilon_{Hf}(t)$ values of the diorite dikes. The chemical modelling experiment proved that a significantly small amount of the sediment-derived fluid (<0.1%) is enough to affect isotopic characteristics of magmas formed in subduction zones (Tatsumi and Takeshi, 2003). Thus, the marine sediments-derived fluid likely plays an important role in magma source (Fig. 10). Additionally, their ($^{206}Pb/^{204}Pb)_i$, ($^{207}Pb/^{204}Pb)_i$, and ($^{208}Pb/^{204}Pb)_i$ isotopic ratios are similar to those of the Mesozoic mafic rocks from the NCC (Fig. 10b-c). These evidences indicate that the Jiaobei and Sulu high-Mg diorite dikes could be derived from the SCLM of NCC which had been metasomatized by fluids liberated from the subducting oceanic slab with marine sediments.

Meanwhile, we also detected slight differences in Sr-Nd-Pb-Hf isotopic compositions between the Jiaobei and Sulu high-Mg diorite dikes (Figs. 5 and 10). The Sulu high-Mg diorite dikes overall show lower ($^{87}Sr/^{86}Sr)_i$, ($^{207}Pb/^{204}Pb)_i$, and ($^{208}Pb/^{204}Pb)_i$ ratios and a wider range of $\varepsilon_{Nd}(t)$ and $\varepsilon_{Hf}(t)$ values than those of the Jiaobei high-Mg diorite dikes (Figs. 5 and 10). However, the Sulu high-Mg diorite dikes displayed strong similarities (e.g. Sr-Nb-Pb isotopic signatures) with the Early Cretaceous mafic dikes in the Dabie orogenic belt (Fig.

ACCEPTED MANUSCRIPT

10), which derived from an enriched lithospheric mantle and was contaminated by the deeply subducted YC during the Triassic collision and northward subduction of YC beneath the NCC (Wang et al., 2005; Xu et al., 2012). The mafic igneous rocks in the Sulu orogenic belt, including the Late Triassic and Early Cretaceaus ones, had been proved to have derived from partial melting of the enriched SCLM source that were generated by reaction of the ancient SCLM peridotite of the NCC with felsic melts from the subducted continental crust of the YC in the Triassic (Dai et al., 2016). Moreover, the mantle xenoliths hosted in the Paleozoic kimberlite from eastern NCC exhibit much higher ($^{87}Sr/^{86}Sr)_i$ values and $\varepsilon_{Nd}(t)$ values than those of the Late Triassic (212-210 Ma) Shidao and Jiazishan alkaline gabbro intrusions in the Sulu orogenic belt. These alkaline gabbro intrusions have been recognized to be derived from the partial melting of the lithospheric mantle which is generated by underplating of hydrous felsic melts derived from the subducted continental crust during the Triassic continental subduction and collision between the NCC and the YC (Chen and Jiang, 2011; Zhao et al., 2012) (Fig. 10a). These chemical and isotopic data suggest that the SCLM beneath the Sulu orogenic belt changed during the Late Triassic subduction of YC. However, the Sulu high-Mg diorite dikes in this study show higher $^{87}Sr/^{86}Sr$ than those of the Shidao and Jiazishan gabbro (Fig. 10), suggesting that another metasomatized agent had been added, besides felsic melts derived from the YC. In the study above, these diorite dikes have been proved to be derived from partial melting of the enriched SCLM source that were modified by fluids liberated from the subducted oceanic slab with marine sediments. These evidences further imply that the Sulu high-Mg diorite dikes derived from partial melting of the SCLM beneath the Sulu orogenic belt had been altered by both of subducted slab-derived melts of

ACCEPTED MANUSCRIPT

YC and fluids liberated from the subducted oceanic slab with marine sediments.

*6.1.3. Nature of mantle source*

Jiaobei and Sulu high-Mg diorite dikes are characterized by high $K_2O$ content and evident LILE enrichment, indicating that LILE- and K-bearing phases, such as amphibole or phlogopite, were present in their source (Foley et al., 1996; Ionov et al., 1997). Partial melting of amphibole is expected to yield significantly lower Rb/Sr (<0.1) and higher Ba/Rb (>20) ratios than melts of a phlogopite-bearing source (Furman and Graham, 1999). The high-Mg diorite dikes in this study record relatively low Rb/Sr (0.06–0.10) ratios and high Ba/Rb (13.66–36.83) ratios, thus indicating a predominance of amphibole in its melting source (Fig. 15a). Furthermore, in the SCLM, partial melts in the garnet stability field generally have high Dy/Yb ratios (>2.5), whereas melting in the spinel stability field would produce melts with low Dy/Yb ratios (<1.5) (Duggen et al., 2005); while the low La/Yb ratios reflect a melting regime dominated by relatively large melt fractions and/or spinel as the predominant residual phase, whereas high La/Yb ratios are indicative of smaller melt fractions and/or garnet control (Yang et al., 2007). In the Dy/Yb versus La/Yb diagram (Fig. 15b), the Jiaobei and Sulu high-Mg diorite dikes show Dy/Yb ratios ranging from 1.98 to 2.68, thus spanning a range between the partial melting curves of garnet-facies and spinel-facies lherzolite. These results thus imply that partial melting have taken place in the spinel-garnet transition zone, with the observed range of La/Yb ratios suggesting that variable and low degrees of partial melting occurred to produce melts. Therefore, we conclude that the Jiaobei and Sulu high-Mg diorite dikes were mostly derived from low-degrees of partial

ACCEPTED MANUSCRIPT

melting of an amphibole-bearing lherzolite lithospheric mantle in the spinel-garnet transition zone.

*6.2. Petrogenesis of adakitic quartz diorite dikes*

Quartz diorite dikes at Jiaobei exhibit adakitic features, including high concentrations of $SiO_2$, $Al_2O_3$ and Sr, and low Y contents, with high Sr/Y (76–149) and La/Yb (41–91) ratios (Fig. 13). Three genetic models have been suggested for the origin of the Mesozoic adakitic rocks in eastern NCC: (1) partial melting of a subducted oceanic crust (Chen and Zhou, 2005; Wang et al., 2016); (2) partial melting of delaminated lower crustal material and interaction with overlying mantle peridotite material (Xu et al., 2002; Gao et al., 2004; Gu et al., 2013); (3) partial melting of thickened lower crust (Yang et al., 2012; Ma et al., 2013; Yang et al., 2014). Firstly, the typical adakites is believed to be generated by the partial melting of subducting oceanic slab (Defant and Drummond, 1990). However, the Sr-Nd isotopic compositions of the Jiaobei adakitic dikes obviously differ from MORB-like components (Fig. 9). Jiaobei adakitic dikes have higher $K_2O/Na_2O$ (0.7-1.1) and Th/U (5.4-7.7) ratios than those of adakites from the partial melting of basaltic ocean crust ($K_2O/Na_2O$ = ~0.4, Th/U = ~0.3, $(^{87}Sr/^{86}Sr)_i$ < 0.7045, $\varepsilon_{Nd}(t)$ > 6; Martin, 1999). Therefore, Jiaobei adakitic dikes are unlikely to have been formed by partial melting of a subducted region of the oceanic crust. Secondly, it is suggested that the adakitic magmas could have been produced by the delamination of lower crustal rocks into the mantle, and followed by interaction with mantle peridotites (Xu et al., 2002; Gao et al., 2004). Nevertheless, the Jiaobei adakitic dikes have

ACCEPTED MANUSCRIPT

lower MgO (1.81–2.34 wt.%) content, lower $\varepsilon_{Nd}(t)$ (-20.1 to -14.7) value, and higher ($^{87}Sr/^{86}Sr)_i$ (0.7098-0.7104) ratio than those of delaminated lower crust-derived Mesozoic adakitic rocks in the eastern NCC (MgO ＞ 3 wt.%, ($^{87}Sr/^{86}Sr)_i$ = 0.7051-0.7075, $\varepsilon_{Nd}(t)$ = -10 to +1; Xu et al., 2002; Gao et al., 2004) (Figs. 9a and 12b). Therefore, the model of delaminated lower crust is also inappropriate for explaining the origin of Jiaobei adakitic dikes.

Alternatively, the model of partial melting of thickened lower crust could explain the origin of Jiaobei adakitic dikes. In the diagrams of $(La/Yb)_N$ versus Sr/Y, the Jiaobei adakitic dikes plot in the field of adakitic rocks derived from melts generated by partial melting of a thickened lower crust (Fig. 12c). Besides, adakitic signatures (e.g. high Sr/Y and La/Yb) and low Y and HREE abundances without negative Eu anomalies have been thought to the presence of residual garnet and the absence of residual plagioclase in the magma source (Yang, 2008; Hou et al., 2013). The flat HREE patterns (Y/Yb = 10-14; $(Ho/Yb)_N$ = 1.05-1.40) of Jiaobei adakitic dikes show that amphibole was also residual mineral (Moyen, 2009; Huang and He, 2010), which is indicative of an amphibole-bearing eclogite or garnet-amphibolite crustal source. Moreover, the mafic crustal rocks can melt to produce adakitic liquids at sufficient depths (＞ 40 km, ~1.2 Gpa) for garnet to be stable within the residual assemblage (amphibole-bearing eclogite, garnet-amphibolite and/or eclogite) (Rapp et al., 2003, and reference therein). Therefore, Jiaobei adakitic dikes originated from partial melting of the amphibole-bearing eclogitic or garnet-amphibolitic thickened lower crust.

Jiaobei quartz diorite dikes also show high $Mg^{\#}$ value (50-60, higher than crustal melts alone; Fig. 12d) and high Cr (30.4-76.6 ppm) and Ni (6.03-45.5 ppm) contents, which

ACCEPTED MANUSCRIPT

indicate likely the involvement of mantle components (Wang et al., 2016; Zeng et al., 2016). In the Jiaodong Peninsula, the Late Jurassic adakitic granites (160-144 Ma; Linglong intrusion) is recognized to be derived from partial melting of the thickened ancient lower crust of the NCC without mixing with mantle-derived materials (Ma et al., 2013). But, the middle Early-Cretaceous granodiorites (135-126 Ma; Guojialing intrusion), which show lower initial $^{87}Sr/^{86}Sr$ ratios and higher $\varepsilon_{Hf}(t)$ and $\varepsilon_{Nd}(t)$ values than those of Late Jurassic Linglong intrusion (Figs. 9a and 16), originated from a crustal magmatic source with involvement of mantle components (Zhang et al., 2010; Jiang et al., 2012; Yang et al., 2012; Yang et al., 2014). Previous study on the Cretaceous felsic rocks in Jiaodong Peninsula revealed that the Guojialing granodiorite (135-126 Ma) carries mafic enclaves (Yang et al., 2014), and the Gushan granite (~120 Ma), located in the Jiaobei terrane of the eastern North China Craton, carries mafic microgranular enclaves as well (Li et al., 2012), which provide support to the hypothesis of involvement of underplated mafic magmas. In this study, combined with the Sr-Nd-Hf isotopic compositions, the Jiaobei quartz diorite dikes display lower initial $^{87}Sr/^{86}Sr$ ratios and higher $\varepsilon_{Hf}(t)$ and $\varepsilon_{Nd}(t)$ values than those of both the middle Early-Cretaceous Guojialing granodiorites and Late Jurassic Linglong intrusion (Figs. 9a and 16), indicating more influx of mantle components into crust-derived melts. It has been studied that there are a large number of mafic dikes which derived from lithospheric mantle and emplaced into Jiaodong Peninsula at early Cretaceous (130-110 Ma) (Liu et al., 2009; Cai et al., 2013, 2015; Ma et al., 2014; Deng et al., 2017; Liang et al., 2017). The underplating of these mafic magmas likely induced the interaction between crust-derived melt and mafic magma. Therefore, Jiaobei adakitic quartz diorite dikes are proposed to be derived from

ACCEPTED MANUSCRIPT

partial melting of thickened ancient lower crust with involvement of underplated mafic magmas.

*6.3. Tectonic implication*

It has been accepted that the late Mesozoic tectonic history of Jiaodong Peninsula, and even to the eastern NCC, was marked by crustal extension and lithospheric thinning with numerous magmatism (Menzies et al., 1993; Yang et al., 2007). The thickness of the NCC lithosphere has been estimated to have been nearly 200 km during the Ordovician (Fan et al., 2000; Gao et al., 2002). The Early Cretaceous OIB-like mafic dikes (123-121 Ma) intruding into Jiaodong Peninsula were proved to be derived from asthenospheric mantle (Ma et al., 2014, 2016), which means that the thickness of the lithosphere is no greater than 80 km at this period (Ma et al., 2014). However, in the Early Cretaceous, the dynamic processes and mechanism leading to the lithospheric thinning as well as magmatism at Jiaodong still remain debated, and those causes mainly include foundering of the lower crust (Gao et al., 2004, 2008; Liu et al., 2009), lithospheric delamination (Wu et al., 2005), and thermo-mechanical erosion resulted by asthosphere mantle convection (Xu et al., 2014) or caused by rollback of Paleo-Pacific slab (Deng et al., 2017). In this paper, the Jiaobei adakitic quartz diorite dikes (127-120 Ma) has proved the existence of a thickened ancient lower crust at Jiaodong, which could also be supported by the Early Cretaceous adakitic rocks in the Luxi area (Gu et al., 2013). Thus, the existence of a thickened ancient lower crust is inconsistent with the foundering of the lower crust beneath eastern NCC in the Createaceous. Furthermore, in

ACCEPTED MANUSCRIPT

combination with the middle Early-Cretaceous granodiorites (135-126 Ma) originated from a crustal magmatic source with involvement of mantle components (Zhang et al., 2010; Jiang et al., 2012; Yang et al., 2012), the high-Mg diorite dikes (116-122 Ma) in this study has the common source of lithospheric mantle with the contemporaneous arc-like mafic dikes (130-110 Ma) at Jiaodong, indicating that lithospheric thinning along with mantle-derived magmatism was a prolonged process since at least 135 Ma rather than the lithospheric delamination during a short event lasting ~10 million years (Wu et al., 2005). Hence, Early Cretaceous magmatism at Jiaodong has revealed an episodic development of the lithospheric thinning through thermo-mechanical-chemical erosion processes during a prolonged process at least from 135 Ma to 110 Ma.

Although the model of thermo-mechanical-chemical erosion processes resulted by asthenospheric mantle convection could explain the dynamic processes of the Early Cretaceous magmatism, however, it could not explain the isotopic discrepancy of the high-Mg diorite dikes between the Jiaobei and Sulu, and that the mantle source of Jiaobei and Sulu high-Mg diorite dikes has been metasomatized by fluids of subducting oceanic slab. In this study, slight differences in Sr-Nd-Pb-Hf isotopic compositions between the Jiaobei and Sulu high-Mg diorite dikes indicate that the SCLM beneath the Sulu orogenic belt had been affected by subducted slab-melts from subducting YC during the Triassic. The lithospheric mantle of the YC has much more radiogenic Pb signatures than those of NCC (Liu et al., 2009; Tan et al., 2013), however, the high-Mg diorite dikes in this study, and even to the mafic dikes from Jiaobei (Liu et al., 2009; Tan et al., 2013; Ma et al., 2014), have Pb isotopic characteristics that are distinct from those of YC lithosphere mantle, so we can rule out the

ACCEPTED MANUSCRIPT

possibility of involvement of YC lithosphere. Arc-like Cretaceous magmatism is widespread all over the NCC rather than areas close to the Dabie-Sulu, hence, the subducted Yangtze crust was impossible thrusted under the NCC even further north (e.g. Yang et al., 2004; Wang et al., 2006; Li et al., 2011). Also, the arc-like trace element signatures, high Rb/Y and Ba/La ratios, and low Nb/Y, Nb/Zr, Th/Zr and Th/Yb of the high-Mg diorite dikes proved that the SCLM beneath Jiaodong, including Jiaobei terrain and Sulu orogenic belt, has been metasomatized by fluids from dehydrated slab. It has been widely accepted that the easternmost NCC had become an active continental margin since ~178 Ma, as it was placed in the upper plate of a shallow-angle subduction zone, consuming the Paleo-Pacific oceanic plate (Maruyama et al., 1997; Li and Li, 2007; Dilek and Sandvol, 2009; Mao et al., 2011). Thus, the SCLM beneath Jiaodong has been metasomatized by fluids from the subducting Paleo-Pacific slab in the Late Mesozoic. Furthermore, Deng et al. (2017) presented eastward younging mafic dikes in the Jiaodong Peninsula, which couldn’t be explained by asthenospheric mantle convection. However, from about 160 Ma onwards, slab rollback of the Paleo-Pacific plate occurred (Wu et al., 2007; Jiang et al., 2010; Mao et al., 2011; Ma et al., 2014), keeping pace with magmatism migrated eastward over time. This process caused strong strain partitioning and regional left-lateral transtensional deformation along and across the eastern part of the NCC (Wu et al., 2007; Jiang et al., 2010; Mao et al., 2011), resulting in upwelling of asthenospheric mantle and prolonged thermo-mechanical-chemical erosion for the lithosphere.

We model that, in the Early Cretaceous, the process of prolonged thermo-mechanical-chemical erosion is caused by rollback of the Paleo-Pacific plate, and

ACCEPTED MANUSCRIPT

further induced delamination and thinning of the lithospheric mantle beneath Jiaodong Peninsula. During this process, the partially melting of SCLM of Jiaodong Peninsula due to heating of the underlying asthenospheric mantle generated the primary lithospheric mantle-derived melts. During ascent to the surface, the lithospheric mantle-derived melts underwent fractionation formed the arc-like mafic dikes and/or high-Mg diorite dikes (130-110 Ma), and decompressive melting of asthenospheric mantle generated the OIB-like mafic dikes (123-121 Ma). Besides, continuous heating by mantle-derived mafic magmas resulted in the partial melting of the thickened ancient lower crust, generating the adakitic quartz diorite dikes (127-120 Ma) with involvement of underplated mafic magmas (Fig. 17).

## 7. Conclusions

(1) LA-ICP-MS zircon U-Pb dating demonstrates that intermediate-felsic dikes, consisting of quartz diorite and diorite dikes, were emplaced in the Jiaodong Peninsula at ca. 128–108 Ma.

(2) Quartz diorite dikes in Jiaobei have adakitic features, and were likely derived from partial melting of thickened ancient lower crust with involvement of underplated mafic magmas. On the other hand, diorite dikes in Jiaobei and Sulu yield the HMAs characteristics, which were derived from low-degree partial melting of amphibole-bearing lherzolitic peridotites in the spinel-garnet transition zone.

(3) The SCLM beneath the Sulu Orogenic belt has been altered by the Triassic continental deep subduction of YC. In the Late Mesozoic, the SCLM beneath the Jiaodong

ACCEPTED MANUSCRIPT

Peninsula was modified by slab-derived hydrous fluids originating from the subduction of the Paleo-Pacific plate with marine sediments.

(4) Early Cretaceous magmatism within the Jiaodong Peninsula may have occurred in an extensional tectonic setting involving lithospheric thinning, which was induced by thermo-mechanical erosion further caused by rollback of Paleo-Pacific slab.

## Acknowledgements

This research was financially supported by the National Natural Science Foundation of China (41230311, 41172295 and 40872068), the National Science and Technology Support Program (2011BAB04B09), and the MOE 111 Project (B07011), and the Fundamental Research Funds for the central Universities (No. 53200959708, 53200859287, 53200859689).

## References

Cai, Y.C., Fan, H.R., Santosh, M., Hu, F.F., Yang, K.F., Hu, Z., 2015. Subduction-related metasomatism of the lithospheric mantle beneath the southeastern north china craton: evidence from mafic to intermediate dykes in the northern Sulu orogen. Tectonophysics 659, 137–151.

Cai, Y.C., Fan, H.R., Santosh, M., Liu, X., Hu, F.F., Yang, K.F., Lan, T.G., Yang, Y.H., Liu, Y.S., 2013. Evolution of the lithospheric mantle beneath the southeastern North China Craton: Constraints from mafic dikes in the Jiaobei terrain. Gondwana Research 24, 601–621.

ACCEPTED MANUSCRIPT

Chen, B., Jahn, B.M., Suzuki, K., 2013. Petrological and Nd-Sr-Os isotopic constraints on the origin of high-Mg adakitic rocks from the North China Craton: Tectonic implications. Geology 41, 91–94.

Chen, J.F., Xie, Z., Li, H.M., Zhang, X.D., Zhou, T.X., Park, Y.S., Ahn, K.S., Chen, D.G., Zhang, X., 2003. U–Pb zircon ages for a collision-related K-rich complex at Shidao in the Sulu ultrahigh pressure terrane. China Geochemical Journal 37, 33–46.

Chen, J.Z., Jiang, N., 2011. Petrogenesis of the Late-Triassic alkaline magmatism in the Jiaodong area: Evidence from U-Pb age，Hf-O isotopes of zircons. Acta Petrologica Sinica 27, 3557–3574.

Chen, L.H., Zhou, X.H., 2005. Subduction-related metasomatism in the thinning lithosphere: evidence from a composite dunite-orthopyroxenite xenolith entrained in Mesozoic Laiwu high-Mg diorite, North China Craton. Geochemistry, Geophysics, Geosystems 6, 1–20.

Dai, L.Q., Zheng, Y.F., Zhao, Z.F., 2016. Termination time of peak decratonization in North China:Geochemical evidence from mafic igneous rocks. Lithos 240, 327-336.

Dai, L.Q., Zhao, Z.F., Zheng, Y.F., An, Y.J., Zheng, F., 2017. Geochemical Distinction between Carbonate and Silicate Metasomatism in Generating the Mantle Sources of Alkali Basalts. Journal of Petrology 58, 863-884.

Davidson, J., Turner, S., Handley, H., Macpherson, C.D.A., 2007. Amphibole “sponge” in arc crust? Geology 35, 787–790.

Defant, M.J., Drummond, M.S., 1990. Derivation of some modern arc magmas by melting of young subducted lithosphere. Nature 347, 662–665.

Deng, J., Liu X.F., Wang Q.F., Pan R.G., 2015a. Origin of the Jiaodong-type Xinli gold deposit, Jiaodong Peninsula, China: Constraints from fluid inclusion and C-D-O-S-Sr isotope compositions. Ore Geology Reviews 65, 674–686.

ACCEPTED MANUSCRIPT

Deng, J., Liu, X.F., Wang, Q.F., Dilek, Y., Liang, Y.Y., 2017. Isotopic Characterization and Petrogenetic Modeling of the Early Cretaceous Mafic Diking-Lithospheric Extension in the North China Craton, Eastern Asia. Geological Society of America Bulletin 129, 1379-1407.

Deng, J., Wang C.M., Bagas L., Carranza E, J.M., Lu Y.J., 2015b. Cretaceous-Cenozoic tectonic history of the Jiaojia Fault and gold mineralization in the Jiaodong Peninsula, China: constraints from zircon U-Pb, illite K-Ar, and apatite fission track thermochronometry. Mineralium Deposita 50, 987–1006.

Deng, J., Wang Q.F., Li, G.J., Santosh, M., 2014a. Cenozoic tectonomagmatic and metallogenic processes in the Sanjiang region, southwestern China. Earth Science Review 138, 268–299.

Deng, J., Wang, Q.F., 2016. Gold mineralization in China: Metallogenic province, deposit types and tectonic framework. Gondwana Research 36, 219–274.

Dilek, Y., Sandvol, E., 2009. Seismic structure, crustal architecture and tectonic evolution of the Anatolian-African plate boundary and the Cenozoic orogenic belts in the Eastern Mediterranean region, in Murphy, J.B., Keppie, J.D., and Hynes, A.J., eds., Ancient Orogens and Modern Analogues. Geological Society of London Special Publications 327, 127–160.

Duggen, S., Hoernle, K., Bogaard, P., Garbe-Schonberg, D., 2005. Post-collisional transition from subduction to intraplatetype magmatism in the westernmost Mediterranean: Evidence for continental edge delamination of subcontinental lithosphere. Journal of Petrology 46, 1155–1201.

Elhlou, S., Belousova, E., Griffin, W.L., O'Reilly, S.Y., 2006. Trace element and isotopic composition of GJ-red zircon standard by laser ablation. Geochim Cosmochim Acta 70, A158.

Elliott, T., Plank, T., Zindler, A., White, W., Bourdon, B., 1997. Element transport from slab to volcanic front at the Mariana arc. Journal of Geophysical Research 102, 14991–15019.

Ernst, R.E., Head, J.W., Parfitt, E., Grosfils, E., Wilson, L., 1995. Giant radiating dyke swarms on Earth

ACCEPTED MANUSCRIPT

and Venus. Earth Sciences Reviews 39, 1–58.

Faure, M., Lin, W., Monie, P., Bruguier, O., 2004. Paleoproterozoic arc magmatism and collision in Liaodong Penisula (north-east China). Terra Nova 16, 75–80.

Foley, S.F., Jackson, S.E., Fryer, B.J., Greenouch, J.D., Jenner G.A., 1996. Trace element partition coefficients for clinopyroxene and phlogopite in an alkaline lamprophyre from Newfoundland by LAM-ICP-MS. Geochimical et Cosmochimica Acta 60, 629–638.

Frey, F.A., Green, D.H., Roy, S.D., 1978. Integrated models of basalt petrogenesis: a study of quartz tholeiites to olivine melilitites from south eastern Australia utilizing geochemical and experimental petrological data. Journal of petrology 19, 463–513.

Furman, T., Graham, D., 1999. Erosion of lithospheric mantle beneath the East African Rift system: Geochemical evidence from the Kivu volcanic province. Lithos 48, 237–262.

Gao, S., Rudnick, R.L., Xu, W., Yuan, H., Liu, Y., Walker, R.J., Puchtel, I.S., Liu, X., Huang, H., Wang, X., Yang, J., 2008. Recycling deep cratonic lithosphere and generation of intraplate magmatism in the North China Craton. Earth and Planetary Science Letters 270, 41–53.

Gao, S., Rudnick, R.L., Yuan, H.L., Liu, X.M., Liu, Y.S., Xu, W.L., Ling, W.L., Ayers, J., Wang, X.C., Wang, Q.H., 2004. Recycling lower continental crust in the North China Craton. Nature 432, 892–897.

Goldfarb, R.J., Taylor, R.D., Collins, G.S., Goryachev, N.A., Orlandini, O.F., 2014. Phanerozoic continental growth and gold metallogeny of Asia. Gondwana Research 25, 48–102.

Goldfarb, R.J., Santosh, M., 2014. The dilemma of the Jiaodong gold deposits: Are they unique? Geoscience Frontiers 5, 139-153.

Gu, H.O., Xiao, Y., Santosh, M., Li, W.Y., Yang, X., Pack, A., Hou, Z., 2013. Spatial and temporal

ACCEPTED MANUSCRIPT

distribution of Mesozoic adakitic rocks along the Tan-Lu fault, Eastern China: constraints on the initiation of lithospheric thinning. Lithos 177, 352–365.

Guo, F., Fan, W.M., Li, C.W., Wang, C.Y., Li, H.X., Zhao, L., Li, J.Y., 2014. Hf-Nd-O isotopic evidence for melting of recycled sediments beneath the Sulu Orogen, North China. Chemical Geology 381, 243–258.

Hanyu, T., Gill, J., Tatsumi, Y., 2012. Across- and along-arc geochemical variations of lava chemistry in the Sangihe arc: Various fluid and melt slab fluxes in response to slab temperature. Geochem. Geophys. Geosyst. 7.

Hart, S.R., 1984. A large-scale isotopic anomaly in the Southern Hemisphere mantle. Nature 309, 753–757.

Hoskin, P.W.O., Schaltegger, U., 2003. The composition of zircon and igneous and metamorphic petrogenesis. Reviews in Mineralogy Geochemistry 53, 27–62.

Hou, G.T., Santosh. M., Qian, X.L., Lister, G.S., Li, J.H., 2008. Configuration of the Late Paleoproterozoic supercontinent Columbia: Insights from radiating mafic dyke swarms. Gondwana Research 14, 395–409.

Hou, K.J., Li, Y.H., Tian, Y.R., 2009. In situ U-Pb zircon dating using laser ablationmulti ion counting-ICP-MS. Mineral Deposit 28, 481–492.

Hou, Z.Q., Zheng, Y.C., Yang, Z.M., Rui, Z.Y., Zhao, Z.D., Jiang, S.H., Qu, X.M., Sun, Q.Z., 2013. Contribution of mantle components within juvenile lower-crust to collisional zone porphyry Cu systems in Tibet. Mineralium Deposita 48, 173–192.

Huang, F.A., He,Y.S., 2010. Partial melting of the dry mafic continental crust: implications for petrogenesis of C-type adakites. Chinese Science Bulletin 55, 2428–2439.

Huang, X.L., Zhong, J.W., Xu, Y.G., 2012. Two tales of the continental lithospheric mantle prior to the

ACCEPTED MANUSCRIPT

destruction of the North China Craton: Insights from Early Cretaceous mafic intrusions in western Shandong, east China. Geochimica et Cosmochimica Acta 96, 193–214.

Ionov, D.A., Griffin, W.L., O’Reilly S.Y., 1997. Volatile bearing minerals and lithophile trace elements in the upper mantle. Chemical Geology 141, 153–184.

Jiang, N., Chen, J., Guo, J., Chang, G., 2012. In situ zircon U-Pb, oxygen and hafnium isotopic compositions of Jurassic granites from the North China craton: Evidence for Triassic subduction of continental crust and subsequent metamorphism-related 18O depletion. Lithos 142, 84–94.

Jiang, Y.H., Jiang, S.Y., Ling, H.F., Ni,P., 2010. Petrogenesis and tectonic implications of Late Jurassic shoshonitic lamprophyre dikes from the Liaodong Peninsula, NE China. Mineral Petrology 100, 127–151.

Kelemen, P.B., Hanghø, J.K., Greene, A.R., 2003. One View of the Geochemistry of Subduction-related Magmatic Arcs, with an Emphasis on Primitive Andesite and Lower Crust. Treatise on Geochemistry 3, 593–659.

Kepezhinskas, P., McDermott, F., Defant, M.J., Hachstaedter, A., Drummond, M.S., Hawkesworth, C.J., Koloskov, A., Maury, R.C., Bellon, H., 1997. Trace element and Sr-Nd-Pb isotopic constraints on a three component model of Kamchatka Arc petrogenesis. Geochimica et Cosmochimica Acta 61, 577–600.

Le Maitre, R.W., Bateman, P., Dudek, A., Keller, J., Le Bas, M.J.L., Sabine, P.A., Schmid, R., Sorensen, H., Streckeisen, A., Woodlley, A.R., Zanettin, B., 1989. A Classification of Igneous Rocks and Glossary of Terms. Blackwell, Oxford.

Li, J.X., Qin, K.Z., Li, G.M., Xiao, B., Zhao, J.X., Cao, M.J., Chen, L., 2013. Petrogenesis of ore-bearing porphyries from the Duolong porphyry Cu-Au deposit, central Tibet: Evidence from U-Pb



ACCEPTED MANUSCRIPT

ACCEPTED MANUSCRIPT

geochronology, petrochemistry and Sr-Nd-Hf-O isotope characteristics. Lithos 160–161, 216–227.

Li, X.C., Fan, H.R., Santosh, M., Hu, F.F., Yang, K.F., Lan, T.G., Liu, Y.S., Yang, Y.H., 2012. An evolving magma chamber within extending lithosphere: An integrated geochemical, isotopic and zircon U-Pb geochronological study of the Gushan granite, eastern North China Craton. Journal of Asian Earth Sciences 50, 27–43.

Li, X.H., Liu, D.Y., Sun, M., Li, W.X., Liang, X.R., Liu, Y., 2004. Precise Sm-Nd and U-Pb isotopic dating of the supergiant Shizhuyuan polymetallic deposit and its host granite, southeast China. Geological Magazine 141, 225–231.

Li, X.H., Long, W.G., Li, Q.L., Zheng, Y.F., Yang, Y.H., Chamberlain, K.R., Wan, D.F., Guo, C.H., Wang, X.C., Tao, H., 2010. Penglai zircon megacrysts: A potential new working reference material for microbeam determination of Hf-O isotopes and U-Pb age. Geostandards and Geoanalytical Research 34, 117–134.

Li, Z.X., Li, X.H., 2007. Formation of the 1300-km-wide intracontinental orogen and postorogenic magmatic province in Mesozoic South China: A flat-slab subduction model. Geology 35, 179–182.

Liang, Y.Y., Liu, X.F., Qin, C., Li, Y., Chen, J., Jiang, J.Y., 2016. Petrogenesis of Early Cretaceous mafc dikes in southeastern Jiaolai basin, Jiaodong Peninsula, China: International Geology Review 2, 131–150.

Liang, Y.Y., Liu, X.F., Qin, C., Li, Y., Chen, J., Jiang, J.Y., 2017. Petrogenesis of Early Cretaceous mafic dikes in southeastern Jiaolai basin, Jiaodong Peninsula, China. International Geology Review 59, 131–150.

Liu, S., Hu, R., Gao, S., Feng, C., Yu, B., Feng, G., Qi, Y., Wang, T., Coulson, I.M., 2009. Petrogenesis of Late Mesozoic mafic dykes in the Jiaodong Peninsula, eastern North China Craton and implications

ACCEPTED MANUSCRIPT

for the foundering of lower crust. Lithos 113, 621–639.

Liu, X.C., Wu, Y.B., Gao, S., Wang, H., Zheng, J.P., Hu, Z.C., Zhou, L., Yang, S.H., 2014. Record of multiple stage channelized fluid and melt activities in deeply subducted slab from zircon U-Pb age and Hf-O isotope compositions. Geochimica et Cosmochimica Acta 144, 1–24.

Liu, Y.S., Gao, S., Hu, Z.C., Gao, C.G., Zong, K.Q., Wang, D.B., 2010. Continental and Oceanic Crust Recycling-induced Melt Peridotite Interactions in the Trans-North China Orogen: U-Pb Dating, Hf Isotopes and Trace Elements in Zircons from Mantle Xenoliths. Journal of Petrology 51, 537–571.

Ma, L., Jiang, S.Y., Dai, B.Z., Jiang, Y.H., Hou, M.L., Pu, W., Xu, B., 2013. Multiple sources for the origin of Late Jurassic Linglong adakitic granite in the Shandong Peninsula, eastern China: Zircon U-Pb geochronological, geochemical and Sr-Nd-Hf isotopic evidence. Lithos 162–163, 251–263.

Ma, L., Jiang, S.Y., Hofman, A.W., Dai, B.Z., Hou, M.L., Zhao, K.D., Chen, L.H., Li, W.J., Jiang, H.Y., 2014. Lithospheric and asthenospheric sources of lamprophyres in the Jiaodong Peninsula: A consequence of rapid lithospheric thinning beneath the North China Craton? Geochimica Cosmochimica Acta 124, 250–271.

Ma, L., Jiang, S.Y., Hofman, A.W., Xu, Y.G., Dai, B.Z., Hou, M.L., 2016. Rapid lithospheric thinning of the North China Craton: New evidence from cretaceous mafic dikes in the Jiaodong Peninsula. Chemical Geology 432, 1–15.

Mao, J.W., Pirajno, F., Cook, N., 2011. Mesozoic metallogeny in East China and corresponding geodynamic settings—An introduction to the special issue. Ore Geology Reviews 43, 1–7.

Martin, H., 1999. Adakitic magmas: modern analogues of Archaean granitoids. Lithos 46, 411–429.

Martin, H., Smithies, R.H., Rapp, R., Moyen, J.F., Champion, D., 2005. An overview of adakite, tonalite-trondhjemite-granodiorite (TTG), and sanukitoid: Relationships and some implications for

ACCEPTED MANUSCRIPT

crustal evolution. Lithos 79, 1–24.

Maruyama, S., Isozaki, Y., Kimura, G., and Terabayashi, M., 1997. Paleogeographic maps of the Japanese Islands: Plate tectonic synthesis from 750 Ma to the present. The Island Arc 6, 121–142.

Menzies, M.A., Fan, W.M., Zhang, M., 1993. Palaeozoic and Cenozoic lithoprobes and the loss of >120 km of Archaean lithosphere, Sino-Korean craton, China. Geological Society, London, Special Publications 76, 71–81.

Menzies, M.A., Xu, Y.G., Zhang, H.F., Fan, W.M., 2007. Integration of geology, geophysics and geochemistry: A key to understanding the North China Craton. Lithos 96, 1–21.

Moyen, J.F., 2009. High Sr/Y and La/Yb ratios: the meaning of the“adakitic signature”. Lithos 112, 556–574.

Nasdala, L., Hofmeister, W., Norberg, N., Martinson, J.M., Cortfu, F., Dörr, W., L.Kamo, S., Kennedy, A.K., Kronz, A., Reiners, P.W., Feri, D., Kosler, J., Wan, Y.S., Götze, J., Häger, T., Kröner, A., Valley, J.W., 2008. Zircon M257-a Homogeneous Natural Reference Material for the Ion Microprobe U-Pb Analysis of Zircon. Geostandards and Geoanalytical Research 32, 247–265.

Ou, Q., Wang, Q., Wyman, D.A., Zhang, H.X., Yang, J.H., Zeng, J.P., Hao, L.L., Chen, Y.W., Liang, H., Qi, Y., 2017. Eocene adakitic porphyries in the central-northern Qiangtang Block, central Tibet: Partial melting of thickened lower crust and implications for initial surface uplifting of the plateau. Journal of Geophysical Research. Solid Earth 122, 1025–1053.

Parman, S.W., Grove, T.L., 2004. Harzburgite melting with and without $H_2O$: experimental data and predictive modeling. Journal of Geophysical Research 109.

Rapp, R.P., Shimizu, N., Norman, M.D., 2003. Growth of early continental crust by partial melting of eclogite. Nature 425, 605–609.

ACCEPTED MANUSCRIPT

Santosh, M., Pirajno, F., 2015. The jiaodong-type gold deposits: Introduction. Ore Geology Reviews 65, 565-567.

Streck, M.J., Leeman, W.P., Chesley, J., 2007. High-magnesian andesite from Mount Shasta: a product of magma mixing and contamination, not a primitive mantle melt. Geology 35, 351–354.

Sun, S.S., McDonough, W.F., 1989. Chemical and isotopic systematics of oceanic basalts: implications for mantle composition and processes In: Saunders, AD, Norry, MJ (eds.), Magmatism in the Oceanic Basins. Geological Society Special Publications 313–345.

Sun, W.D., Ding, X,. Hu, Y.H., Li, X.H., 2007. The golden transformation of the Cretaceous plate subduction in the west Pacific. Earth and Planetary Science Letters 262, 533–542.

Tan, J., Wei, J.H., Guo, L.L., Zhang, K.Q., Yao, C.L., Lu, J.P., Li, H.M., 2008. LA-ICP-MS zircon U-Pb dating and phenocryst EPMA of dikes, Guocheng, Jiaodong Peninsula: Implications for North China Craton lithosphere evolution. Science in China (D) 51, 1483–1500.

Tan, J., Wei, J.H., Li, Y.G., Tan, W.J., Dazhao, G., Yang, C., 2007. Geochemical Characteristics of Late Mesozoic Dikes, Jiaodong Peninsula, North China Craton: Petrogenesis and Geodynamic Setting. International Geology Review 49, 931–946.

Tatsumi, Y., 2001. Geochemical modeling of partial melting of subducting sediments and subsequent melt-mantle interaction: Generation of High-Mg andesites in the Setouchi volcanic belt, southwest Japan. Geology 29, 323–326.

Tatsumi, Y., 2006. High-Mg andesites in the Setouchi volcanic belt, southwestern Japan: Analogy to Archean magmatism and continental crust formation? Annu. Rev. Earth Planet. Sci. 34, 467–499.

Wang, C.M., Deng, J., Santosh, M., Emmanuel, J.M.C., Gong, Q.J., Guo, C.Y., Xia, R., Lai, X.R., 2015. Timing, tectonic implications and genesis of gold mineralization in the Xincheng gold deposit, China:

ACCEPTED MANUSCRIPT

C-H-O isotopes, pyrite Rb-Sr and zircon fission track thermochronometry. Ore Geology Reviews 65, 659–673.

Wang, C.M., Lu, Y.J., He, X.Y., Wang, Q.H., Zhang, J., 2016a. The Paleoproterozoic diorite dykse in the southern margin of the North China Craton: Insight into rift-related magmatism. Precambrian Research 277, 26–46.

Wang, Q., Mcdermott, F., Xu, J.F., Bellon, H., Zhu, Y.T., 2005. Cenozoic k-rich adakitic volcanic rocks in the hohxil area, northern tibet: lower-crustal melting in an intracontinental setting. Geology 33, 465-468.

Wang, Q.F., Deng, J., Liu, X.F., Zhao, R., Cai, S.H., 2016b. Provenance of late carboniferous bauxite deposits in the North China Craton: New constraints on marginal arc construction and accretion processes. Gondwana Research 38, 86–98.

Wang, Y.J., Fan, W.M., Peng, T.P., Zhang, H.F., Guo, F., 2005. Nature of the Mesozoic lithospheric mantle and tectonic decoupling beneath the Dabie Orogen, Central China: Evidence from $^{40}Ar/^{39}Ar$ geochronology, elemental and Sr-Nd-Pb isotopic compositions of early Cretaceous mafic igneous rocks. Chemical Geology 220, 165–189.

Wei, G.J., Liang, X.R., Li, X.H., Liu, Y., 2002. Precise measurement of Sr isotopic composition of liquid and solid base using (LP) MC-ICPMS. Geochimica 31, 295–299.

White, W.M., Albarède, F., Télouk, P., 2000. High–precision analysis of Pb isotope ratios by multi-collector ICP-MS. Chemical Geology 167, 257–270.

Woodhead, J.D., Hergt, J.M., Davidson, J.P., Eggins, S.M., 2001. Hafnium isotope evidence for ‘conservative’ element mobility during subduction zone processes. Earth and Planetary Science Letters 192, 331–346.

ACCEPTED MANUSCRIPT

Wu, F.Y., Lin, J.Q., Wilde, S.A., Zhang, X.O., Yang, J.H., 2005. Nature and significance of the early cretaceous giant igneous event in Eastern China. Earth and Planetary Science Letters 233, 103–119.

Wu, F.Y., Yang, J.H., Lo, C.H., Wilde, S.A., Sun, D.Y., and Jahn, B.M., 2007. The Heilongjiang Group: A Jurassic accretionary complex in the Jiamusi Massif at the western Pacifc margin of northeastern China. The Island Arc 16, 156–172.

Wu, F.Y., Yang, Y.H., Xie, L.W., Yang, J.H., Xu, P., 2006. Hf isotopic compositions of the standard zircons and baddeleyites used in U-Pb geochronology. Chemical Geology 234, 105–126.

Xie, Z., Li, Q.Z., Gao, T.S., 2006. Comment on "Petrogenesis of post-orogenic syenites in the Sulu orogenic belt, east China: Geochronological, geochemical and Nd–Sr isotopic evidence" by Yang et al. Chemical Geology 235, 191–194.

Xu, H.J., Ma, C.Q., Song, Y.R., Zhang, J.F., Ye, K., 2012. Early Cretaceous intermediate-mafic dykes in the Dabie orogen, eastern China: Petrogenesis and implications for crust–mantle interaction. Lithos 154, 83–99.

Xu, J.F., Shinjo, R., Defant, M.J., Wang, Q., Rapp, R.P., 2002. Origin of Mesozoic adakitic intrusive rocks in the Ningzhen area of east China: Partial melting of delaminated lower continental crust? Geology 30, 1111–1114.

Xu, W.L., Gao, S., Wang, Q.H., Wang, D.Y., Liu, Y.S., 2006. Mesozoic crustal thickening of the eastern North China craton: evidence from eclogite xenoliths and petrologic implications. Geology 34, 721–724.

Xu, Y.G., 2014. Recycled oceanic crust in the source of 90–40 Ma basalts in North and Northeast China: Evidence, provenance and significance. Geochimica et Cosmochimica Acta 143, 49–67.

Xu, Y.G., Huang, X.L., Ma, J.L., Wang, Y.B., Iizuka, Y., Xu, J.F., Wang, Q., Wu, X.Y., 2004. Crust-mantle



ACCEPTED MANUSCRIPT

ACCEPTED MANUSCRIPT

interaction during the tectono-thermal reactivation of the North China Craton: constraints from SHRIMP zircon U-Pb chronology and geochemistry of Mesozoic plutons from western Shandong. Contributions to Mineralogy and Petrology 147, 750–767.

Yan, J., Chen, J.F., Yu, G., Qian, H., Zhou, T.X., 2003. Pb isotopic characteristics of late Mesozoic mafic rocks from the Lower Yangtze Region: evidence for enriched mantle. Journal of China University of Geosciences 9, 195–206.

Yang, C.H., Xu, W.L., Yang, D.B., Wang, W., Wang, W.D., Liu, J.M., 2008. Petrogenesis of Shangyu gabbro-diorites in western Shandong: geochronological and geochemical evidence. Science China (Series D) 51, 481–492.

Yang, J.H., Wu, F.Y., Chung, S.L., Lo, C.H., Wilde, S.A., Davis, G.A., 2007. Rapid exhumation and cooling of the Liaonan metamorphic core complex: Inferences from $^{40}Ar/^{39}Ar$ thermochronology and implications for Late Mesozoic extension in the eastern North China Craton. Geological Society of America Bulletin 119, 1405–1414.

Yang, K.F., Fan, H.R., Santosh, M., Hu, F.F., Simon, A.W., Lan, T.G., Lu, L.N., Liu, Y.S., 2012. Reactivation of the Archean lower crust: Implications for zircon geochronology, elemental and Sr-Nd-Hf isotopic geochemistry of late Mesozoic granitoids from northwestern Jiaodong Terrane, the North China Craton. Lithos 146–147, 112–127.

Yang, L.Q., Deng, J., Guo, L.N., Wang, Z.L., Li, X. Z., Li, J.L., 2016a. Origin and evolution of ore fluid, and gold-deposition processes at the giant Taishang gold deposit, Jiaodong Peninsula, eastern China. Ore Geology Reviews 72, 585–602.

Yang, L.Q., Deng, J., Wang, Z.L., Guo, L.N., Li, H.R., Groves, D.I., Danyushevsky, L.V., Zhang, C., Zheng, X.L., Zhao, H., 2016b. Relationships between Gold and Pyrite at the Xincheng gold deposit,

ACCEPTED MANUSCRIPT

Jiaodong Peninsula, China: Implications for gold source and deposition in a brittle epizonal environment. Economic Geology 111, 105–126.

Yang, Q.Y., Santosh, M., Shen, J.F., Li, S.R., 2014. Juvenile vs. recycled crust in NE China: Zircon U-Pb geochronology, Hf isotope and an integrated model for Mesozoic gold mineralization in the Jiaodong Peninsula. Gondwana Research 25, 1445-1468.

Yang, Q.Y., Santosh, M., 2015. Early Cretaceous magma flare-up and its implications on gold mineralization in the Jiaodong Peninsula, China. Ore Geology Reviews 626-642.Goss, S.C., Wilde, S.A., Wu, F.Y., Yang, J.H., 2010.

Yang, Z.M., Lu, Y.J., Hou, Z.Q., Chang, Z.S., 2015. High-Mg diorite from Qulong in southern Tibet: Implications for the genesis of adakitic intrusions and associated porphyry, Cu deposits in collisional orogens. Journal of Petrology 56, 227–254.

Ye, K., Cong, B.L., Ye, D.N., 2000. The possible subduction of continental material to depths greater than 200 km. Nature 407, 734–736.

Zeng, Y.C., Chen, J.L., Xu, J.F., Wang, B.D., Huang, F., 2016. Sediment melting during subduction initiation: Geochronological and geochemical evidence from the Darutso high-Mg andesites within ophiolite melange, central Tibet. Geochemistry, Geophysics, Geosystems. 17, 4859-4877.

Zeng, Y.C., Chen, J.L., Xu, J.F., Lei, M., Xiong, Q.W., 2017. Origin of Miocene Cu-bearing porphyries in the Zhunuo region of the southern Lhasa subterrane: Constraints from geochronology and geochemistry. Gondwana Research 41, 51–64.

Zhai, M.G., Santosh, M., 2013. Metallogeny of the North China Craton: Link with secular changes in the evolving Earth. Gondwana Research 24, 275–297.

Zhang, H.F., 2012. Destruction of ancient lower crust through magma underplating beneath Jiaodong

ACCEPTED MANUSCRIPT

Peninsula, North China Craton: U-Pb and Hf isotopic evidence from granulite xenoliths. Gondwana Research 21, 281–292.

Zhang, H.F., Sun, M., Zhou, M.F., Fan, W.M., Zhou, X.H., Zhai, M.G., 2004. Highly heterogeneous Late Mesozoic lithospheric mantle beneath the North China Craton: evidence from Sr-Nd-Pb isotopic systematics of mafic igneous rocks. Geological Magazine 141, 55–62.

Zhang, H.F., Sun, M., Zhou, X.H., Fan, W.M., Zhai, M.G., Yin, J.F., 2002. Mesozoic lithosphere destruction beneath the North China Craton:evidence from major-trace-element and Sr-Nd-Pb isotope studies of Fangcheng basalts. Contrib Mineral Petrol 144, 241–253.

Zhang, J., Zhao, Z.F., Zheng, Y.F., Dai, M., 2010. Postcollisional magmatism: Geochemical constraints on the petrogenesis of Mesozoic granitoids in the Sulu orogen, China. Lithos 119, 512–536.

Zhao, G.C., Zhai, M. G., 2013. Lithotectonic elements of Precambrian basement in the North China Craton: Review and tectonic implications. Gondwana Research 23, 1207–1240.

Zhao, Z.F., Zheng, Y.F., Zhang, J., Dai, L.Q., Li, Q., Liu, X., 2012. Syn-exhumation magmatism during continental collision: evidence from alkaline intrusives of Triassic age in the Sulu orogen. Chemical Geology 328, 70–88.

Zheng, J.P., Lu, F. X., 1999. Mantle xenoliths from kimberlites, Shandong and Liaoning: Paleozoic mantle character and its heterogeneity. Acta Petrology Sinica 15, 65–74.

ACCEPTED MANUSCRIPT

ACCEPTED MANUSCRIPT

## Figure captions

**Fig. 1.** (a) Tectonic outline of the North China Craton. (b) Simplified geological map of the Jiaodong Peninsula (modified after Deng et al., 2017), showing the distribution of dike swarms and the locations of samples used in this study. Data sources: Tan et al., 2008; Liu et al., 2009; Cai et al., 2013, 2015; Ma et al., 2014, 2016; Deng et al., 2017.

**Fig. 2.** Representative field photographs and micrographs showing a quartz diorite dike (a) and its major mineral assemblages (b), a diorite dike (c) and its main mineral assemblages (d) in the Jiaobei terrane; a diorite dike (e) and its dominant minerals (f); and a diorite porphyry dike (g) and its major minerals (h) in the Sulu orogenic belt. Qtz: quartz; Pl: plagioclase; Am: amphibole.

**Fig. 3.** Cathodoluminescence images (a–c) and zircon U–Pb concordia diagrams (e–g) of quartz diorite dikes from the Jiaobei terrane; Cathodoluminescence images (d) and zircon U–Pb concordia diagrams (h) of diorite dikes from the Jiaobei terrane in the Jiaodong Peninsula.

**Fig. 4.** Cathodoluminescence images (a–b) and zircon U–Pb concordia diagrams (c–d) of diorite dikes from the Sulu orogenic belt in the Jiaodong Peninsula.

**Fig. 5.** Histograms of zircon $\varepsilon_{Hf}$(t) values and $T_{DM2}$(t) for quartz diorite dikes (a-b) and diorite dikes (c-d) from Jiaobei terrane, and diorite dikes from Sulu orogenic belt (e-f) in Jiaodong Peninsula.

**Fig. 6.** Plots (a) of $Na_2O+K_2O$ vs. $SiO_2$ and (b) $K_2O$ vs. $SiO_2$ (after Le et al., 1989) for quartz diorite dikes and diorite dikes from the Jiaobei terrane and Sulu orogenic belt in the

ACCEPTED MANUSCRIPT

Jiaodong Peninsula. Smaller gray circles and squares represent data from previous studies (Tan et al., 2007; Cai et al., 2013, 2015).

**Fig. 7.** $SiO_2$ vs. selected major and trace element contents for quartz diorite dikes and diorite dikes from the Jiaobei terrane and Sulu orogenic belt in the Jiaodong Peninsula. Smaller gray circles and squares represent data from previous studies (Tan et al., 2007; Cai et al., 2013, 2015).

**Fig. 8.** Chondrite-normalized REE patterns of Jiaobei quartz diorite dikes (a), Jiaobei diorite dikes (c) and Sulu diorite dikes (e); primitive mantle-normalized immobile trace element patterns of Jiaobei quartz diorite dikes (b), Jiaobei diorite dikes (d) and Sulu diorite dikes (f). Data sources: 123-121 Ma OIB-like mafic dikes in the Jiaodong Peninsula are from Ma et al. (2014, 2016); 130–110 Ma arc-like mafic dikes in the Jiaodong Peninsula are from Liu et al. (2009) and Ma et al. (2014); 120-110 Ma granites in Jiaodong Peninsula are from Goss et al. (2010) and Li et al. (2012); average OIB and N-MORB lines are from Sun and McDonough (1989); Aleutian arc basalts are from Kelemen et al. (2003); and chondrite and primitive mantle values are from Sun and McDonough (1989).

**Fig. 9.** Plots of (a) $(^{87}Sr/^{86}Sr)_i$ vs. $\varepsilon_{Nd}(t)$, (b) Initial $^{206}Pb/^{204}Pb$ vs. $^{208}Pb/^{204}Pb$, and (c) initial $^{206}Pb/^{204}Pb$ vs. $^{207}Pb/^{204}Pb$ values for the quartz diorite dikes from the Jiaobei terrane in the Jiaodong Peninsula. Data sources: The Late Jurassic granite are from Yang et al. (2012); the middle Early-Cretaceous granodiorite are from Zhang et al. (2010); Yang et al. (2012); the late Early-Cretaceous monzogranite are from Li et al. (2012); Cretaceous arc-like mafic dikes in Jiaodong are from Liu et al. (2009), Ma et al. (2014), Cai et al. (2015) and Deng et al. (2017); delaminated lower crust-derived adakitic rocks in Mesozoic are from

ACCEPTED MANUSCRIPT

Gao et al. (2004); subducted oceanic crust-derived adakites in Cenozoic are from Defant and Drummond (1990) and Sajona et al. (2000); mafic rocks from the NCC are from Zhang et al. (2004) and Xie et al. (2006); mafic rocks from the YC are from Yan et al. (2003); fields for MORB, OIB and NHRL (north hemisphere reference line) are from Hart (1984).

**Fig. 10.** Plots of (a) $(^{87}Sr/^{86}Sr)_i$ vs. $\varepsilon_{Nd}(t)$, (b) initial $^{206}Pb/^{204}Pb$ vs. $^{208}Pb/^{204}Pb$, and (c) initial $^{206}Pb/^{204}Pb$ vs. $^{207}Pb/^{204}Pb$ values of diorite dikes from the Jiaobei terrane and Sulu orogenic belt in the Jiaodong Peninsula. Data sources: Paleozoic kimberlites and peridotites are from Zheng and Lu (1999); Triassic mafic rocks in Sulu orogenic dikes are from Zhao et al. (2012); Cretaceous arc-like mafic dikes in Jiaobei are from Liu et al. (2009), Ma et al. (2014) and Deng et al. (2017); Cretaceous OIB-like mafic dikes in Jiaobei are from Ma et al. (2014, 2016); Cretaceous arc-like mafic dikes in Sulu are from Cai et al.(2015) and Deng et al. (2017); Cretaceous arc-like mafic dikes in Dabie are from Wang et al. (2005) and Xu et al. (2012); subducted oceanic crust-derived adakites in Cenozoic are from Defant and Drummond (1990) and Sajona et al. (2000); mafic rocks from the NCC are from Zhang et al. (2004) and Xie et al. (2006); mafic rocks from the YC are from Yan et al. (2003); fields for MORB, OIB and NHRL (north hemisphere reference line) are from Hart (1984).

**Fig. 11.** Plots of $\varepsilon_{Nd}(t)$ vs. $SiO_2$ (a) and $(^{87}Sr/^{86}Sr)i$ vs. $SiO_2$ (b) for quartz diorite dikes and diorite dikes from the Jiaobei terrane and the Sulu orogenic belt in the Jiaodong Peninsula. Smaller gray circles and squares represent data from previous studies (Tan et al., 2007; Cai et al., 2013, 2015).

ACCEPTED MANUSCRIPT

**Fig. 12.** Plots of (a) Th vs. Th/La for quartz diorite dikes and diorite dikes from the Jiaobei terrane and Sulu orogenic belt (MORB data are from Niu and Batiza, 1997); (b) $SiO_2$ vs. MgO (after Wang et al., 2007 and Moyen, 2009), (c) $(La/Yb)_N$ vs. Sr/Y (after Liu et al., 2010) and (d) $SiO_2$ vs. $Mg^{\#}$ of in the Jiaodong Peninsula (after Wang et al., 2016) for quartz diorite dikes from Jiaobei terrane.

**Fig. 13.** Diagrams of Sr/Y vs. Y (a) and $(La/Yb)_N$ vs. $Yb_N$ (b) for quartz diorite dikes and diorite dikes from the Jiaobei terrane and Sulu orogenic belt in the Jiaodong Peninsula (after Defant and Drummond, 1990; Martin et al., 2005). Data sources: partial melting curves for basalt residues of eclogite, garnet amphibolite, and amphibolite are from Defant and Drummond, 1990 and Ou et al. (2017). Smaller gray circles and squares represent data from previous studies (Tan et al., 2007; Cai et al., 2013, 2015).

**Fig. 14.** Plots of (a) Rb/Y vs. Nb/Y (Kepezhinskas et al., 1997), (b) Nb/Zr vs. Th/Zr (Kepezhinskas et al., 1997), (c) Th/Yb vs. Ba/La (Woodhead et al. 2001) and (d) Hf/Sm vs. Zr/Hf (Liu et al. 2014) for quartz diorite dikes and diorite dikes from the Jiaobei terrane and Sulu orogenic belt in the Jiaodong Peninsula. Smaller gray circles and squares represent data from previous studies (Tan et al., 2007; Cai et al., 2013, 2015).

**Fig. 15.** (a) Rb/Sr vs. Ba/Rb (Furman and Graham, 1999) and (b) plot of La/Yb vs. Dy/Yb (Yang et al., 2007) for diorite dikes from the Jiaobei terrane and Sulu orogenic belt in the Jiaodong Peninsula. Smaller gray circles and squares represent data from previous studies (Tan et al., 2007; Cai et al., 2013, 2015).

**Fig. 16.** Plots of zircon $\varepsilon_{Hf}(t)$ vs. ages of Late Mesozoic magmatic rocks in the Jiaodong Peninsula. Data sources: The Late Jurassic granite are from Yang et al. (2012); the middle

ACCEPTED MANUSCRIPT

Early-Cretaceous granodiorite are from Zhang et al. (2010) and Yang et al. (2012); the late Early-Cretaceous monzogranite are from Li et al. (2012).

**Fig. 17.** A proposed model for the origin of the Cretaceous dike swarms in Jiaodong Peninsula (Modified from Deng et al., 2017).

## Table captions

**Table 1:** Lithology and mineralogy of intermediate-felsic dikes from the Jiaobei terrane and the Sulu orogenic belt in the Jiaodong Peninsula

**Table 2:** Results of LA–ICP–MS zircon U–Pb dating of intermediate-felsic dikes from the Jiaobei terrane and the Sulu orogenic belt in the Jiaodong Peninsula

**Table 3:** Zircon Hf isotopic compositions of intermediate-felsic dikes from the Jiaobei terrane and the Sulu orogenic belt in the Jiaodong Peninsula

**Table 4:** Whole-rock major (wt.%) and trace element (ppm) compositions of intermediate-felsic dikes from the Jiaobei terrane and the Sulu orogenic belt in the Jiaodong Peninsula

**Table 5:** Sr, Nd and Pb isotopic compositions of intermediate-felsic dikes from the Jiaobei terrane and the Sulu orogenic belt in the Jiaodong Peninsula

ACCEPTED MANUSCRIPT

ACCEPTED MANUSCRIPT

**Table 1:** Lithology and mineralogy of intermediate-felsic dikes from the Jiaobei terrane and the Sulu orogenic belt in the Jiaodong Peninsula

| No | Sample | GPS | Lithology | Texture | Mineralogy |
|---|---|---|---|---|---|
| ***Jiaobei*** | | | | | |
| LKXDJ-1 | LKXDJ-1-1<br>LKXDJ-1-2 | N：37°32′8.8″<br>E：120°30′13″ | Quartz diorite | Subhedral granula | Pl(45%), Am(15%), Qtz(15%), Kfs(10%), Bt |
| LZYD-1 | LZYD-1-11<br>LZYD-1-12 | N：37°12′45″<br>E：120°10′53″ | Quartz diorite | Euhedral granula | Pl(40%), Am(15%) Qtz(15%), Kfs(10%), Bt(5%), Py(5%) |
| PDDZ-1 | PDDZ-1-1<br>PDDZ-1-2 | N：36°58′25.9″<br>E：119°59′56.2″ | Diorite | Subhedral granula | Pl(50%), Am(30%), Cpx(10%), Py(5%) |
| PDDZ-2 | PDDZ-2-1<br>PDDZ-2-2 | N：36°58′28.8″<br>E：120°00′23″ | Quartz diorite porphyrite | Porphyritic | Phenocrysts: Pl(10%), Am(10%); groundmass: Pl＞Am＞Qtz |
| PDDZ-3 | PDDZ-3-1<br>PDDZ-3-2<br>PDDZ-3-3 | N：36°58'28.8"<br>E：120°00'23" | Diorite | Subhedral granula | Pl(40%), Am(30%), Kfs(15%), Py(5%) |
| ***Sulu*** | | | | | |
| RSYZ-1 | RSYZ-1-1<br>RSYZ-1-2<br>RSYZ-1-4 | N:37°5'15"<br>E:121°25'10.1" | Diorite | Subhedral granula | Pl(35%), Am(30%), Kfs(10%), Py(5%) |
| RSZT-1 | RSZT-1-1<br>RSZT-1-2<br>RSZT-1-3 | N:37°0′38.8″<br>E:121°47′56″ | Diorite | Subhedral granula | Pl(40%), Am(30%), Kfs(10%), Qtz(5%) |
| RSZT-2 | RSZT-2-1<br>RSZT-2-2<br>RSZT-2-5 | N:37°0′52.3″<br>E:121°52′32.9″ | Diorite | Subhedral granula | Pl(40%), Am(30%), Kfs(10%), Qtz(5%), Py(5%) |
| RSZT-3 | RSZT-3-2<br>RSZT-3-3<br>RSZT-3-4 | N:37°0′52.3″<br>E:121°52′32.9″ | Diorite | Subhedral granula | Pl(45%), Am(30%), Kfs(10%), Py(5%) |
| RCYT-1 | RCYT-1-1<br>RCYT-1-2<br>RCYT-1-3 | N:37°10′41.5″<br>E:122°24′53.4″ | Diorite porphyrite | Porphyritic | Phenocrysts: Am(10%); groundmass:Pl＞Am＞Bt＞Qtz＞Py |

Pl: Plagioclase; Am: Amphibole; Bt: Biotite; Py: Pyrite; Qtz: Quartz; Kfs: K-feldspar

ACCEPTED MANUSCRIPT

**Table 2:** Results of LA–ICP–MS zircon U–Pb dating of intermediate-felsic dikes from the Jiaobei terrane and the Sulu orogenic belt in the Jiaodong Peninsula

| Spot | Th(ppm) | U(ppm) | Th/U | Isotopic ratios | | | | | | Age (Ma) | | | |
|---|---|---|---|---|---|---|---|---|---|---|---|---|---|
| | | | | $^{207}Pb/^{206}Pb$ | 1σ | $^{207}Pb/^{235}U$ | 1σ | $^{206}Pb/^{238}U$ | 1σ | $^{207}Pb/^{235}U$ | 1σ | $^{206}Pb/^{238}U$ | 1σ |
| **LKXDJ-1** | | | | | | | | | | | | | |
| 1 | 486.2 | 874.0 | 0.5563 | 0.1305 | 0.0062 | 0.0201 | 0.0002 | 0.25871 | 0.00025 | 124.6 | 5.6 | 128.2 | 1.6 |
| 2 | 133.6 | 265.8 | 0.5027 | 0.0509 | 0.0032 | 0.1422 | 0.0086 | 0.02034 | 0.00031 | 135.0 | 7.6 | 129.8 | 2.0 |
| 3 | 137.0 | 277.8 | 0.4931 | 0.0521 | 0.0036 | 0.1452 | 0.0097 | 0.01989 | 0.00032 | 137.6 | 8.6 | 126.9 | 2.0 |
| 4 | 246.0 | 365.6 | 0.6730 | 0.0490 | 0.0028 | 0.1354 | 0.0078 | 0.01976 | 0.00031 | 128.9 | 6.9 | 126.1 | 2.0 |
| 5 | 327.4 | 779.1 | 0.4202 | 0.0484 | 0.0077 | 0.1322 | 0.0205 | 0.01980 | 0.00043 | 126.1 | 18.4 | 126.4 | 2.7 |
| 6 | 982.9 | 709.0 | 1.3862 | 0.0495 | 0.0024 | 0.1391 | 0.0067 | 0.02034 | 0.00031 | 132.3 | 6.0 | 129.8 | 2.0 |
| 7 | 494.7 | 698.0 | 0.7088 | 0.0486 | 0.0021 | 0.1375 | 0.0057 | 0.02045 | 0.00026 | 130.8 | 5.1 | 130.5 | 1.6 |
| 8 | 269.4 | 591.7 | 0.4554 | 0.0528 | 0.0026 | 0.1433 | 0.0069 | 0.01963 | 0.00032 | 136.0 | 6.1 | 125.3 | 2.0 |
| 9 | 156.9 | 403.6 | 0.3887 | 0.0501 | 0.0028 | 0.1355 | 0.0071 | 0.01978 | 0.00036 | 129.0 | 6.4 | 126.3 | 2.3 |
| 10 | 206.9 | 297.7 | 0.6950 | 0.0467 | 0.0022 | 0.1305 | 0.0062 | 0.02009 | 0.00025 | 130.8 | 10.5 | 126.3 | 2.3 |
| 11 | 304.2 | 408.6 | 0.7446 | 0.0502 | 0.0027 | 0.1357 | 0.0072 | 0.01965 | 0.00027 | 129.2 | 6.5 | 125.4 | 1.7 |
| 12 | 221.2 | 735.4 | 0.3008 | 0.0472 | 0.0019 | 0.1289 | 0.0049 | 0.01969 | 0.00024 | 123.1 | 4.4 | 125.7 | 1.5 |
| 13 | 142.4 | 231.8 | 0.6141 | 0.0537 | 0.0054 | 0.1465 | 0.0136 | 0.01995 | 0.00036 | 138.8 | 12.0 | 127.3 | 2.3 |
| **LZYD-11** | | | | | | | | | | | | | |
| 1 | 124.2 | 74.9 | 1.6594 | 0.0518 | 0.0078 | 0.1292 | 0.0154 | 0.01898 | 0.00052 | 123.4 | 13.8 | 121.2 | 3.3 |
| 2 | 114.0 | 83.5 | 1.3643 | 0.0521 | 0.0065 | 0.1264 | 0.0138 | 0.01891 | 0.00069 | 120.8 | 12.4 | 120.7 | 4.4 |
| 3 | 64.2 | 56.2 | 1.1415 | 0.0518 | 0.0098 | 0.1189 | 0.0170 | 0.01846 | 0.00073 | 114.1 | 15.5 | 117.9 | 4.6 |
| 4 | 143.2 | 98.7 | 1.4504 | 0.0518 | 0.0066 | 0.1296 | 0.0149 | 0.01858 | 0.00065 | 123.7 | 13.4 | 118.7 | 4.1 |
| 5 | 113.5 | 95.3 | 1.1913 | 0.0497 | 0.0058 | 0.1250 | 0.0121 | 0.01871 | 0.00046 | 119.6 | 10.9 | 119.5 | 2.9 |
| 6 | 62.7 | 58.9 | 1.0647 | 0.0483 | 0.0076 | 0.1178 | 0.0149 | 0.01872 | 0.00056 | 113.0 | 13.5 | 119.5 | 3.5 |
| 7 | 262.0 | 179.5 | 1.4596 | 0.0504 | 0.0045 | 0.1321 | 0.0098 | 0.01871 | 0.00039 | 126.0 | 8.8 | 119.5 | 2.5 |
| 8 | 135.5 | 85.4 | 1.5865 | 0.0559 | 0.0126 | 0.1350 | 0.0187 | 0.01852 | 0.00087 | 128.6 | 16.7 | 118.3 | 5.5 |
| 9 | 129.1 | 112.2 | 1.1506 | 0.0500 | 0.0067 | 0.1289 | 0.0137 | 0.01909 | 0.00052 | 123.1 | 12.3 | 121.9 | 3.3 |
| 10 | 126.9 | 116.6 | 1.0887 | 0.0477 | 0.0050 | 0.1280 | 0.0115 | 0.01908 | 0.00059 | 122.3 | 10.4 | 121.8 | 3.7 |
| 11 | 87.7 | 92.9 | 0.9435 | 0.0496 | 0.0081 | 0.1301 | 0.0183 | 0.01908 | 0.00076 | 124.2 | 16.4 | 121.8 | 4.8 |
| 12 | 126.2 | 113.5 | 1.1119 | 0.0514 | 0.0060 | 0.1322 | 0.0126 | 0.01933 | 0.00055 | 126.1 | 11.3 | 123.4 | 3.5 |
| 13 | 198.9 | 129.4 | 1.5368 | 0.0473 | 0.0043 | 0.1252 | 0.0110 | 0.01930 | 0.00051 | 119.8 | 9.9 | 123.2 | 3.2 |
| 14 | 233.8 | 139.7 | 1.6730 | 0.0507 | 0.0046 | 0.1335 | 0.0117 | 0.01875 | 0.00043 | 127.3 | 10.5 | 119.7 | 2.7 |
| 15 | 116.5 | 118.9 | 0.9793 | 0.0480 | 0.0068 | 0.1246 | 0.0173 | 0.01915 | 0.00047 | 119.2 | 15.6 | 122.3 | 3.0 |
| 16 | 161.2 | 96.0 | 1.6788 | 0.0485 | 0.0087 | 0.1221 | 0.0165 | 0.01879 | 0.00080 | 117.0 | 15.0 | 120.0 | 5.0 |
| 17 | 354.4 | 197.2 | 1.7974 | 0.0473 | 0.0041 | 0.1244 | 0.0116 | 0.01869 | 0.00041 | 119.1 | 10.5 | 119.3 | 2.6 |
| 18 | 173.5 | 185.0 | 0.9382 | 0.0482 | 0.0057 | 0.1218 | 0.0134 | 0.01919 | 0.00050 | 116.7 | 12.1 | 122.5 | 3.1 |
| 19 | 217.8 | 173.3 | 1.2568 | 0.0441 | 0.0038 | 0.1140 | 0.0089 | 0.01890 | 0.00039 | 109.6 | 8.2 | 120.7 | 2.5 |
| **PDDZ-2** | | | | | | | | | | | | | |
| 1 | 302.0 | 391.7 | 0.7710 | 0.0517 | 0.0033 | 0.1347 | 0.0083 | 0.01901 | 0.00042 | 128.3 | 7.5 | 121.4 | 2.6 |
| 2 | 512.6 | 411.9 | 1.2445 | 0.0513 | 0.0031 | 0.1343 | 0.0078 | 0.01907 | 0.00033 | 128.0 | 7.0 | 121.8 | 2.1 |
| 3 | 818.7 | 620.6 | 1.3193 | 0.0498 | 0.0024 | 0.1333 | 0.0065 | 0.01947 | 0.00033 | 127.0 | 5.9 | 124.3 | 2.1 |
| 4 | 510.1 | 365.2 | 1.3967 | 0.0515 | 0.0033 | 0.1345 | 0.0082 | 0.01923 | 0.00031 | 128.1 | 7.4 | 122.8 | 2.0 |
| 5 | 368.8 | 481.3 | 0.7662 | 0.0493 | 0.0030 | 0.1275 | 0.0074 | 0.01892 | 0.00030 | 121.9 | 6.6 | 120.8 | 1.9 |

ACCEPTED MANUSCRIPT

| | | | | | | | | | | | | | |
|---|---|---|---|---|---|---|---|---|---|---|---|---|---|
| 6 | 416.4 | 356.2 | 1.1689 | 0.0510 | 0.0033 | 0.1343 | 0.0078 | 0.01923 | 0.00030 | 127.9 | 7.0 | 122.8 | 1.9 |
| 7 | 506.1 | 487.6 | 1.0378 | 0.0509 | 0.0029 | 0.1348 | 0.0078 | 0.01893 | 0.00032 | 128.4 | 7.0 | 120.9 | 2.0 |
| 8 | 635.2 | 592.1 | 1.0729 | 0.0496 | 0.0028 | 0.1340 | 0.0081 | 0.01920 | 0.00029 | 127.6 | 7.3 | 122.6 | 1.8 |
| 9 | 645.1 | 539.2 | 1.1964 | 0.0500 | 0.0029 | 0.1304 | 0.0074 | 0.01903 | 0.00028 | 124.5 | 6.7 | 121.6 | 1.7 |
| 10 | 518.6 | 590.3 | 0.8785 | 0.0486 | 0.0031 | 0.1264 | 0.0077 | 0.01901 | 0.00040 | 120.9 | 7.0 | 121.4 | 2.5 |
| 11 | 691.1 | 626.4 | 1.1032 | 0.0494 | 0.0023 | 0.1335 | 0.0063 | 0.01965 | 0.00026 | 127.3 | 5.6 | 125.5 | 1.7 |
| 12 | 418.4 | 380.0 | 1.1010 | 0.0477 | 0.0030 | 0.1272 | 0.0077 | 0.01962 | 0.00032 | 121.6 | 7.0 | 125.2 | 2.0 |
| 13 | 269.0 | 349.4 | 0.7701 | 0.0488 | 0.0027 | 0.1277 | 0.0067 | 0.01933 | 0.00070 | 122.0 | 6.1 | 123.4 | 4.4 |
| 14 | 261.5 | 368.1 | 0.7106 | 0.0518 | 0.0032 | 0.1324 | 0.0074 | 0.01892 | 0.00032 | 126.3 | 6.6 | 120.9 | 2.0 |
| 15 | 344.9 | 313.9 | 1.0987 | 0.0485 | 0.0027 | 0.1304 | 0.0077 | 0.01936 | 0.00036 | 124.5 | 6.9 | 123.6 | 2.3 |
| **PDDZ-3** | | | | | | | | | | | | | |
| 1 | 240.7 | 655.0 | 0.3676 | 0.0531 | 0.0047 | 0.1351 | 0.0129 | 0.01927 | 0.00058 | 128.7 | 11.6 | 123.0 | 3.7 |
| 2 | 225.7 | 387.5 | 0.5825 | 0.0509 | 0.0037 | 0.1302 | 0.0095 | 0.01900 | 0.00061 | 124.2 | 8.5 | 121.3 | 3.8 |
| 3 | 232.3 | 578.3 | 0.4017 | 0.0501 | 0.0035 | 0.1277 | 0.0085 | 0.01887 | 0.00042 | 122.0 | 7.6 | 120.5 | 2.7 |
| 4 | 222.9 | 415.1 | 0.5369 | 0.0541 | 0.0039 | 0.1374 | 0.0089 | 0.01950 | 0.00060 | 130.8 | 8.0 | 124.5 | 3.8 |
| 5 | 208.7 | 357.3 | 0.5840 | 0.0548 | 0.0048 | 0.1400 | 0.0121 | 0.01894 | 0.00064 | 133.0 | 10.7 | 121.0 | 4.0 |
| 6 | 203.3 | 797.3 | 0.2550 | 0.0514 | 0.0024 | 0.1331 | 0.0060 | 0.01901 | 0.00038 | 126.9 | 5.3 | 121.4 | 2.4 |
| 7 | 184.3 | 756.6 | 0.2436 | 0.0507 | 0.0036 | 0.1322 | 0.0077 | 0.01936 | 0.00045 | 126.1 | 6.9 | 123.6 | 2.9 |
| 8 | 178.0 | 1033.0 | 0.1723 | 0.0487 | 0.0024 | 0.1277 | 0.0062 | 0.01916 | 0.00041 | 122.0 | 5.6 | 122.3 | 2.6 |
| 9 | 220.5 | 539.1 | 0.4090 | 0.0478 | 0.0028 | 0.1228 | 0.0074 | 0.01881 | 0.00048 | 117.6 | 6.7 | 120.1 | 3.0 |
| 10 | 126.1 | 533.9 | 0.2363 | 0.0529 | 0.0036 | 0.1355 | 0.0090 | 0.01913 | 0.00055 | 129.1 | 8.0 | 122.1 | 3.5 |
| 11 | 175.5 | 960.2 | 0.1827 | 0.0523 | 0.0024 | 0.1368 | 0.0061 | 0.01923 | 0.00044 | 130.2 | 5.4 | 122.8 | 2.8 |
| 12 | 903.0 | 1180.1 | 0.7652 | 0.0503 | 0.0027 | 0.1327 | 0.0066 | 0.01944 | 0.00038 | 126.5 | 5.9 | 124.1 | 2.4 |
| 13 | 267.7 | 596.3 | 0.4489 | 0.0468 | 0.0032 | 0.1203 | 0.0074 | 0.01913 | 0.00046 | 115.3 | 6.7 | 122.1 | 2.9 |
| 14 | 215.8 | 578.6 | 0.3730 | 0.0514 | 0.0030 | 0.1321 | 0.0077 | 0.01914 | 0.00053 | 126.0 | 6.9 | 122.2 | 3.3 |
| 15 | 374.5 | 554.7 | 0.6752 | 0.0478 | 0.0032 | 0.1227 | 0.0073 | 0.01934 | 0.00056 | 117.5 | 6.6 | 123.5 | 3.5 |
| 16 | 299.5 | 689.5 | 0.4344 | 0.0509 | 0.0031 | 0.1318 | 0.0071 | 0.01924 | 0.00044 | 125.7 | 6.3 | 122.8 | 2.8 |
| 17 | 205.5 | 340.1 | 0.6043 | 0.0507 | 0.0037 | 0.1309 | 0.0094 | 0.01950 | 0.00056 | 124.9 | 8.4 | 124.5 | 3.5 |
| **RSZT-3** | | | | | | | | | | | | | |
| 1 | 251.5 | 327.3 | 0.7684 | 0.0525 | 0.0033 | 0.1290 | 0.0079 | 0.01852 | 0.00049 | 123.2 | 7.1 | 118.3 | 3.1 |
| 2 | 455.7 | 464.7 | 0.9807 | 0.0574 | 0.0041 | 0.1368 | 0.0074 | 0.01943 | 0.00059 | 130.2 | 6.6 | 124.0 | 3.7 |
| 3 | 541.5 | 387.1 | 1.3988 | 0.0487 | 0.0039 | 0.1225 | 0.0109 | 0.01887 | 0.00063 | 117.4 | 9.9 | 120.5 | 4.0 |
| 4 | 628.9 | 540.0 | 1.1647 | 0.0530 | 0.0032 | 0.1240 | 0.0074 | 0.01812 | 0.00042 | 118.7 | 6.7 | 115.7 | 2.7 |
| 5 | 322.3 | 260.1 | 1.2392 | 0.0564 | 0.0038 | 0.1326 | 0.0086 | 0.01836 | 0.00049 | 126.5 | 7.7 | 117.3 | 3.1 |
| 6 | 331.1 | 355.9 | 0.9302 | 0.0527 | 0.0037 | 0.1324 | 0.0082 | 0.01889 | 0.00041 | 126.3 | 7.4 | 120.7 | 2.6 |
| 7 | 551.7 | 598.7 | 0.9216 | 0.0490 | 0.0027 | 0.1263 | 0.0070 | 0.01890 | 0.00036 | 120.8 | 6.3 | 120.7 | 2.3 |
| **RCYT-1** | | | | | | | | | | | | | |
| 1 | 262.6 | 206.1 | 1.2739 | 0.0588 | 0.0043 | 0.1356 | 0.0086 | 0.01837 | 0.00054 | 129.1 | 7.7 | 117.4 | 3.4 |
| 2 | 211.2 | 214.4 | 0.9853 | 0.0556 | 0.0036 | 0.1285 | 0.0074 | 0.01755 | 0.00048 | 122.8 | 6.7 | 112.2 | 3.1 |
| 3 | 217.0 | 222.9 | 0.9735 | 0.0576 | 0.0048 | 0.1368 | 0.0107 | 0.01879 | 0.00064 | 130.2 | 9.5 | 120.0 | 4.1 |
| 4 | 261.3 | 245.1 | 1.0660 | 0.0544 | 0.0044 | 0.1278 | 0.0099 | 0.01780 | 0.00059 | 122.2 | 8.9 | 113.7 | 3.7 |
| 5 | 206.6 | 203.1 | 1.0173 | 0.0582 | 0.0046 | 0.1373 | 0.0098 | 0.01833 | 0.00056 | 130.6 | 8.7 | 117.1 | 3.6 |
| 6 | 182.5 | 215.0 | 0.8486 | 0.0560 | 0.0037 | 0.1330 | 0.0083 | 0.01801 | 0.00048 | 126.8 | 7.4 | 115.0 | 3.0 |
| 7 | 359.0 | 414.4 | 0.8661 | 0.0532 | 0.0033 | 0.1236 | 0.0065 | 0.01770 | 0.00038 | 118.3 | 5.9 | 113.1 | 2.4 |

ACCEPTED MANUSCRIPT

| | | | | | | | | | | | | | |
|---|---|---|---|---|---|---|---|---|---|---|---|---|---|
| 8 | 314.5 | 326.7 | 0.9627 | 0.0516 | 0.0039 | 0.1310 | 0.0095 | 0.01881 | 0.00051 | 125.0 | 8.5 | 120.1 | 3.3 |
| 9 | 225.7 | 261.8 | 0.8622 | 0.0555 | 0.0047 | 0.1325 | 0.0114 | 0.01762 | 0.00063 | 126.3 | 10.2 | 112.6 | 4.0 |
| 10 | 239.6 | 282.6 | 0.8479 | 0.0624 | 0.0087 | 0.1348 | 0.0096 | 0.01842 | 0.00077 | 128.4 | 8.6 | 117.7 | 4.9 |
| 11 | 283.8 | 288.0 | 0.9853 | 0.0565 | 0.0047 | 0.1367 | 0.0105 | 0.01886 | 0.00065 | 130.1 | 9.4 | 120.4 | 4.1 |
| 12 | 993.1 | 666.6 | 1.4899 | 0.0494 | 0.0023 | 0.1174 | 0.0055 | 0.01770 | 0.00039 | 112.7 | 5.0 | 113.1 | 2.4 |
| 13 | 281.5 | 298.2 | 0.9440 | 0.0497 | 0.0041 | 0.1295 | 0.0118 | 0.01892 | 0.00081 | 123.7 | 10.6 | 120.8 | 5.1 |
| 14 | 371.5 | 395.7 | 0.9390 | 0.0496 | 0.0044 | 0.1138 | 0.0098 | 0.01888 | 0.00072 | 109.5 | 9.0 | 120.6 | 4.5 |
| 15 | 368.9 | 317.6 | 1.1616 | 0.0574 | 0.0042 | 0.1366 | 0.0089 | 0.01889 | 0.00062 | 130.0 | 8.0 | 120.6 | 3.9 |

ACCEPTED MANUSCRIPT

ACCEPTED MANUSCRIPT

**Table 3**: Zircon Hf isotopic compositions of intermediate-felsic dikes from the Jiaobei terrane and the Sulu orogenic belt in the Jiaodong Peninsula

| Spot | Age(Ma) | $^{176}Yb/^{177}Hf$ | $^{176}Lu/^{177}Hf$ | $^{176}Hf/^{177}Hf$ | 2σ | $\varepsilon_{Hf}(0)$ | $\varepsilon_{Hf}(t)$ | 2σ | $t_{DM1}$(Ma) | $t_{DM2}$(Ma) | $f_{Lu/Hf}$ |
|---|---|---|---|---|---|---|---|---|---|---|---|
| **LKXDJ** | | | | | | | | | | | |
| 1 | 128 | 0.041984 | 0.000784 | 0.282298 | 0.000014 | -16.8 | -14.0 | 0.5 | 1338 | 2074 | -0.98 |
| 2 | 130 | 0.079699 | 0.001503 | 0.282295 | 0.000015 | -16.9 | -14.2 | 0.5 | 1369 | 2084 | -0.95 |
| 3 | 127 | 0.036770 | 0.000737 | 0.282316 | 0.000015 | -16.1 | -13.4 | 0.5 | 1312 | 2035 | -0.98 |
| 4 | 126 | 0.047997 | 0.000979 | 0.282308 | 0.000013 | -16.4 | -13.7 | 0.5 | 1332 | 2054 | -0.97 |
| 5 | 126 | 0.067793 | 0.001234 | 0.282255 | 0.000015 | -18.3 | -15.6 | 0.5 | 1415 | 2173 | -0.96 |
| 6 | 130 | 0.077502 | 0.001330 | 0.282426 | 0.000019 | -12.2 | -9.5 | 0.7 | 1177 | 1789 | -0.96 |
| 7 | 131 | 0.069195 | 0.001252 | 0.282420 | 0.000012 | -12.5 | -9.7 | 0.4 | 1184 | 1803 | -0.96 |
| 8 | 125 | 0.053235 | 0.000963 | 0.282332 | 0.000014 | -15.6 | -12.9 | 0.5 | 1298 | 2002 | -0.97 |
| 9 | 126 | 0.036204 | 0.000737 | 0.282339 | 0.000013 | -15.3 | -12.6 | 0.5 | 1280 | 1983 | -0.98 |
| 10 | 126 | 0.049402 | 0.000910 | 0.282333 | 0.000013 | -15.5 | -12.8 | 0.5 | 1295 | 1999 | -0.97 |
| 11 | 125 | 0.051796 | 0.000896 | 0.282267 | 0.000015 | -17.9 | -15.2 | 0.5 | 1386 | 2145 | -0.97 |
| 12 | 126 | 0.042914 | 0.000862 | 0.282317 | 0.000011 | -16.1 | -13.4 | 0.4 | 1315 | 2034 | -0.97 |
| 13 | 127 | 0.035668 | 0.000619 | 0.282337 | 0.000014 | -15.4 | -12.6 | 0.5 | 1279 | 1987 | -0.98 |
| **LZYD-11** | | | | | | | | | | | |
| 1 | 121 | 0.064670 | 0.000992 | 0.282211 | 0.000014 | -19.8 | -17.3 | 0.5 | 1467 | 2273 | -0.97 |
| 2 | 121 | 0.051003 | 0.000826 | 0.282181 | 0.000013 | -20.9 | -18.3 | 0.5 | 1503 | 2340 | -0.98 |
| 3 | 118 | 0.110086 | 0.001715 | 0.282310 | 0.000016 | -16.3 | -13.9 | 0.6 | 1356 | 2058 | -0.95 |
| 4 | 119 | 0.080562 | 0.001280 | 0.282201 | 0.000015 | -20.2 | -17.7 | 0.5 | 1493 | 2299 | -0.96 |
| 5 | 120 | 0.090578 | 0.001419 | 0.282281 | 0.000015 | -17.4 | -14.8 | 0.5 | 1385 | 2119 | -0.96 |
| 6 | 120 | 0.051215 | 0.000820 | 0.282137 | 0.000013 | -22.4 | -19.9 | 0.5 | 1563 | 2437 | -0.98 |
| 7 | 120 | 0.092017 | 0.001508 | 0.282202 | 0.000017 | -20.2 | -17.7 | 0.6 | 1500 | 2297 | -0.95 |
| 8 | 118 | 0.083679 | 0.001320 | 0.282332 | 0.000016 | -15.6 | -13.1 | 0.6 | 1310 | 2006 | -0.96 |
| 9 | 122 | 0.084866 | 0.001347 | 0.282251 | 0.000016 | -18.4 | -15.9 | 0.6 | 1426 | 2186 | -0.96 |
| 10 | 122 | 0.076577 | 0.001263 | 0.282190 | 0.000016 | -20.6 | -18.0 | 0.6 | 1507 | 2321 | -0.96 |
| 11 | 122 | 0.070820 | 0.001171 | 0.282213 | 0.000015 | -19.8 | -17.2 | 0.5 | 1472 | 2270 | -0.96 |
| 12 | 123 | 0.091713 | 0.001430 | 0.282163 | 0.000014 | -21.5 | -19.0 | 0.5 | 1553 | 2381 | -0.96 |
| 13 | 123 | 0.091489 | 0.001491 | 0.282206 | 0.000014 | -20.0 | -17.4 | 0.5 | 1494 | 2286 | -0.96 |
| 14 | 120 | 0.088353 | 0.001352 | 0.282229 | 0.000015 | -19.2 | -16.7 | 0.5 | 1456 | 2236 | -0.96 |
| 15 | 122 | 0.072072 | 0.001123 | 0.282197 | 0.000013 | -20.3 | -17.8 | 0.5 | 1492 | 2305 | -0.97 |
| 16 | 120 | 0.053069 | 0.000868 | 0.282185 | 0.000018 | -20.7 | -18.2 | 0.6 | 1498 | 2331 | -0.97 |
| 17 | 119 | 0.109540 | 0.001721 | 0.282349 | 0.000015 | -15.0 | -12.5 | 0.5 | 1300 | 1970 | -0.95 |
| 18 | 123 | 0.059430 | 0.000968 | 0.282168 | 0.000016 | -21.3 | -18.7 | 0.6 | 1526 | 2367 | -0.97 |
| 19 | 121 | 0.107149 | 0.001747 | 0.282185 | 0.000017 | -20.8 | -18.3 | 0.6 | 1535 | 2336 | -0.95 |
| **PDDZ-2** | | | | | | | | | | | |
| 1 | 121 | 0.099420 | 0.001650 | 0.282236 | 0.000014 | -19.0 | -16.4 | 0.5 | 1458 | 2220 | -0.95 |
| 2 | 122 | 0.081309 | 0.001304 | 0.282240 | 0.000016 | -18.8 | -16.3 | 0.6 | 1439 | 2211 | -0.96 |
| 3 | 124 | 0.123623 | 0.001986 | 0.282186 | 0.000014 | -20.7 | -18.2 | 0.5 | 1543 | 2332 | -0.94 |
| 4 | 123 | 0.089418 | 0.001459 | 0.282213 | 0.000015 | -19.8 | -17.2 | 0.5 | 1482 | 2269 | -0.96 |
| 5 | 121 | 0.121890 | 0.001933 | 0.282193 | 0.000014 | -20.5 | -18.0 | 0.5 | 1531 | 2318 | -0.94 |
| 6 | 123 | 0.118110 | 0.001848 | 0.282319 | 0.000014 | -16.0 | -13.5 | 0.5 | 1347 | 2034 | -0.94 |

ACCEPTED MANUSCRIPT

| | | | | | | | | | | | |
|---|---|---|---|---|---|---|---|---|---|---|---|
| 7 | 121 | 0.101861 | 0.001633 | 0.282252 | 0.000014 | -18.4 | -15.9 | 0.5 | 1434 | 2184 | -0.95 |
| 8 | 123 | 0.123976 | 0.001996 | 0.282256 | 0.000015 | -18.3 | -15.7 | 0.5 | 1443 | 2177 | -0.94 |
| 9 | 122 | 0.142293 | 0.002031 | 0.282392 | 0.000013 | -13.5 | -11.0 | 0.5 | 1250 | 1875 | -0.94 |
| 10 | 121 | 0.117875 | 0.001825 | 0.282195 | 0.000016 | -20.4 | -17.9 | 0.6 | 1523 | 2312 | -0.95 |
| 11 | 125 | 0.126995 | 0.001915 | 0.282218 | 0.000016 | -19.6 | -17.0 | 0.6 | 1494 | 2259 | -0.94 |
| 12 | 125 | 0.109186 | 0.001673 | 0.282146 | 0.000015 | -22.1 | -19.5 | 0.5 | 1586 | 2418 | -0.95 |
| 13 | 123 | 0.117775 | 0.001836 | 0.282157 | 0.000017 | -21.7 | -19.2 | 0.6 | 1578 | 2396 | -0.94 |
| 14 | 121 | 0.127276 | 0.001978 | 0.282277 | 0.000017 | -17.5 | -15.0 | 0.6 | 1412 | 2130 | -0.94 |
| 15 | 124 | 0.148544 | 0.002181 | 0.282490 | 0.000018 | -10.0 | -7.4 | 0.6 | 1112 | 1653 | -0.93 |
| **PDDZ-3** | | | | | | | | | | | |
| 1 | 123 | 0.052176 | 0.000928 | 0.282050 | 0.000011 | -25.5 | -22.9 | 0.4 | 1688 | 2629 | -0.97 |
| 2 | 121 | 0.068880 | 0.001210 | 0.282047 | 0.000012 | -25.6 | -23.1 | 0.4 | 1704 | 2637 | -0.96 |
| 3 | 120 | 0.063828 | 0.001092 | 0.282037 | 0.000010 | -26.0 | -23.4 | 0.3 | 1714 | 2661 | -0.97 |
| 4 | 125 | 0.096494 | 0.001507 | 0.282081 | 0.000010 | -24.4 | -21.8 | 0.3 | 1670 | 2562 | -0.95 |
| 5 | 121 | 0.065263 | 0.001025 | 0.282038 | 0.000011 | -26.0 | -23.4 | 0.4 | 1709 | 2658 | -0.97 |
| 6 | 121 | 0.065606 | 0.001032 | 0.282015 | 0.000009 | -26.8 | -24.2 | 0.3 | 1742 | 2710 | -0.97 |
| 7 | 124 | 0.064489 | 0.001013 | 0.281983 | 0.000011 | -27.9 | -25.3 | 0.4 | 1784 | 2777 | -0.97 |
| 8 | 122 | 0.075852 | 0.001265 | 0.281867 | 0.000012 | -32.0 | -29.4 | 0.4 | 1959 | 3036 | -0.96 |
| 9 | 120 | 0.063061 | 0.001017 | 0.281922 | 0.000013 | -30.1 | -27.5 | 0.4 | 1870 | 2916 | -0.97 |
| 10 | 122 | 0.072175 | 0.001195 | 0.281943 | 0.000011 | -29.3 | -26.8 | 0.4 | 1850 | 2869 | -0.96 |
| 11 | 123 | 0.051089 | 0.000873 | 0.281987 | 0.000011 | -27.8 | -25.1 | 0.4 | 1773 | 2769 | -0.97 |
| 12 | 124 | 0.101312 | 0.001529 | 0.282037 | 0.000011 | -26.0 | -23.4 | 0.4 | 1734 | 2660 | -0.95 |
| 13 | 122 | 0.081814 | 0.001331 | 0.281963 | 0.000011 | -28.6 | -26.0 | 0.4 | 1828 | 2824 | -0.96 |
| 14 | 122 | 0.049205 | 0.000759 | 0.282068 | 0.000010 | -24.9 | -22.3 | 0.3 | 1656 | 2589 | -0.98 |
| 15 | 124 | 0.058359 | 0.000936 | 0.282063 | 0.000010 | -25.1 | -22.5 | 0.3 | 1671 | 2602 | -0.97 |
| 16 | 123 | 0.082666 | 0.001311 | 0.282070 | 0.000009 | -24.8 | -22.3 | 0.3 | 1678 | 2588 | -0.96 |
| 17 | 124 | 0.067330 | 0.001112 | 0.282058 | 0.000010 | -25.3 | -22.6 | 0.3 | 1686 | 2613 | -0.97 |
| **RCYT-1** | | | | | | | | | | | |
| 1 | 117 | 0.061939 | 0.000915 | 0.282417 | 0.000011 | -12.5 | -10.0 | 0.4 | 1177 | 1814 | -0.97 |
| 2 | 112 | 0.056345 | 0.000868 | 0.282313 | 0.000011 | -16.2 | -13.8 | 0.4 | 1320 | 2050 | -0.97 |
| 3 | 120 | 0.060013 | 0.000967 | 0.282355 | 0.000011 | -14.7 | -12.2 | 0.4 | 1265 | 1952 | -0.97 |
| 4 | 114 | 0.053239 | 0.000834 | 0.282341 | 0.000010 | -15.2 | -12.8 | 0.4 | 1280 | 1986 | -0.97 |
| 5 | 117 | 0.053076 | 0.000848 | 0.282398 | 0.000010 | -13.2 | -10.7 | 0.4 | 1202 | 1858 | -0.97 |
| 6 | 115 | 0.043436 | 0.000686 | 0.282361 | 0.000011 | -14.5 | -12.1 | 0.4 | 1248 | 1940 | -0.98 |
| 7 | 113 | 0.062543 | 0.000982 | 0.282344 | 0.000012 | -15.1 | -12.7 | 0.4 | 1282 | 1982 | -0.97 |
| 8 | 120 | 0.059534 | 0.000954 | 0.282321 | 0.000011 | -15.9 | -13.4 | 0.4 | 1312 | 2028 | -0.97 |
| 9 | 113 | 0.056785 | 0.000904 | 0.282285 | 0.000014 | -17.2 | -14.8 | 0.5 | 1362 | 2114 | -0.97 |
| 10 | 118 | 0.052728 | 0.000909 | 0.282254 | 0.000013 | -18.3 | -15.8 | 0.5 | 1405 | 2180 | -0.97 |
| 11 | 120 | 0.081813 | 0.001266 | 0.282400 | 0.000013 | -13.1 | -10.6 | 0.5 | 1212 | 1852 | -0.96 |
| 12 | 121 | 0.065920 | 0.001018 | 0.282348 | 0.000013 | -15.0 | -12.4 | 0.5 | 1277 | 1968 | -0.97 |
| 13 | 121 | 0.055400 | 0.000853 | 0.282341 | 0.000011 | -15.3 | -12.7 | 0.4 | 1282 | 1984 | -0.97 |
| 14 | 121 | 0.076694 | 0.001172 | 0.282424 | 0.000014 | -12.3 | -9.8 | 0.5 | 1176 | 1799 | -0.96 |

ACCEPTED MANUSCRIPT

| | | | | | | | | | | | |
|---|---|---|---|---|---|---|---|---|---|---|---|
| **RSZT-3** | | | | | | | | | | | |
| 1 | 124 | 0.088577 | 0.001477 | 0.282202 | 0.000011 | -20.2 | -17.6 | 0.4 | 1499 | 2293 | -0.96 |
| 2 | 121 | 0.127532 | 0.002082 | 0.282297 | 0.000017 | -16.8 | -14.3 | 0.6 | 1388 | 2087 | -0.94 |
| 3 | 116 | 0.029790 | 0.000516 | 0.282246 | 0.000015 | -18.6 | -16.1 | 0.5 | 1401 | 2196 | -0.98 |
| 4 | 121 | 0.132400 | 0.002125 | 0.281900 | 0.000014 | -30.8 | -28.4 | 0.5 | 1957 | 2968 | -0.94 |

$\varepsilon_{Hf}(t)=10{,}000\{[(^{176}Hf/^{177}Hf)_S-(^{176}Lu/^{177}Hf)_S\times(e^{\lambda t}-1)]/[(^{176}Hf/^{177}Hf)_{CHUR,0}-(^{176}Lu/^{177}Hf)_{CHUR}\times(e^{\lambda t}-1)]-1\}$

$T_{DM1}=1/\lambda\times\ln\{1+(^{176}Hf/^{177}Hf)_S-(^{176}Hf/^{177}Hf)_{DM}]/[(^{176}Lu/^{177}Hf)_S-(^{176}Lu/^{177}Hf)_{DM}]\}.$

$T_{DM2}=1/\lambda\times\ln\{1+[(^{176}Hf/^{177}Hf)_{S,t}-(^{176}Hf/^{177}Hf)_{DM,t}]/[(^{176}Lu/^{177}Hf)_C-(^{176}Lu/^{177}Hf)_{DM}]\}+t.$

ACCEPTED MANUSCRIPT

ACCEPTED MANUSCRIPT

**Table 4:** Whole-rock major (wt.%) and trace element (ppm) compositions of intermediate-felsic dikes from the Jiaobei terrane and the Sulu orogenic belt in the Jiaodong Peninsula

| Site | Jiaobei terane | | | | | | | | | | | | |
|---|---|---|---|---|---|---|---|---|---|---|---|---|---|
| Sample | LKXDJ-1-1 | LKXDJ-1-2 | LZYD-1-11 | LZYD-1-12 | PDDZ-2-1 | PDDZ-2-2 | PDDZ-1-1 | PDDZ-1-2 | PDDZ-3-1 | PDDZ-3-2 | PDDZ-3-3 | RSYZ-1-1 | RSYZ-1-2 |
| Rock type | Quartz diorite | Quartz-diorite | Quartz-diorite | Quartz-diorite | Quartz-diorite | Quartz-diorite | Diorite | Diorite | Diorite | Diorite | Diorite | Diorite | Diorite |
| *wt.%* | | | | | | | | | | | | | |
| $SiO_2$ | 67.50 | 67.22 | 66.26 | 66.45 | 66.63 | 67.15 | 54.00 | 54.24 | 56.43 | 56.29 | 55.68 | 51.75 | 51.69 |
| $TiO_2$ | 0.34 | 0.35 | 0.37 | 0.39 | 0.33 | 0.33 | 0.85 | 0.84 | 0.78 | 0.78 | 0.79 | 0.96 | 0.99 |
| $Al_2O_3$ | 15.18 | 15.27 | 16.49 | 16.21 | 16.29 | 15.67 | 13.92 | 13.87 | 14.27 | 14.25 | 14.86 | 13.54 | 13.20 |
| $TFe_2O_3$ | 2.69 | 2.73 | 2.87 | 3.16 | 3.09 | 2.94 | 7.04 | 6.89 | 6.46 | 6.43 | 6.49 | 7.10 | 6.94 |
| FeO | 2.02 | 1.94 | 1.66 | 1.96 | 1.96 | 1.92 | 5.42 | 5.05 | 4.98 | 4.51 | 4.89 | 5.94 | 5.18 |
| $Fe_2O_3$ | 0.74 | 0.88 | 1.34 | 1.34 | 1.26 | 1.13 | 1.80 | 2.05 | 1.64 | 2.13 | 1.78 | 1.29 | 1.96 |
| MnO | 0.05 | 0.05 | 0.05 | 0.05 | 0.062 | 0.059 | 0.123 | 0.114 | 0.11 | 0.11 | 0.11 | 0.123 | 0.122 |
| MgO | 2.28 | 2.34 | 1.92 | 2.04 | 1.76 | 1.81 | 9.71 | 9.71 | 6.86 | 6.97 | 6.77 | 10.18 | 9.92 |
| CaO | 3.25 | 3.25 | 3.19 | 2.93 | 2.78 | 2.95 | 7.81 | 7.85 | 6.36 | 6.34 | 6.39 | 7.66 | 7.91 |
| $Na_2O$ | 3.94 | 3.91 | 4.20 | 4.29 | 3.88 | 3.68 | 2.58 | 2.63 | 2.87 | 2.87 | 2.90 | 2.50 | 2.63 |
| $K_2O$ | 3.58 | 3.66 | 3.18 | 3.00 | 4.05 | 4.20 | 2.57 | 2.39 | 4.14 | 4.08 | 4.30 | 2.53 | 2.43 |
| $P_2O_5$ | 0.20 | 0.20 | 0.18 | 0.17 | 0.19 | 0.19 | 0.42 | 0.38 | 0.75 | 0.72 | 0.75 | 0.71 | 0.68 |
| LOI | 0.66 | 0.69 | 0.95 | 0.98 | 0.59 | 0.72 | 0.57 | 0.65 | 0.60 | 0.78 | 0.58 | 2.67 | 3.08 |
| Total | 99.76 | 99.75 | 99.79 | 99.80 | 99.78 | 99.82 | 99.78 | 99.77 | 99.80 | 99.83 | 99.81 | 99.85 | 99.79 |
| Mg# | 60 | 60 | 54 | 53 | 50 | 52 | 71 | 72 | 65 | 66 | 65 | 72 | 72 |
| *ppm* | | | | | | | | | | | | | |
| La | 68.4 | 65.4 | 34.6 | 35.6 | 65.9 | 65.3 | 71.1 | 72.6 | 54.6 | 57.1 | 54.7 | 49.0 | 54.0 |
| Ce | 137 | 129 | 67 | 68 | 131 | 127 | 155 | 160 | 125 | 132 | 132 | 119 | 128 |
| Pr | 14.9 | 14.4 | 7.80 | 7.60 | 13.7 | 13.3 | 17.9 | 17.9 | 15.2 | 16.1 | 16.0 | 14.5 | 14.8 |
| Nd | 52.6 | 51.2 | 29.2 | 26.8 | 45.1 | 43.2 | 65.9 | 65.7 | 58.7 | 61.0 | 61.4 | 56.2 | 56.6 |
| Sm | 7.62 | 7.42 | 5.10 | 4.20 | 5.78 | 5.49 | 9.61 | 9.79 | 9.77 | 10.09 | 9.90 | 8.99 | 8.91 |
| Eu | 1.84 | 1.83 | 1.26 | 1.08 | 1.48 | 1.42 | 2.44 | 2.48 | 2.63 | 2.76 | 2.75 | 2.47 | 2.41 |
| Gd | 5.27 | 5.06 | 3.91 | 3.16 | 4.23 | 3.95 | 6.93 | 7.08 | 7.45 | 7.79 | 7.99 | 6.88 | 6.77 |



ACCEPTED MANUSCRIPT

ACCEPTED MANUSCRIPT

| | | | | | | | | | | | | | |
|---|---|---|---|---|---|---|---|---|---|---|---|---|---|
| Tb | 0.57 | 0.56 | 0.52 | 0.39 | 0.48 | 0.47 | 0.84 | 0.85 | 0.96 | 1.01 | 1.03 | 0.92 | 0.90 |
| Dy | 2.27 | 2.20 | 2.39 | 1.78 | 2.19 | 2.04 | 3.96 | 3.96 | 4.62 | 4.56 | 4.81 | 4.38 | 4.37 |
| Ho | 0.35 | 0.35 | 0.39 | 0.30 | 0.39 | 0.37 | 0.68 | 0.72 | 0.78 | 0.77 | 0.81 | 0.75 | 0.76 |
| Er | 0.96 | 0.95 | 1.06 | 0.79 | 1.16 | 1.10 | 1.97 | 1.97 | 2.15 | 2.08 | 2.23 | 2.06 | 2.07 |
| Tm | 0.11 | 0.12 | 0.13 | 0.11 | 0.16 | 0.16 | 0.26 | 0.27 | 0.29 | 0.28 | 0.30 | 0.27 | 0.27 |
| Yb | 0.75 | 0.75 | 0.85 | 0.65 | 1.10 | 1.06 | 1.70 | 1.69 | 1.78 | 1.72 | 1.85 | 1.66 | 1.70 |
| Lu | 0.12 | 0.12 | 0.13 | 0.11 | 0.18 | 0.17 | 0.28 | 0.28 | 0.29 | 0.29 | 0.29 | 0.25 | 0.28 |
| Be | 2.05 | 2.44 | 3.03 | 1.67 | 1.67 | 1.65 | 1.26 | 1.41 | 1.99 | 1.96 | 2.22 | 1.62 | 1.40 |
| Sc | 6.55 | 6.86 | 10.54 | 5.80 | 6.61 | 5.92 | 23.58 | 25.22 | 18.88 | 19.25 | 19.22 | 20.91 | 22.98 |
| V | 51.8 | 48.8 | 35.9 | 44.1 | 48.3 | 42.1 | 172.4 | 166.3 | 132.3 | 132.9 | 136.6 | 171.7 | 161.2 |
| Cr | 76.6 | 75.6 | 30.4 | 35.8 | 26.3 | 27.9 | 497.4 | 505.8 | 297.0 | 297.2 | 283.8 | 379.4 | 386.4 |
| Co | 8.91 | 9.20 | 12.74 | 7.33 | 9.07 | 7.10 | 35.60 | 40.05 | 27.65 | 27.97 | 27.99 | 35.49 | 34.02 |
| Ni | 43.5 | 45.5 | 11.3 | 6.0 | 9.1 | 8.8 | 151.3 | 164.4 | 112.9 | 113.6 | 108.8 | 145.4 | 154.2 |
| Zn | 64.1 | 66.6 | 113.1 | 60.8 | 53.9 | 35.9 | 85.1 | 88.2 | 84.7 | 77.3 | 82.6 | 87.1 | 90.3 |
| Ga | 21.9 | 23.6 | 43.0 | 23.1 | 20.9 | 19.0 | 17.7 | 18.7 | 17.9 | 17.4 | 18.2 | 17.3 | 17.8 |
| Rb | 87.9 | 88.0 | 75.7 | 78.2 | 81.6 | 90.5 | 81.0 | 79.8 | 121.0 | 124.3 | 126.8 | 65.2 | 64.4 |
| Sr | 1282 | 1238 | 891 | 840 | 918 | 921 | 1122 | 1115 | 1039 | 1042 | 1068 | 1037 | 961 |
| Y | 10.6 | 10.5 | 11.1 | 8.6 | 11.9 | 11.1 | 19.4 | 19.9 | 23.5 | 23.2 | 24.3 | 21.1 | 21.1 |
| Zr | 171 | 170 | 149 | 140 | 163 | 167 | 172 | 170 | 224 | 221 | 227 | 230 | 224 |
| Nb | 6.58 | 7.20 | 14.28 | 6.78 | 7.22 | 7.25 | 6.41 | 6.60 | 12.66 | 12.60 | 12.99 | 15.50 | 13.83 |
| Mo | 0.26 | 0.24 | 1.22 | 0.68 | 0.19 | 0.28 | 0.26 | 0.45 | 0.38 | 0.49 | 0.35 | 0.17 | 0.15 |
| Ba | 1993 | 1914 | 1733 | 1561 | 2816 | 2758 | 2173 | 2108 | 2446 | 2387 | 2470 | 2401 | 2269 |
| Hf | 6.44 | 6.45 | 5.02 | 4.63 | 4.87 | 5.06 | 4.60 | 4.57 | 5.69 | 5.65 | 5.60 | 5.96 | 5.39 |
| Ta | 0.37 | 0.39 | 1.03 | 0.45 | 0.51 | 0.50 | 0.36 | 0.37 | 0.73 | 0.76 | 0.74 | 0.72 | 0.73 |
| Pb | 31.3 | 33.6 | 24.9 | 12.8 | 24.2 | 22.2 | 8.67 | 8.56 | 13.55 | 13.5 | 16.1 | 39.3 | 21.3 |
| Th | 12.6 | 13.5 | 12.9 | 7.1 | 17.1 | 16.3 | 11.86 | 12.51 | 10.00 | 9.72 | 9.98 | 6.72 | 7.55 |
| U | 2.33 | 2.33 | 1.98 | 0.92 | 2.76 | 2.61 | 1.89 | 2.02 | 4.38 | 2.02 | 3.69 | 1.00 | 1.00 |
| Sr/Y | 120.7 | 118.0 | 80.5 | 97.7 | 77.5 | 83.2 | 57.8 | 55.9 | 44.2 | 44.9 | 44.0 | 49.1 | 45.4 |

ACCEPTED MANUSCRIPT

ACCEPTED MANUSCRIPT

*Continued*

| site | Sulu orogenic belt | | | | | | | | | | | | |
|---|---|---|---|---|---|---|---|---|---|---|---|---|---|
| Sample | RSYZ-1-4 | RSZT-1-1 | RSZT-1-2 | RSZT-1-3 | RSZT-2-1 | RSZT-2-2 | RSZT-2-5 | RSZT-3-2 | RSZT-3-3 | RSZT-3-4 | RCYT-1-1 | RCYT-1-2 | RCYT-1-3 |
| Rock type | Diorite | Diorite | Diorite | Diorite | Diorite | Diorite | Diorite | Diorite | Diorite | Diorite | Diorite | Diorite | Diorite |
| *wt.%* | | | | | | | | | | | | | |
| $SiO_2$ | 51.76 | 57.31 | 57.94 | 57.54 | 57.16 | 57.28 | 57.10 | 55.40 | 55.45 | 55.23 | 57.85 | 58.15 | 58.37 |
| $TiO_2$ | 0.99 | 0.85 | 0.86 | 0.82 | 0.84 | 0.83 | 0.85 | 0.88 | 0.89 | 0.88 | 0.79 | 0.78 | 0.79 |
| $Al_2O_3$ | 13.46 | 16.13 | 15.99 | 16.39 | 15.05 | 15.09 | 14.78 | 14.90 | 14.93 | 14.68 | 14.27 | 14.35 | 14.22 |
| $TFe_2O_3$ | 7.22 | 4.50 | 4.49 | 4.29 | 6.12 | 6.10 | 6.18 | 6.47 | 6.36 | 6.58 | 6.62 | 6.45 | 6.66 |
| FeO | 5.64 | 3.35 | 3.27 | 3.18 | 3.80 | 4.11 | 3.90 | 4.14 | 4.01 | 4.06 | 4.13 | 4.19 | 4.07 |
| $Fe_2O_3$ | 1.75 | 1.28 | 1.35 | 1.23 | 2.58 | 2.21 | 2.53 | 2.59 | 2.61 | 2.80 | 2.77 | 2.51 | 2.87 |
| MnO | 0.122 | 0.09 | 0.09 | 0.09 | 0.13 | 0.12 | 0.12 | 0.11 | 0.12 | 0.11 | 0.16 | 0.15 | 0.14 |
| MgO | 9.67 | 5.49 | 5.40 | 4.91 | 6.29 | 6.13 | 6.47 | 6.96 | 7.00 | 7.12 | 6.00 | 5.64 | 5.67 |
| CaO | 7.80 | 6.57 | 6.46 | 6.44 | 6.34 | 6.26 | 6.39 | 6.90 | 6.90 | 6.94 | 6.66 | 6.54 | 6.61 |
| $Na_2O$ | 2.58 | 3.99 | 3.96 | 4.28 | 3.58 | 3.63 | 3.49 | 3.73 | 3.71 | 3.57 | 3.14 | 3.15 | 3.20 |
| $K_2O$ | 2.54 | 2.88 | 2.90 | 2.93 | 2.82 | 2.78 | 2.79 | 2.62 | 2.54 | 2.82 | 2.74 | 2.84 | 2.75 |
| $P_2O_5$ | 0.68 | 0.58 | 0.60 | 0.58 | 0.57 | 0.56 | 0.57 | 0.69 | 0.70 | 0.71 | 0.35 | 0.33 | 0.33 |
| LOI | 2.75 | 1.32 | 1.01 | 1.36 | 0.67 | 0.86 | 0.85 | 0.88 | 0.94 | 0.91 | 0.94 | 1.13 | 0.77 |
| TOTAL | 99.76 | 99.83 | 99.83 | 99.76 | 99.80 | 99.84 | 99.84 | 99.81 | 99.80 | 99.83 | 99.79 | 99.76 | 99.80 |
| Mg# | 70 | 69 | 68 | 67 | 65 | 64 | 65 | 66 | 66 | 66 | 62 | 61 | 60 |
| *ppm* | | | | | | | | | | | | | |
| La | 53.3 | 45.9 | 41.8 | 42.9 | 52.8 | 53.6 | 55.1 | 61.3 | 53.5 | 51.7 | 42.0 | 42.5 | 39.3 |
| Ce | 130.8 | 96.6 | 90.3 | 92.1 | 113.2 | 119.6 | 120.1 | 129.1 | 116.7 | 112.7 | 88.0 | 93.9 | 85.3 |
| Pr | 15.6 | 11.4 | 10.9 | 11.0 | 13.3 | 13.9 | 14.3 | 14.8 | 13.4 | 13.3 | 10.3 | 10.9 | 10.0 |
| Nd | 59.5 | 42.2 | 41.1 | 41.3 | 49.6 | 52.7 | 53.6 | 54.2 | 49.3 | 49.7 | 38.5 | 41.1 | 37.6 |
| Sm | 9.56 | 6.41 | 6.35 | 6.31 | 8.02 | 8.22 | 8.59 | 8.27 | 7.80 | 7.93 | 6.57 | 6.87 | 6.53 |
| Eu | 2.65 | 2.06 | 1.97 | 2.02 | 2.27 | 2.32 | 2.39 | 2.36 | 2.21 | 2.25 | 1.88 | 1.90 | 1.78 |
| Gd | 7.35 | 4.89 | 4.75 | 4.88 | 6.23 | 6.39 | 6.56 | 6.69 | 6.31 | 6.29 | 5.35 | 5.62 | 5.12 |



ACCEPTED MANUSCRIPT

ACCEPTED MANUSCRIPT

| | | | | | | | | | | | | | |
|---|---|---|---|---|---|---|---|---|---|---|---|---|---|
| Tb | 0.98 | 0.59 | 0.59 | 0.60 | 0.79 | 0.82 | 0.85 | 0.87 | 0.82 | 0.85 | 0.72 | 0.75 | 0.71 |
| Dy | 4.66 | 2.66 | 2.68 | 2.64 | 3.82 | 3.81 | 4.02 | 4.26 | 4.09 | 4.07 | 3.58 | 3.79 | 3.63 |
| Ho | 0.81 | 0.43 | 0.42 | 0.42 | 0.67 | 0.67 | 0.70 | 0.75 | 0.72 | 0.72 | 0.65 | 0.69 | 0.65 |
| Er | 2.18 | 1.14 | 1.14 | 1.10 | 1.82 | 1.94 | 1.92 | 2.12 | 2.01 | 2.04 | 1.88 | 1.98 | 1.85 |
| Tm | 0.29 | 0.13 | 0.15 | 0.14 | 0.26 | 0.26 | 0.27 | 0.30 | 0.29 | 0.29 | 0.27 | 0.28 | 0.27 |
| Yb | 1.74 | 0.83 | 0.82 | 0.80 | 1.66 | 1.74 | 1.77 | 1.88 | 1.81 | 1.78 | 1.81 | 1.87 | 1.80 |
| Lu | 0.28 | 0.12 | 0.11 | 0.10 | 0.28 | 0.29 | 0.29 | 0.30 | 0.29 | 0.29 | 0.30 | 0.31 | 0.30 |
| Be | 1.56 | 1.32 | 1.22 | 1.26 | 1.76 | 1.55 | 1.61 | 1.71 | 1.78 | 1.56 | 1.38 | 1.53 | 1.47 |
| Sc | 22.1 | 12.6 | 12.2 | 12.3 | 17.7 | 17.3 | 18.1 | 17.8 | 18.2 | 17.7 | 20.2 | 21.2 | 20.9 |
| V | 163 | 113 | 114 | 108 | 139 | 133 | 135 | 137 | 135 | 136 | 160 | 155 | 165 |
| Cr | 372 | 154 | 151 | 146 | 220 | 214 | 221 | 257 | 251 | 261 | 157 | 150 | 155 |
| Co | 38.3 | 15.7 | 14.5 | 14.8 | 26.2 | 26.1 | 25.8 | 26.6 | 23.2 | 34.2 | 21.7 | 22.0 | 22.3 |
| Ni | 152.2 | 93.3 | 87.4 | 88.8 | 109.0 | 108.9 | 107.9 | 144.0 | 147.9 | 137.0 | 30.4 | 30.5 | 31.7 |
| Zn | 89.9 | 71.5 | 62.3 | 70.1 | 98.9 | 99.1 | 101.4 | 94.3 | 99.9 | 94.1 | 85.8 | 85.3 | 86.2 |
| Ga | 18.0 | 21.6 | 20.8 | 21.2 | 19.6 | 19.3 | 19.5 | 19.3 | 19.8 | 19.1 | 19.4 | 19.9 | 19.4 |
| Rb | 64.8 | 89.7 | 83.5 | 89.8 | 71.0 | 68.9 | 67.7 | 69.1 | 70.1 | 64.9 | 79.7 | 81.6 | 70.5 |
| Sr | 983 | 1154 | 1206 | 1173 | 1015 | 994 | 996 | 1142 | 1163 | 1112 | 821 | 781 | 706 |
| Y | 22.4 | 12.2 | 12.5 | 11.7 | 19.3 | 19.6 | 20.4 | 21.9 | 21.6 | 21.3 | 19.0 | 19.6 | 19.0 |
| Zr | 212 | 192 | 194 | 193 | 204 | 198 | 200 | 209 | 216 | 205 | 172 | 165 | 148 |
| Nb | 15.3 | 11.1 | 10.5 | 10.7 | 12.1 | 11.7 | 11.7 | 16.6 | 17.5 | 16.4 | 8.3 | 8.7 | 8.3 |
| Mo | 0.14 | 0.15 | 0.13 | 0.16 | 0.18 | 0.15 | 0.11 | 0.14 | 0.15 | 0.17 | 0.92 | 1.00 | 0.86 |
| Ba | 2291 | 1847 | 2064 | 1844 | 1905 | 1906 | 1868 | 2065 | 1927 | 2015 | 1090 | 1115 | 1055 |
| Hf | 5.50 | 5.31 | 5.24 | 5.32 | 4.32 | 4.59 | 4.20 | 4.86 | 5.24 | 5.15 | 4.46 | 4.79 | 4.19 |
| Ta | 0.75 | 0.56 | 0.54 | 0.58 | 0.68 | 0.65 | 0.66 | 0.86 | 0.91 | 0.84 | 0.60 | 0.65 | 0.63 |
| Pb | 46.4 | 13.7 | 14.9 | 16.7 | 13.3 | 14.7 | 14.2 | 17.3 | 17.9 | 17.2 | 10.5 | 10.1 | 10.4 |
| Th | 6.80 | 5.00 | 4.73 | 4.72 | 8.47 | 8.04 | 8.09 | 9.04 | 9.15 | 8.42 | 12.16 | 13.23 | 12.86 |
| U | 1.05 | 0.79 | 0.79 | 0.78 | 1.38 | 1.35 | 1.38 | 1.58 | 1.65 | 1.45 | 4.27 | 5.27 | 4.68 |
| Sr/Y | 43.8 | 94.5 | 96.8 | 100.0 | 52.5 | 50.8 | 48.9 | 52.1 | 53.9 | 52.2 | 43.1 | 39.8 | 37.1 |

Mg# = 100* molar Mg/(Mg +∑Fe).



ACCEPTED MANUSCRIPT

ACCEPTED MANUSCRIPT

**Table 5:** Sr, Nd and Pb isotopic compositions of intermediate-felsic dikes from the Jiaobei terrane and the Sulu orogenic belt in the Jiaodong Peninsula

| Sample | **Rb (ppm)** | **Sr (ppm)** | **$^{87}Rb/^{86}Sr$** | **$^{87}Sr/^{86}Sr$** | **2δ** | **$(^{87}Sr/^{86}Sr)_i$** | **Sm (ppm)** | **Nd (ppm)** | **$^{147}Sm/^{144}Nd$** | **$^{143}Nd/^{144}Nd$** | **2δ** | **$\varepsilon Nd(t)$** | **T** | **$^{206}Pb/^{204}Pb$** | **$^{207}Pb/^{204}Pb$** | **$^{208}Pb/^{204}Pb$** | **$(^{206}Pb/^{204}Pb)_i$** | **$(^{207}Pb/^{204}Pb)_i$** | **$(^{208}Pb/^{204}Pb)_i$** |
|---|---|---|---|---|---|---|---|---|---|---|---|---|---|---|---|---|---|---|---|
| LKXDJ-1-1 | 87.9 | 1282 | 0.1979 | 0.710656 | 7 | 0.7103185 | 7.62 | 52.6 | 0.0877 | 0.511797 | 6 | -14.7 | 2113 | 17.3032 | 15.5086 | 38.1084 | 17.2042 | 15.5038 | 37.9379 |
| LKXDJ-1-2 | 88.0 | 1238 | 0.2052 | 0.710717 | 9 | 0.7103673 | 7.42 | 51.2 | 0.0876 | 0.511784 | 6 | -15.0 | 2133 | 17.3093 | 15.5111 | 38.1202 | 17.2167 | 15.5066 | 37.9494 |
| LZYD-1-11 | 75.7 | 891 | 0.2453 | 0.710675 | 7 | 0.7102563 | 5.10 | 29.2 | 0.1055 | 0.511550 | 5 | -19.8 | 2522 | 17.1936 | 15.4829 | 37.8892 | 17.0873 | 15.4778 | 37.6687 |
| LZYD-1-12 | 78.2 | 840 | 0.2687 | 0.710698 | 6 | 0.7102398 | 4.20 | 26.8 | 0.0948 | 0.511528 | 5 | -20.1 | 2545 | 17.2003 | 15.4830 | 37.9270 | 17.1048 | 15.4783 | 37.6913 |
| PDDZ-2-1 | 81.6 | 918 | 0.2566 | 0.710219 | 7 | 0.7097813 | 5.78 | 45.1 | 0.0776 | 0.511616 | 6 | -18.1 | 2388 | 17.0580 | 15.4584 | 37.6745 | 16.9059 | 15.4510 | 37.3731 |
| PDDZ-2-2 | 90.5 | 921 | 0.2836 | 0.710355 | 10 | 0.7098716 | 5.49 | 43.2 | 0.0769 | 0.511615 | 6 | -18.1 | 2389 | 17.0670 | 15.4583 | 37.6860 | 16.9104 | 15.4507 | 37.3742 |
| PDDZ-1-1 | 81.0 | 1122 | 0.2083 | 0.709268 | 7 | 0.7089129 | 9.61 | 65.9 | 0.0882 | 0.511719 | 6 | -16.3 | 2237 | 17.2307 | 15.4546 | 38.0150 | 16.9395 | 15.4405 | 37.4329 |
| PDDZ-1-2 | 79.8 | 1115 | 0.2066 | 0.709284 | 7 | 0.7089322 | 9.79 | 65.7 | 0.0901 | 0.511724 | 5 | -16.2 | 2232 | 17.2447 | 15.4557 | 38.0657 | 16.9308 | 15.4405 | 37.4443 |
| PDDZ-3-1 | 121.0 | 1039 | 0.3361 | 0.709982 | 7 | 0.7094086 | 9.77 | 58.7 | 0.1008 | 0.511728 | 5 | -16.3 | 2238 | 17.0862 | 15.4577 | 37.6358 | 16.6552 | 15.4369 | 37.3220 |

ACCEPTED MANUSCRIPT

ACCEPTED MANUSCRIPT

| | | | | | | | | | | | | | | | | | | | |
|---|---|---|---|---|---|---|---|---|---|---|---|---|---|---|---|---|---|---|---|
| PDDZ-3-2 | 124.3 | 1042 | 0.3443 | 0.710002 | 8 | 0.7094145 | 10.09 | 61.0 | 0.1000 | 0.511740 | 5 | -16.0 | 2218 | 17.0801 | 15.4591 | 37.6350 | 16.8813 | 15.4495 | 37.3294 |
| PDDZ-3-3 | 126.8 | 1068 | 0.3425 | 0.709906 | 7 | 0.7093216 | 9.90 | 61.4 | 0.0976 | 0.511739 | 5 | -16.0 | 2215 | | | | | | |
| RSYZ-1-1 | 65.2 | 1037 | 0.1815 | 0.709353 | 8 | 0.7090434 | 8.99 | 56.2 | 0.0968 | 0.511711 | 5 | -16.6 | 2260 | 17.0870 | 15.4605 | 37.6190 | 17.0533 | 15.4589 | 37.5462 |
| RSYZ-1-2 | 64.4 | 961 | 0.1935 | 0.709420 | 8 | 0.7090895 | 8.91 | 56.6 | 0.0952 | 0.511701 | 5 | -16.7 | 2274 | 17.1104 | 15.4634 | 37.6806 | 17.0476 | 15.4604 | 37.5297 |
| RSYZ-1-4 | 64.8 | 983 | 0.1902 | 0.709364 | 8 | 0.7090400 | 9.56 | 59.5 | 0.0972 | 0.511711 | 5 | -16.6 | 2260 | 16.8850 | 15.4103 | 37.2023 | 16.8548 | 15.4089 | 37.1399 |
| RSZT-1-1 | 89.7 | 1154 | 0.2243 | 0.707692 | 7 | 0.7073099 | 6.41 | 42.2 | 0.0919 | 0.511835 | 5 | -14.1 | 2058 | 17.0266 | 15.4246 | 37.3669 | 16.9492 | 15.4209 | 37.2112 |
| RSZT-1-2 | 83.5 | 1206 | 0.1998 | 0.707610 | 8 | 0.7072695 | 6.35 | 41.1 | 0.0933 | 0.511841 | 5 | -14.0 | 2051 | 17.0120 | 15.4236 | 37.3423 | 16.9416 | 15.4202 | 37.2071 |
| RSZT-1-3 | 89.8 | 1173 | 0.2210 | 0.707704 | 8 | 0.7073274 | 6.31 | 41.3 | 0.0924 | 0.511839 | 5 | -14.0 | 2052 | 17.0131 | 15.4216 | 37.3406 | 16.9506 | 15.4186 | 37.2204 |
| RSZT-2-1 | 71.0 | 1015 | 0.2019 | 0.707800 | 6 | 0.7074561 | 8.02 | 49.6 | 0.0978 | 0.511915 | 5 | -12.6 | 1939 | 17.1240 | 15.4333 | 37.4673 | 16.9853 | 15.4266 | 37.1958 |
| RSZT-2-2 | 68.9 | 994 | 0.2000 | 0.707798 | 7 | 0.7074566 | 8.22 | 52.7 | 0.0943 | 0.511916 | 5 | -12.5 | 1933 | 17.1107 | 15.4338 | 37.4508 | 16.9880 | 15.4279 | 37.2184 |
| RSZT-2-5 | 67.7 | 996 | 0.1961 | 0.707772 | 7 | 0.7074379 | 8.59 | 53.6 | 0.0969 | 0.511915 | 5 | -12.6 | 1937 | 17.1149 | 15.4332 | 37.4568 | 16.9858 | 15.4270 | 37.2150 |

| | | | | | | | | | | | | | | | | | | | |
|---|---|---|---|---|---|---|---|---|---|---|---|---|---|---|---|---|---|---|---|
| RSZT-3-2 | 69.1 | 1142 | 0.1746 | 0.708917 | 7 | 0.7086188 | 8.27 | 54.2 | 0.0923 | 0.511859 | 5 | -13.6 | 2020 | 17.1558 | 15.4436 | 37.4035 | 17.0343 | 15.4377 | 37.1814 |
| RSZT-3-3 | 70.1 | 1163 | 0.1739 | 0.708898 | 8 | 0.7086016 | 7.80 | 49.3 | 0.0957 | 0.511878 | 5 | -13.3 | 1995 | 17.1580 | 15.4437 | 37.3970 | 17.0351 | 15.4378 | 37.1799 |
| RSZT-3-4 | 64.9 | 1112 | 0.1685 | 0.708909 | 8 | 0.7086214 | 7.93 | 49.7 | 0.0965 | 0.511884 | 5 | -13.2 | 1985 | 17.1389 | 15.4413 | 37.3765 | 17.0269 | 15.4359 | 37.1681 |
| RCYT-1-1 | 79.7 | 821 | 0.2802 | 0.706848 | 7 | 0.7063704 | 6.57 | 38.5 | 0.1033 | 0.512067 | 5 | -9.7 | 1703 | 17.7301 | 15.4476 | 37.9629 | 17.1879 | 15.4214 | 37.4697 |
| RCYT-1-2 | 81.6 | 781 | 0.3015 | 0.707216 | 10 | 0.7067019 | 6.87 | 41.1 | 0.1013 | 0.512047 | 5 | -10.1 | 1734 | 17.8831 | 15.4550 | 38.0323 | 17.1909 | 15.4215 | 37.4775 |
| RCYT-1-3 | 70.5 | 706 | 0.2884 | 0.706797 | 8 | 0.7063052 | 6.53 | 37.6 | 0.1051 | 0.512072 | 5 | -9.6 | 1699 | 17.7761 | 15.4513 | 38.0017 | 17.1757 | 15.4222 | 37.4745 |

$\lambda_{Rb}$= 1.393 × $10^{-11}$ $year^{-1}$ (Nebel *et al*., 2011); $\lambda_{Sm}$ = 6.54 × $10^{-12}$ $year^{-1}$ (Lugmair and Marti, 1978); $(^{147}Sm/^{144}Nd)_{CHUR}$ = 0.1967 (Jacobsen and Wasserburg, 1980); $(^{143}Nd/^{144}Nd)_{CHUR}$ = 0.512638 (Goldstein *et al*., 1984)

ACCEPTED MANUSCRIPT

# Highlights

1. Early Cretaceous felsic dikes characterized by adakite-like features indicate the existence of a thickened ancient lower crust at Jiaodong.
2. Early Cretaceous intermediate dikes with the HMAs characteristics provide new evidence for the SCLM beneath Jiaodong Peninsula which has been metasomatized by the subducting Paleo-Pacific plate with marine sediments.
3. We clarified that the Early Cretaceous magmatism within the Jiaodong Peninsula represents a magmatic response to lithospheric thinning caused prolonged thermo-mechanical-chemical erosion induced by rollback of Paleo-Pacific plate.
4. This newly study focus on the petrogenesis of Early Cretaceous intermediate-felsic dikes in the Jiaodong Peninsula.

ACCEPTED MANUSCRIPT

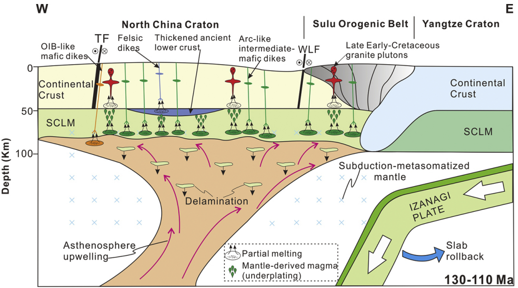


Graphics Abstract

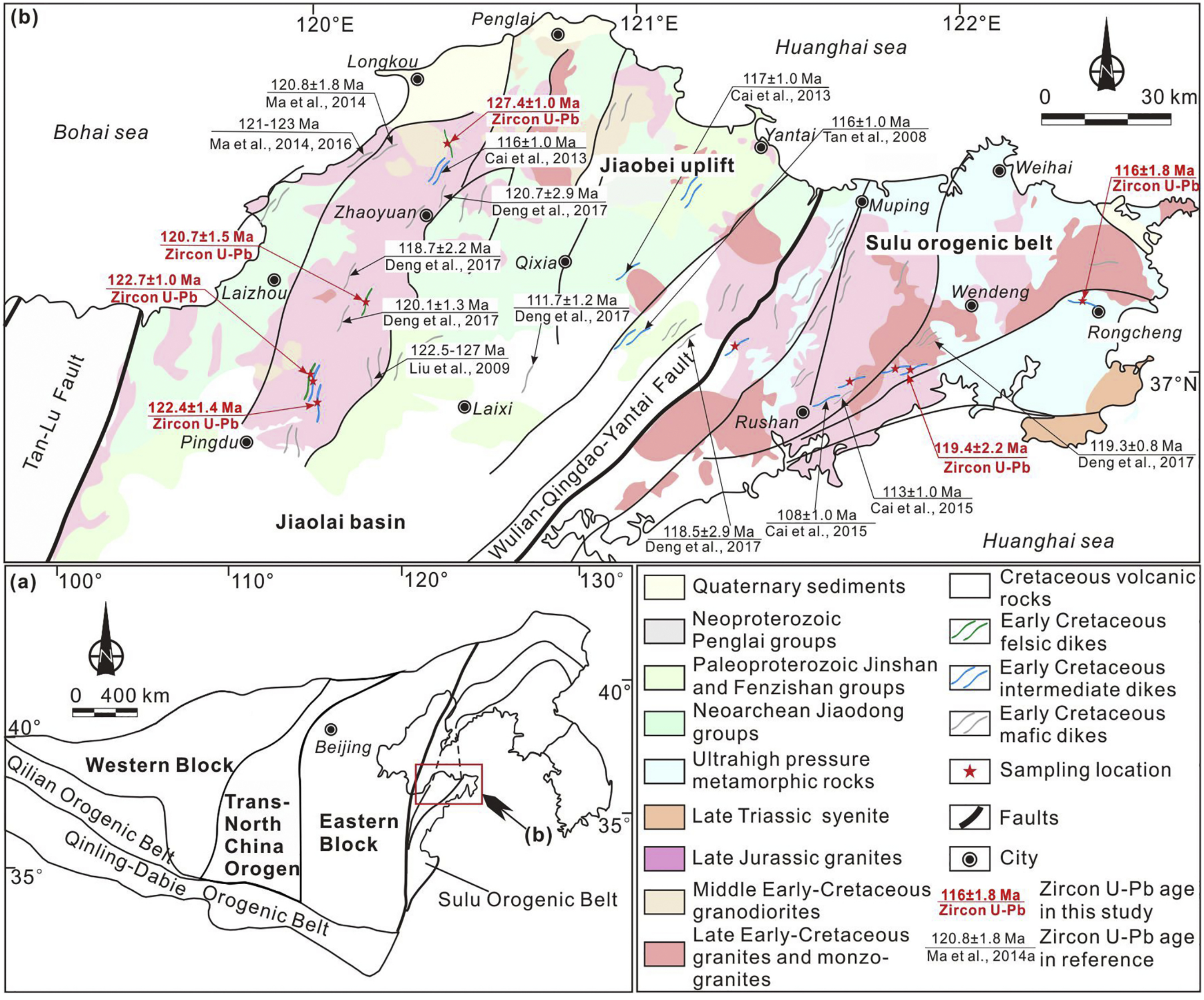
(b)
120°E
121°E
122°E
Penglai
Longkou
Huanghai sea
Bohai sea
0
30 km
120.8±1.8 Ma
Ma et al., 2014
127.4±1.0 Ma
Zircon U-Pb
121-123 Ma
Ma et al., 2014, 2016
116±1.0 Ma
Cai et al., 2013
117±1.0 Ma
Cai et al., 2013
116±1.0 Ma
Tan et al., 2008
Yantai
Jiaobei uplift
Weihai
116±1.8 Ma
Zircon U-Pb
120.7±2.9 Ma
Deng et al., 2017
Zhaoyuan
Muping
120.7±1.5 Ma
Zircon U-Pb
Sulu orogenic belt
118.7±2.2 Ma
Deng et al., 2017
Qixia
122.7±1.0 Ma
Zircon U-Pb
Laizhou
120.1±1.3 Ma
Deng et al., 2017
111.7±1.2 Ma
Deng et al., 2017
Wendeng
Rongcheng
122.5-127 Ma
Liu et al., 2009
Tan-Lu Fault
Wulian-Qingdao-Yantai Fault
37°N
122.4±1.4 Ma
Zircon U-Pb
Laixi
Rushan
Pingdu
119.4±2.2 Ma
Zircon U-Pb
119.3±0.8 Ma
Deng et al., 2017
113±1.0 Ma
Cai et al., 2015
108±1.0 Ma
Cai et al., 2015
118.5±2.9 Ma
Deng et al., 2017
Jiaolai basin
Huanghai sea
(a)
100°
110°
120°
130°
0 400 km
40°
35°
Beijing
Western Block
Trans-North China Orogen
Eastern Block
Qilian Orogenic Belt
Qinling-Dabie Orogenic Belt
Sulu Orogenic Belt
(b)
Quaternary sediments
Neoproterozoic Penglai groups
Paleoproterozoic Jinshan and Fenzishan groups
Neoarchean Jiaodong groups
Ultrahigh pressure metamorphic rocks
Late Triassic syenite
Late Jurassic granites
Middle Early-Cretaceous granodiorites
Late Early-Cretaceous granites and monzo-granites
Cretaceous volcanic rocks
Early Cretaceous felsic dikes
Early Cretaceous intermediate dikes
Early Cretaceous mafic dikes
Sampling location
Faults
City
116±1.8 Ma
Zircon U-Pb
Zircon U-Pb age in this study
120.8±1.8 Ma
Ma et al., 2014a
Zircon U-Pb age in reference

Figure 1

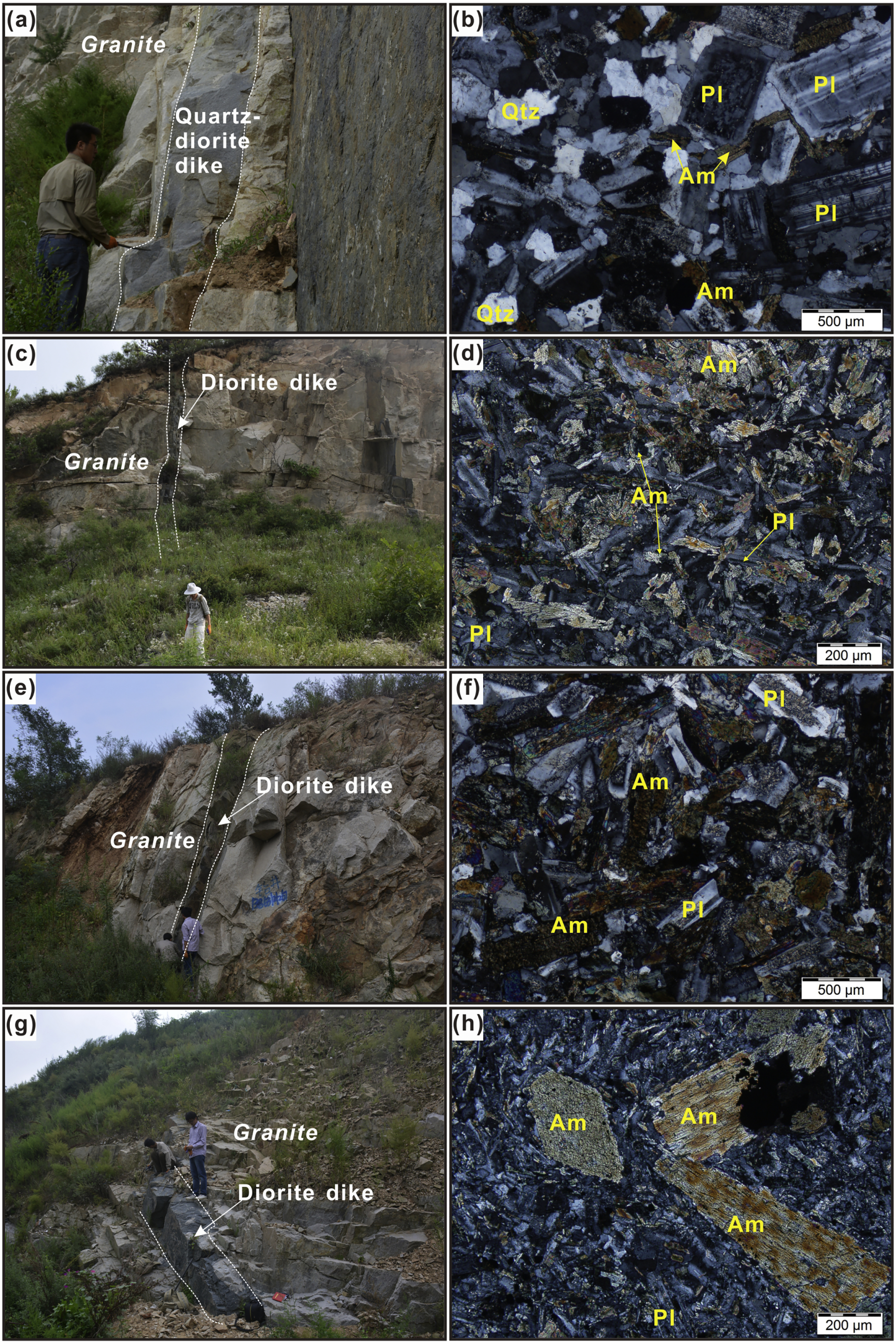
(a)
Granite
Quartz-
diorite
dike
(b)
Qtz
Pl
Pl
Am
Pl
Am
Qtz
500 μm
(c)
Diorite dike
Granite
(d)
Am
Am
Pl
Pl
200 μm
(e)
Diorite dike
Granite
(f)
Pl
Am
Pl
Am
500 μm
(g)
Granite
Diorite dike
(h)
Am
Am
Am
Pl
200 μm

Figure 2

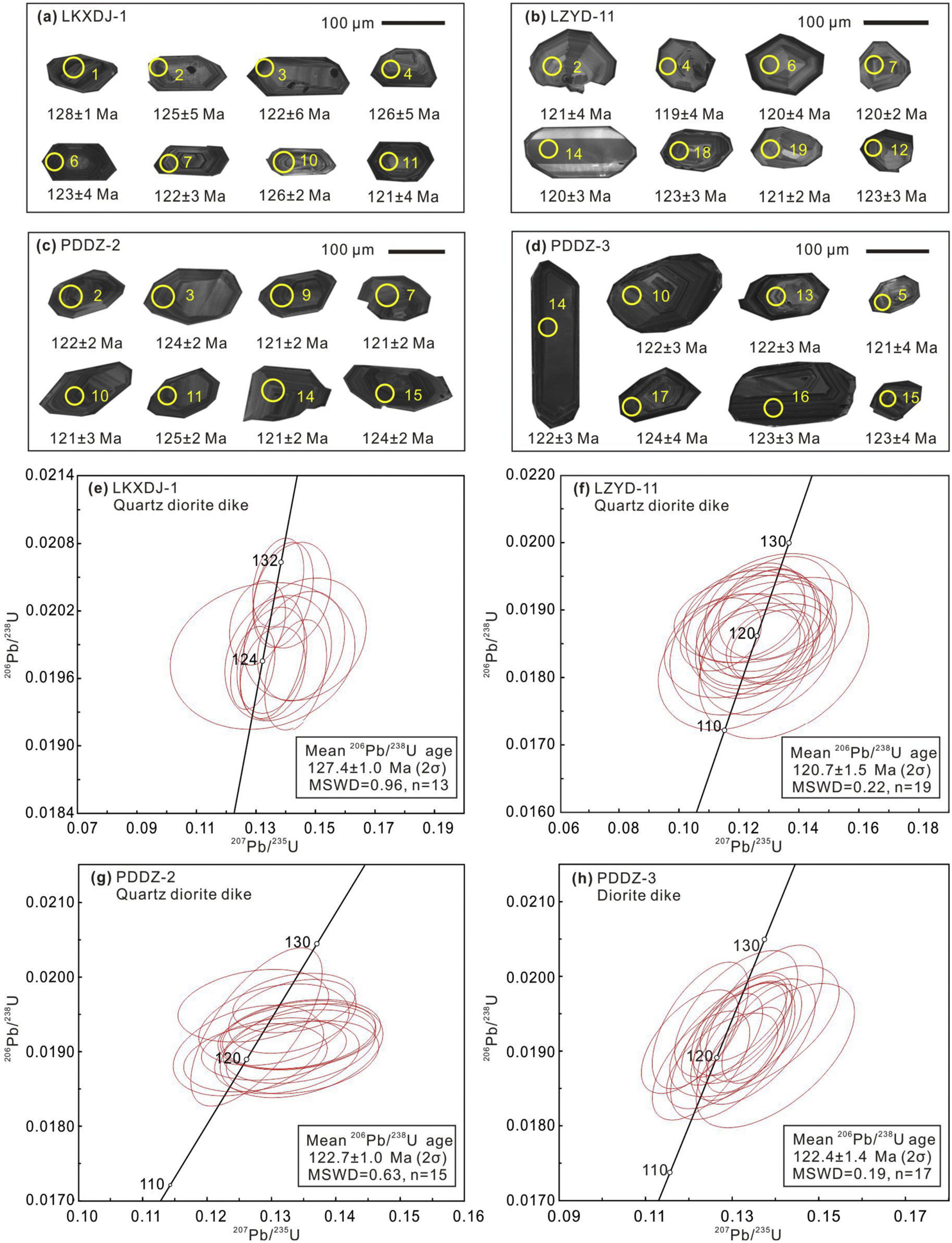
(a) LKXDJ-1
100 μm
128±1 Ma
125±5 Ma
122±6 Ma
126±5 Ma
123±4 Ma
122±3 Ma
126±2 Ma
121±4 Ma
(b) LZYD-11
100 μm
121±4 Ma
119±4 Ma
120±4 Ma
120±2 Ma
120±3 Ma
123±3 Ma
121±2 Ma
123±3 Ma
(c) PDDZ-2
100 μm
122±2 Ma
124±2 Ma
121±2 Ma
121±2 Ma
121±3 Ma
125±2 Ma
121±2 Ma
124±2 Ma
(d) PDDZ-3
100 μm
122±3 Ma
122±3 Ma
121±4 Ma
122±3 Ma
124±4 Ma
123±3 Ma
123±4 Ma
(e) LKXDJ-1
Quartz diorite dike
Mean $^{206}Pb/^{238}U$ age
127.4±1.0 Ma (2σ)
MSWD=0.96, n=13
(f) LZYD-11
Quartz diorite dike
Mean $^{206}Pb/^{238}U$ age
120.7±1.5 Ma (2σ)
MSWD=0.22, n=19
(g) PDDZ-2
Quartz diorite dike
Mean $^{206}Pb/^{238}U$ age
122.7±1.0 Ma (2σ)
MSWD=0.63, n=15
(h) PDDZ-3
Diorite dike
Mean $^{206}Pb/^{238}U$ age
122.4±1.4 Ma (2σ)
MSWD=0.19, n=17
$^{206}Pb/^{238}U$
$^{207}Pb/^{235}U$

Figure 3

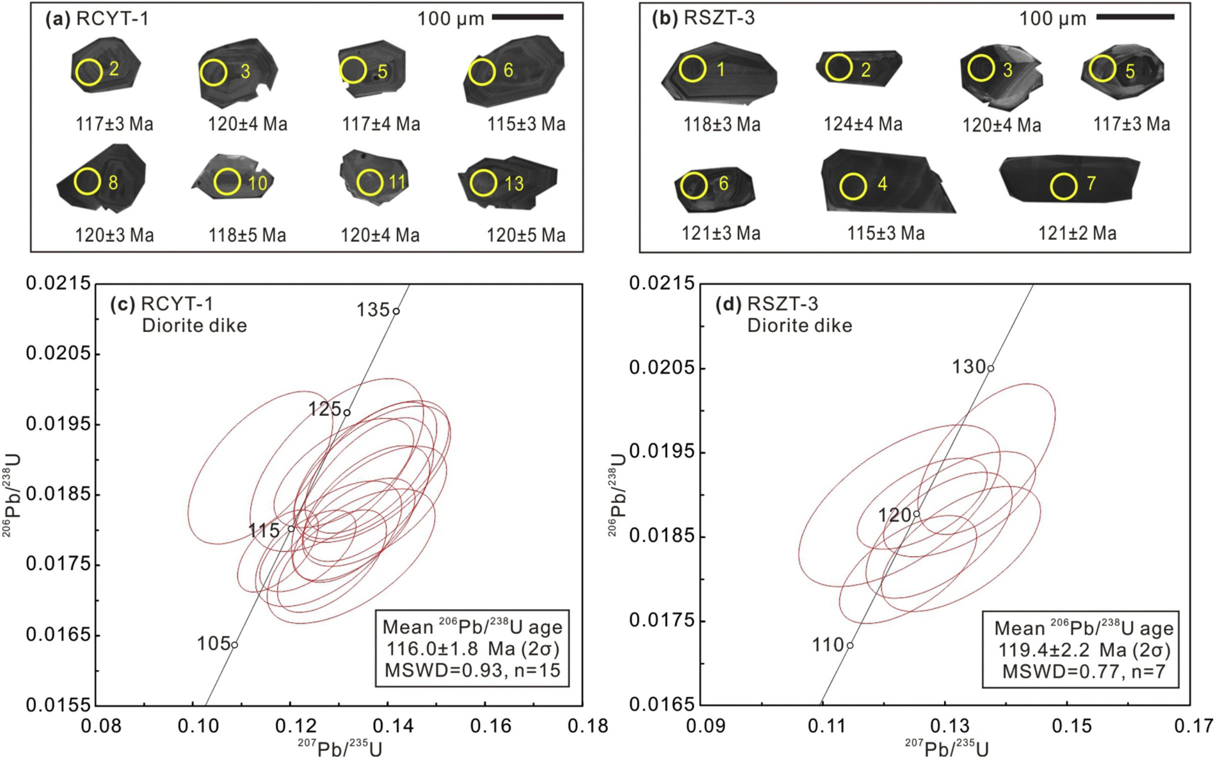
(a) RCYT-1
100 μm
2
3
5
6
117±3 Ma
120±4 Ma
117±4 Ma
115±3 Ma
8
10
11
13
120±3 Ma
118±5 Ma
120±4 Ma
120±5 Ma
(b) RSZT-3
100 μm
1
2
3
5
118±3 Ma
124±4 Ma
120±4 Ma
117±3 Ma
6
4
7
121±3 Ma
115±3 Ma
121±2 Ma
(c) RCYT-1
Diorite dike
135
125
115
105
Mean $^{206}Pb/^{238}U$ age
116.0±1.8 Ma (2σ)
MSWD=0.93, n=15
$^{206}Pb/^{238}U$
$^{207}Pb/^{235}U$
0.0215
0.0205
0.0195
0.0185
0.0175
0.0165
0.0155
0.08
0.10
0.12
0.14
0.16
0.18
(d) RSZT-3
Diorite dike
130
120
110
Mean $^{206}Pb/^{238}U$ age
119.4±2.2 Ma (2σ)
MSWD=0.77, n=7
$^{206}Pb/^{238}U$
$^{207}Pb/^{235}U$
0.0215
0.0205
0.0195
0.0185
0.0175
0.0165
0.09
0.11
0.13
0.15
0.17

Figure 4

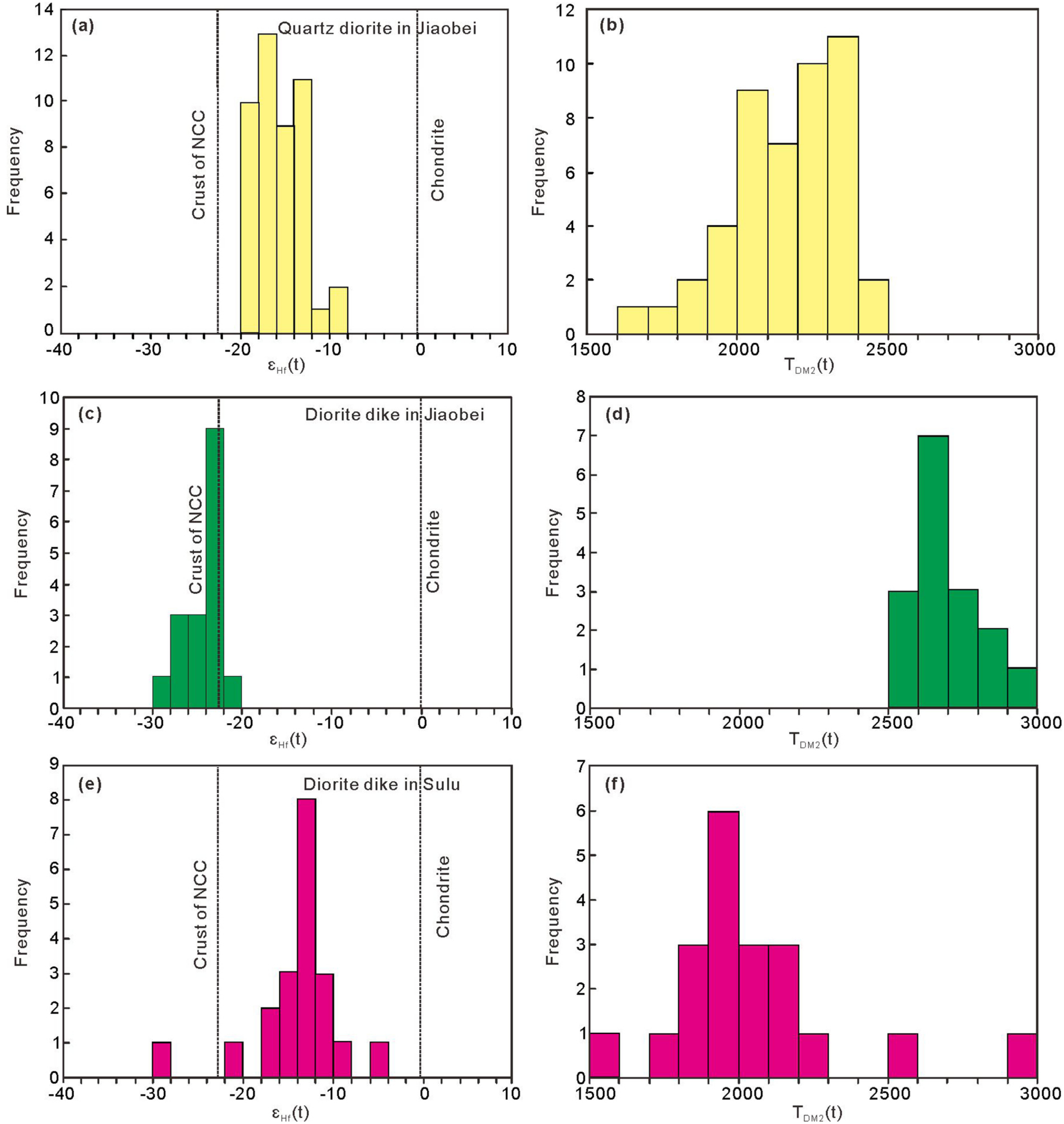

(a)
Quartz diorite in Jiaobei
Crust of NCC
Chondrite
Frequency
εHf(t)
(b)
Frequency
TDM2(t)
(c)
Diorite dike in Jiaobei
Crust of NCC
Chondrite
Frequency
εHf(t)
(d)
Frequency
TDM2(t)
(e)
Diorite dike in Sulu
Crust of NCC
Chondrite
Frequency
εHf(t)
(f)
Frequency
TDM2(t)


Figure 5

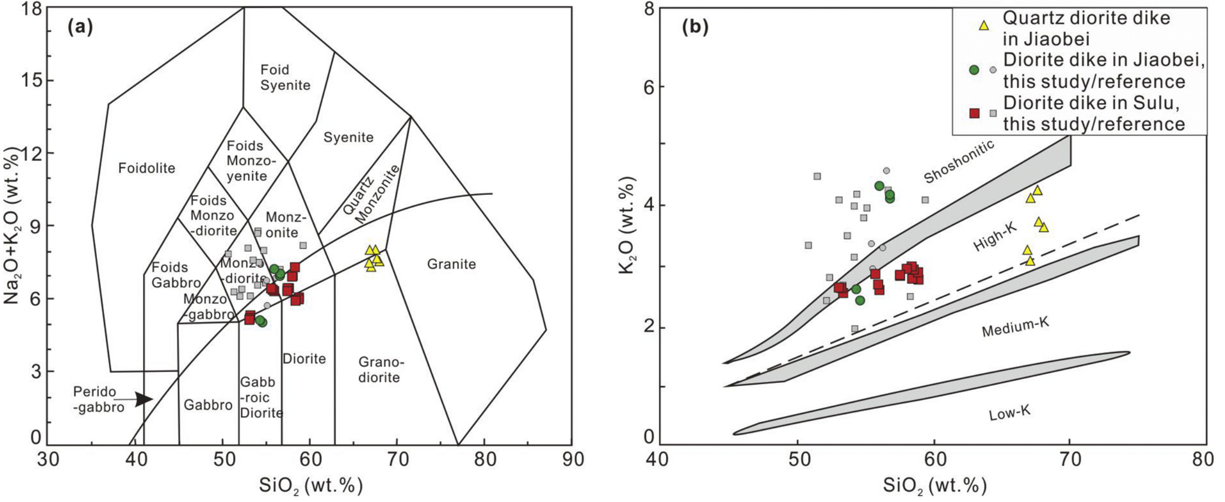

(a)
18
15
12
9
6
3
0
30
40
50
60
70
80
90
$Na_2O+K_2O$ (wt.%)
$SiO_2$ (wt.%)
Foid Syenite
Syenite
Foidolite
Foids Monzo-yenite
Foids Monzo -diorite
Monz- onite
Quartz Monzonite
Foids Gabbro
Monzo -diorite
Monzo -gabbro
Granite
Perido -gabbro
Gabbro
Gabb -roic Diorite
Diorite
Grano- diorite
(b)
8
6
4
2
0
40
50
60
70
80
$K_2O$ (wt.%)
$SiO_2$ (wt.%)
Quartz diorite dike in Jiaobei
Diorite dike in Jiaobei, this study/reference
Diorite dike in Sulu, this study/reference
Shoshonitic
High-K
Medium-K
Low-K


Figure 6

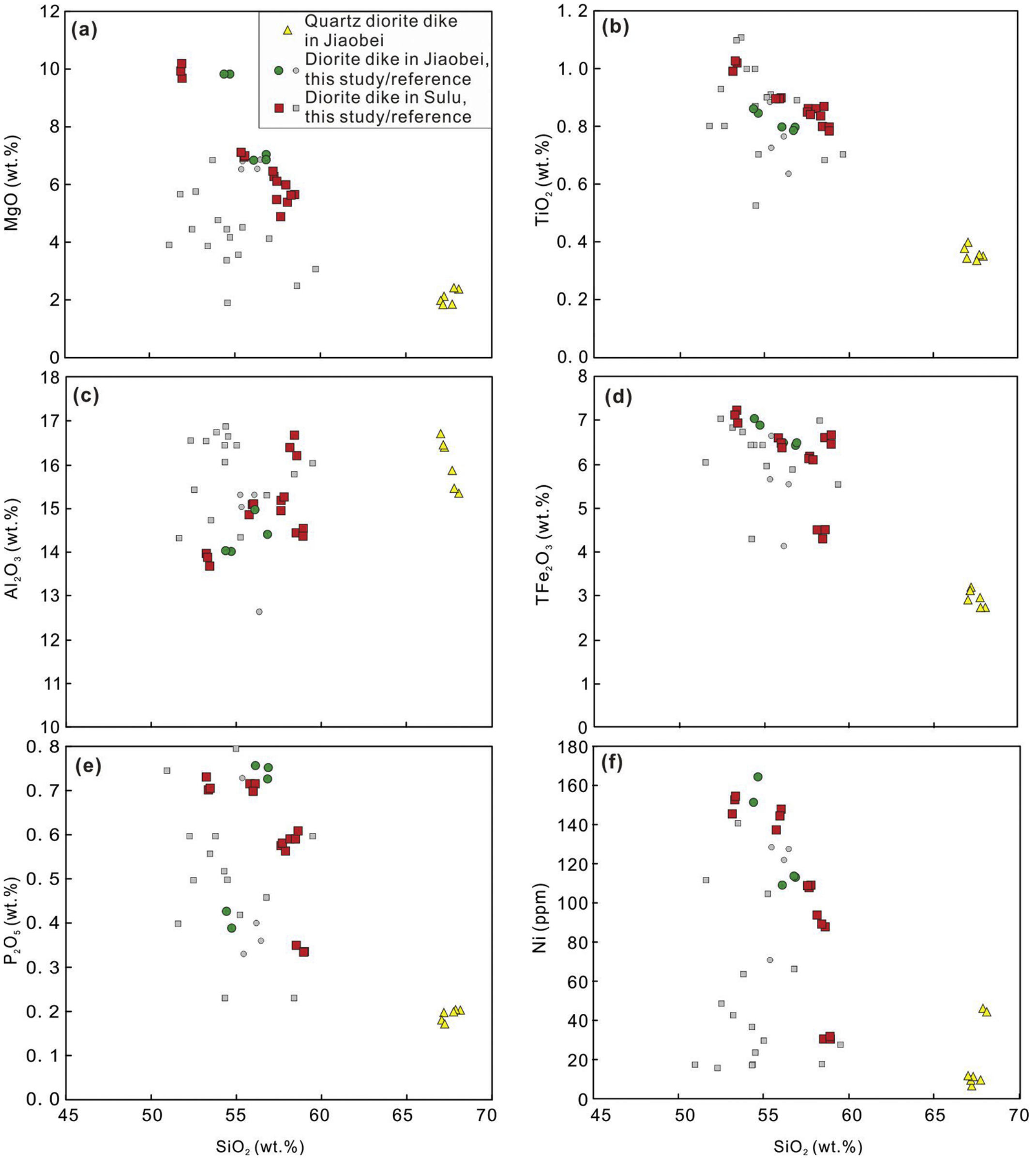
(a)
Quartz diorite dike
in Jiaobei
Diorite dike in Jiaobei,
this study/reference
Diorite dike in Sulu,
this study/reference
MgO (wt.%)
(b)
TiO2 (wt.%)
(c)
Al2O3 (wt.%)
(d)
TFe2O3 (wt.%)
(e)
P2O5 (wt.%)
(f)
Ni (ppm)
SiO2 (wt.%)
SiO2 (wt.%)

Figure 7

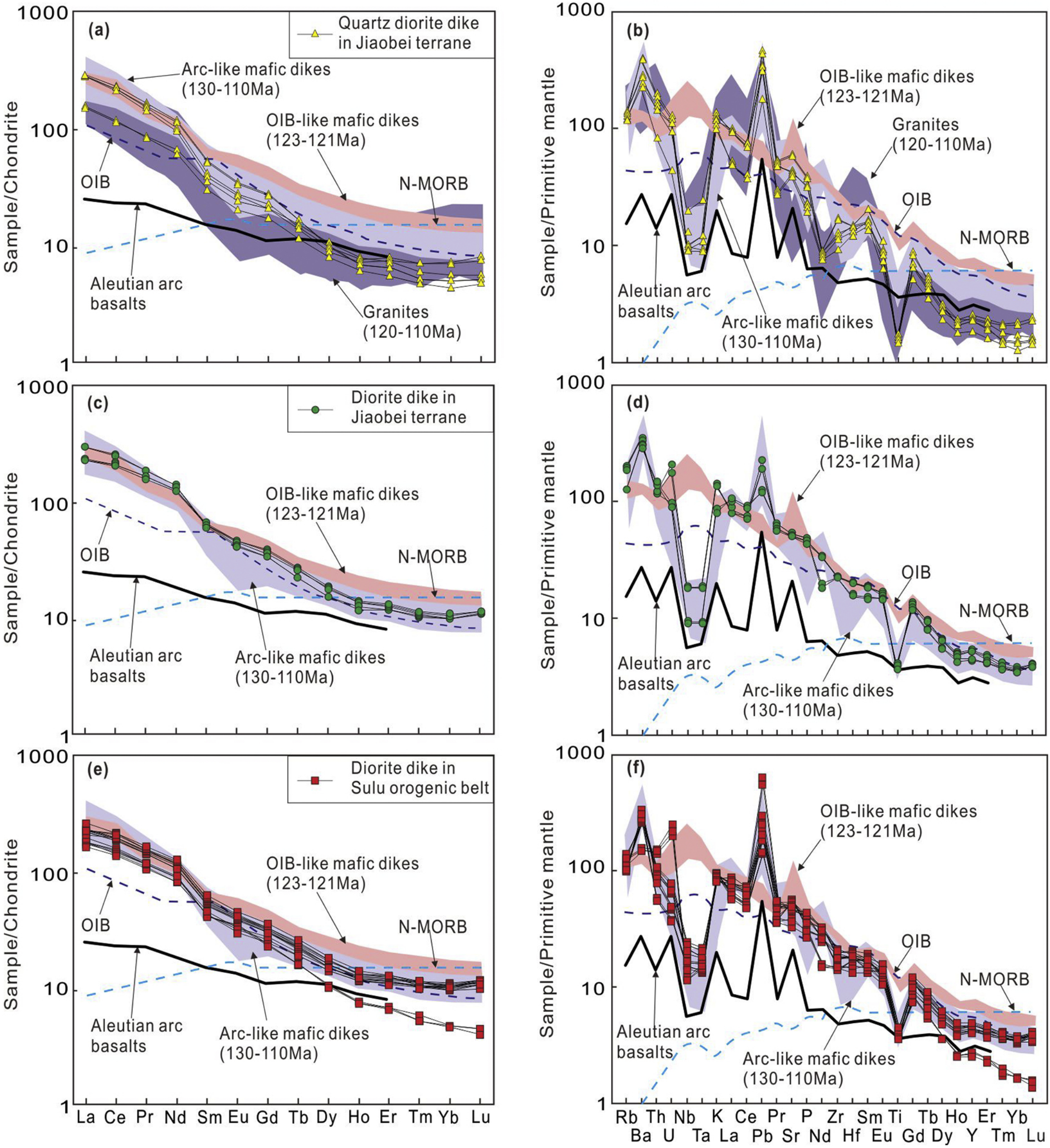

(a)
Quartz diorite dike in Jiaobei terrane
Arc-like mafic dikes (130-110Ma)
OIB-like mafic dikes (123-121Ma)
OIB
N-MORB
Aleutian arc basalts
Granites (120-110Ma)
Sample/Chondrite
(b)
OIB-like mafic dikes (123-121Ma)
Granites (120-110Ma)
OIB
N-MORB
Aleutian arc basalts
Arc-like mafic dikes (130-110Ma)
Sample/Primitive mantle
(c)
Diorite dike in Jiaobei terrane
OIB-like mafic dikes (123-121Ma)
OIB
N-MORB
Aleutian arc basalts
Arc-like mafic dikes (130-110Ma)
Sample/Chondrite
(d)
OIB-like mafic dikes (123-121Ma)
OIB
N-MORB
Aleutian arc basalts
Arc-like mafic dikes (130-110Ma)
Sample/Primitive mantle
(e)
Diorite dike in Sulu orogenic belt
OIB-like mafic dikes (123-121Ma)
OIB
N-MORB
Aleutian arc basalts
Arc-like mafic dikes (130-110Ma)
Sample/Chondrite
La Ce Pr Nd Sm Eu Gd Tb Dy Ho Er Tm Yb Lu
(f)
OIB-like mafic dikes (123-121Ma)
OIB
N-MORB
Aleutian arc basalts
Arc-like mafic dikes (130-110Ma)
Sample/Primitive mantle
Rb Ba Th U Nb Ta K La Ce Pb Pr Sr P Nd Zr Hf Sm Eu Ti Gd Tb Dy Ho Y Er Tm Yb Lu
1000
100
10
1


Figure 8

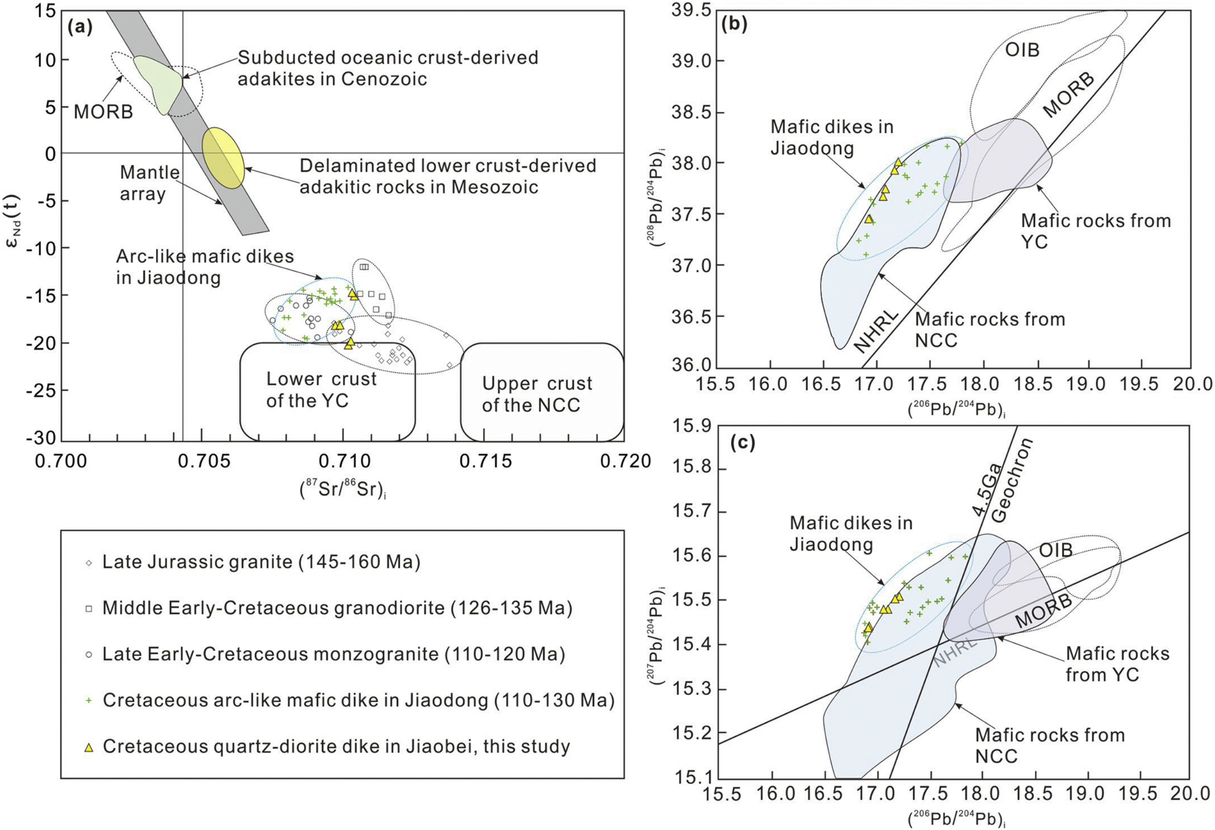

(a)
Subducted oceanic crust-derived adakites in Cenozoic
MORB
Mantle array
Delaminated lower crust-derived adakitic rocks in Mesozoic
Arc-like mafic dikes in Jiaodong
Lower crust of the YC
Upper crust of the NCC
εNd(t)
(87Sr/86Sr)i
Late Jurassic granite (145-160 Ma)
Middle Early-Cretaceous granodiorite (126-135 Ma)
Late Early-Cretaceous monzogranite (110-120 Ma)
Cretaceous arc-like mafic dike in Jiaodong (110-130 Ma)
Cretaceous quartz-diorite dike in Jiaobei, this study
(b)
OIB
MORB
Mafic dikes in Jiaodong
Mafic rocks from YC
NHRL
Mafic rocks from NCC
(208Pb/204Pb)i
(206Pb/204Pb)i
(c)
4.5Ga Geochron
Mafic dikes in Jiaodong
OIB
MORB
NHRL
Mafic rocks from YC
Mafic rocks from NCC
(207Pb/204Pb)i
(206Pb/204Pb)i


Figure 9

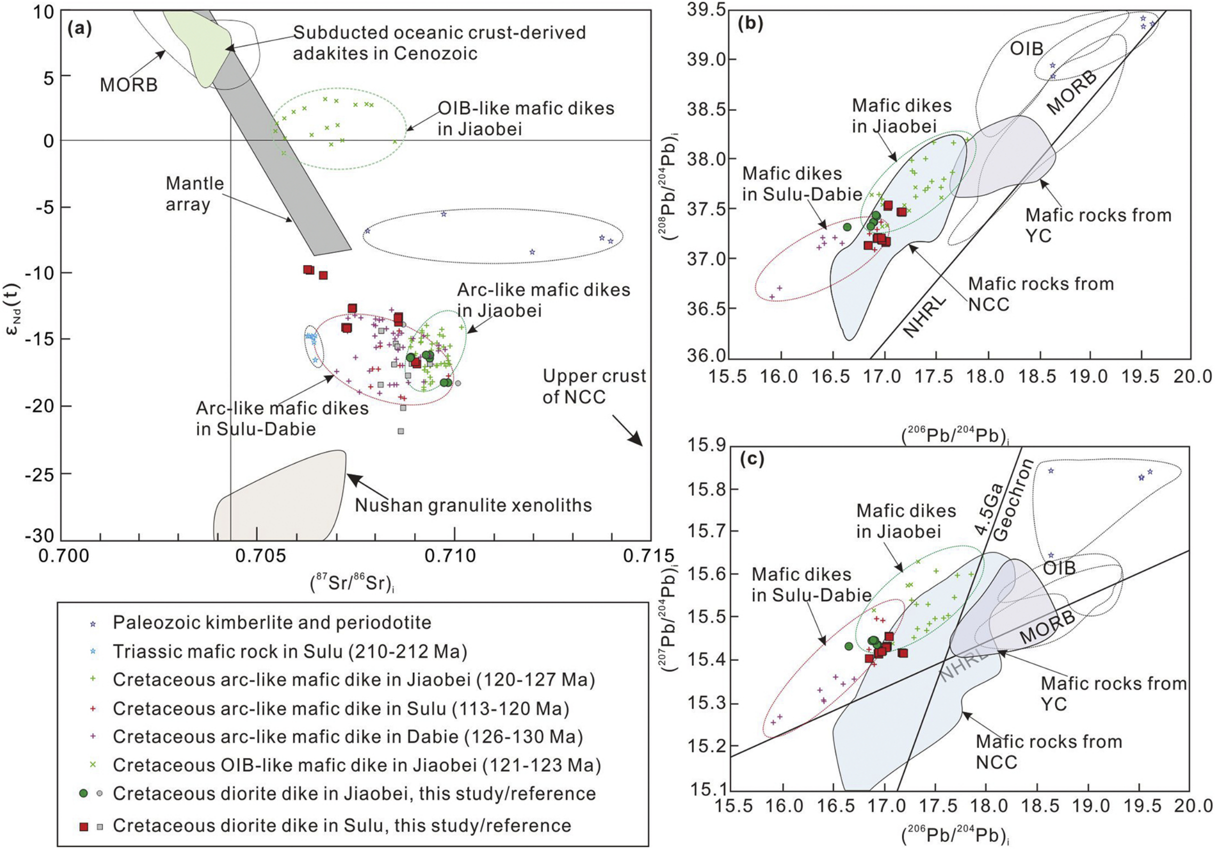
(a)
Subducted oceanic crust-derived adakites in Cenozoic
MORB
OIB-like mafic dikes in Jiaobei
Mantle array
Arc-like mafic dikes in Jiaobei
Arc-like mafic dikes in Sulu-Dabie
Upper crust of NCC
Nushan granulite xenoliths
εNd(t)
(87Sr/86Sr)i
Paleozoic kimberlite and periodotite
Triassic mafic rock in Sulu (210-212 Ma)
Cretaceous arc-like mafic dike in Jiaobei (120-127 Ma)
Cretaceous arc-like mafic dike in Sulu (113-120 Ma)
Cretaceous arc-like mafic dike in Dabie (126-130 Ma)
Cretaceous OIB-like mafic dike in Jiaobei (121-123 Ma)
Cretaceous diorite dike in Jiaobei, this study/reference
Cretaceous diorite dike in Sulu, this study/reference
(b)
OIB
MORB
Mafic dikes in Jiaobei
Mafic dikes in Sulu-Dabie
Mafic rocks from YC
Mafic rocks from NCC
NHRL
(208Pb/204Pb)i
(206Pb/204Pb)i
(c)
4.5Ga Geochron
Mafic dikes in Jiaobei
Mafic dikes in Sulu-Dabie
OIB
MORB
NHRL
Mafic rocks from YC
Mafic rocks from NCC
(207Pb/204Pb)i
(206Pb/204Pb)i

Figure 10

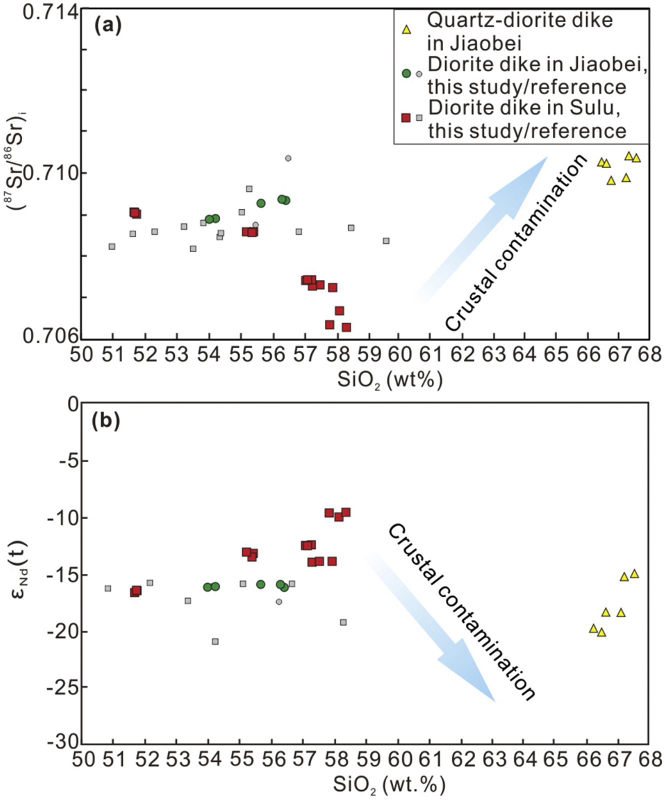

(a)
Quartz-diorite dike in Jiaobei
Diorite dike in Jiaobei, this study/reference
Diorite dike in Sulu, this study/reference
Crustal contamination
$(^{87}Sr/^{86}Sr)_i$
0.714
0.710
0.706
50 51 52 53 54 55 56 57 58 59 60 61 62 63 64 65 66 67 68
$SiO_2$ (wt%)
(b)
Crustal contamination
$\varepsilon_{Nd}(t)$
0
-5
-10
-15
-20
-25
-30
50 51 52 53 54 55 56 57 58 59 60 61 62 63 64 65 66 67 68
$SiO_2$ (wt.%)


Figure 11

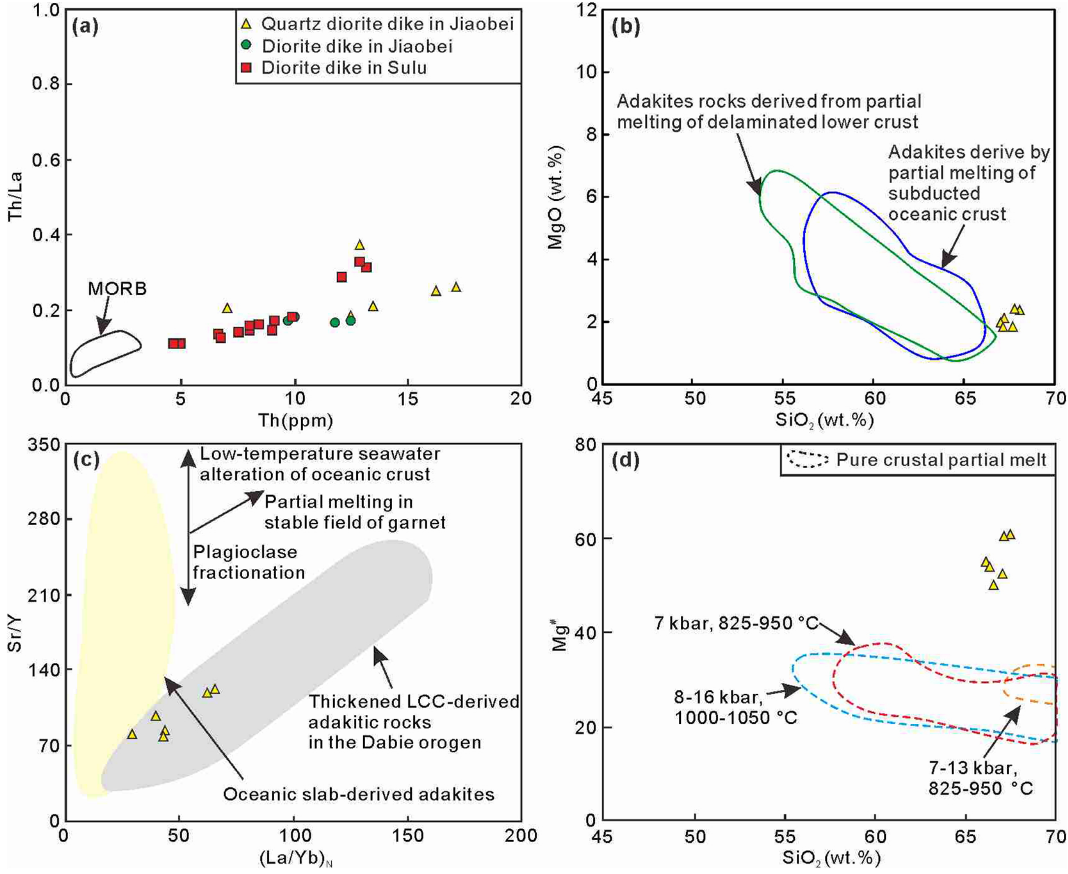

(a)
Quartz diorite dike in Jiaobei
Diorite dike in Jiaobei
Diorite dike in Sulu
MORB
Th/La
Th(ppm)
(b)
Adakites rocks derived from partial melting of delaminated lower crust
Adakites derive by partial melting of subducted oceanic crust
MgO (wt.%)
SiO2 (wt.%)
(c)
Low-temperature seawater alteration of oceanic crust
Partial melting in stable field of garnet
Plagioclase fractionation
Thickened LCC-derived adakitic rocks in the Dabie orogen
Oceanic slab-derived adakites
Sr/Y
(La/Yb)N
(d)
Pure crustal partial melt
7 kbar, 825-950 °C
8-16 kbar, 1000-1050 °C
7-13 kbar, 825-950 °C
Mg#
SiO2 (wt.%)


Figure 12

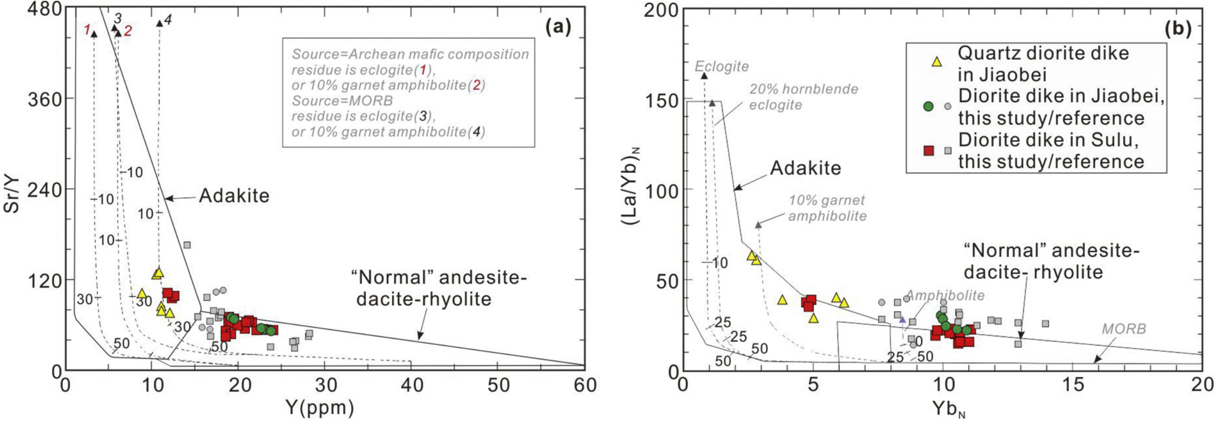

(a)
Sr/Y
Y(ppm)
Source=Archean mafic composition
residue is eclogite(1),
or 10% garnet amphibolite(2)
Source=MORB
residue is eclogite(3),
or 10% garnet amphibolite(4)
Adakite
"Normal" andesite-dacite-rhyolite
(b)
(La/Yb)N
YbN
Quartz diorite dike in Jiaobei
Diorite dike in Jiaobei, this study/reference
Diorite dike in Sulu, this study/reference
Eclogite
20% hornblende eclogite
10% garnet amphibolite
Amphibolite
MORB
Adakite
"Normal" andesite-dacite- rhyolite


Figure 13

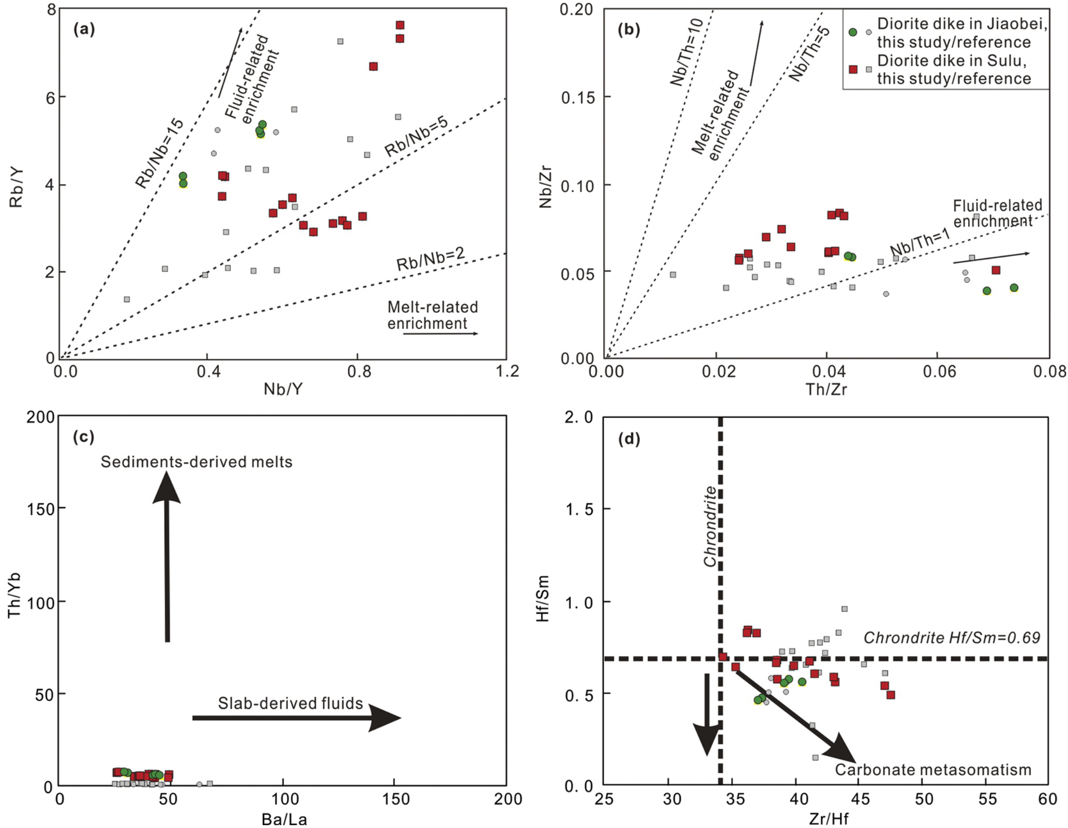
(a)
Rb/Y
Nb/Y
Rb/Nb=15
Fluid-related enrichment
Rb/Nb=5
Rb/Nb=2
Melt-related enrichment
(b)
Nb/Zr
Th/Zr
Nb/Th=10
Melt-related enrichment
Nb/Th=5
Nb/Th=1
Fluid-related enrichment
Diorite dike in Jiaobei, this study/reference
Diorite dike in Sulu, this study/reference
(c)
Th/Yb
Ba/La
Sediments-derived melts
Slab-derived fluids
(d)
Hf/Sm
Zr/Hf
Chrondrite
Chrondrite Hf/Sm=0.69
Carbonate metasomatism

Figure 14

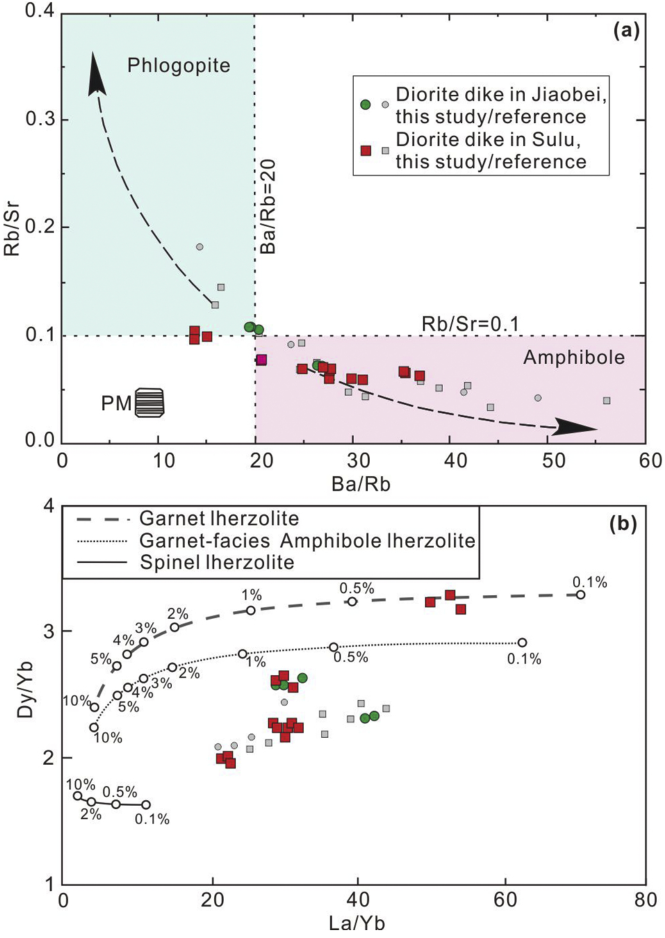

(a)
Phlogopite
Diorite dike in Jiaobei, this study/reference
Diorite dike in Sulu, this study/reference
Ba/Rb=20
Rb/Sr=0.1
Amphibole
PM
Rb/Sr
Ba/Rb
(b)
Garnet lherzolite
Garnet-facies Amphibole lherzolite
Spinel lherzolite
Dy/Yb
La/Yb


Figure 15

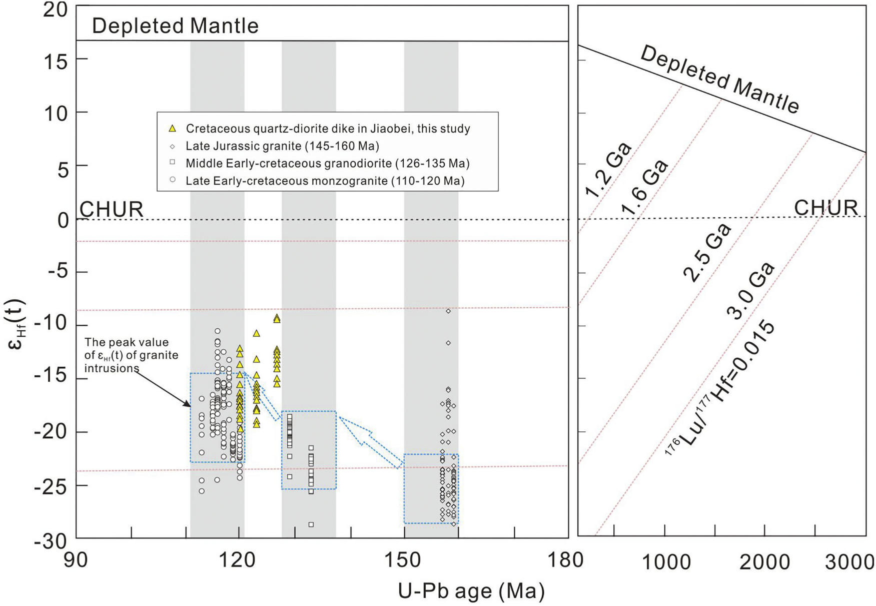

Depleted Mantle
CHUR
Cretaceous quartz-diorite dike in Jiaobei, this study
Late Jurassic granite (145-160 Ma)
Middle Early-cretaceous granodiorite (126-135 Ma)
Late Early-cretaceous monzogranite (110-120 Ma)
The peak value of $\varepsilon_{Hf}(t)$ of granite intrusions
$\varepsilon_{Hf}(t)$
U-Pb age (Ma)
Depleted Mantle
CHUR
1.2 Ga
1.6 Ga
2.5 Ga
3.0 Ga
$^{176}Lu/^{177}Hf=0.015$


Figure 16

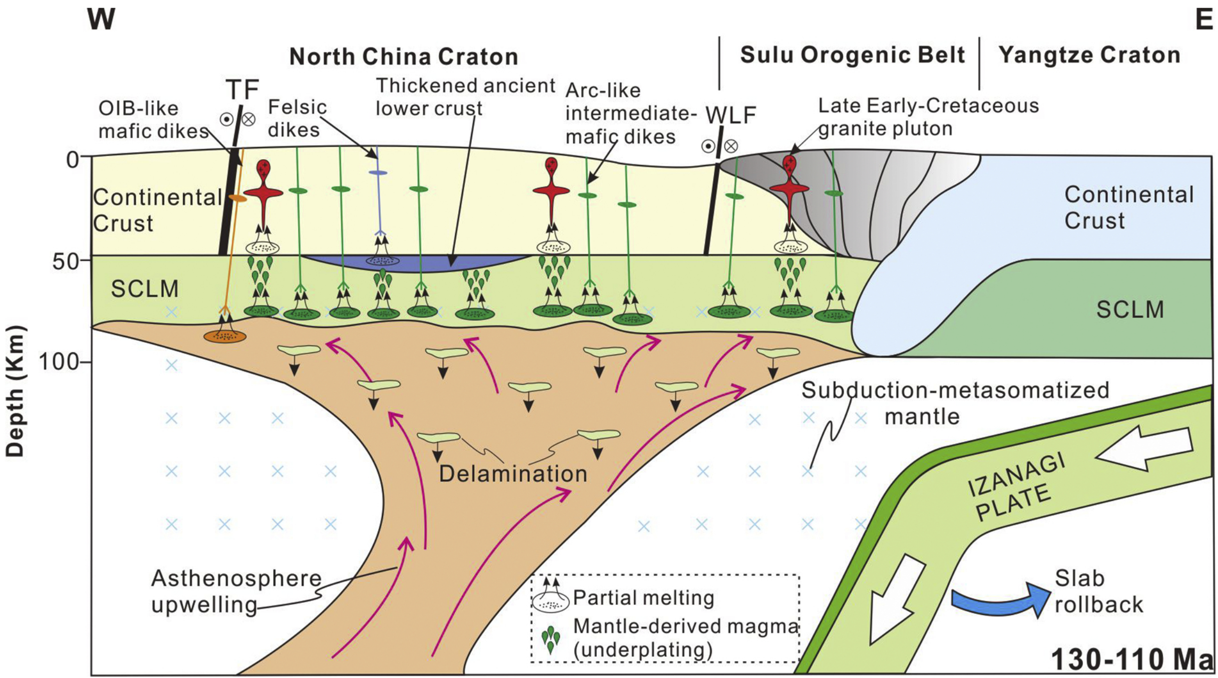
W
E
North China Craton
Sulu Orogenic Belt
Yangtze Craton
TF
OIB-like mafic dikes
Felsic dikes
Thickened ancient lower crust
Arc-like intermediate-mafic dikes
WLF
Late Early-Cretaceous granite pluton
0
50
100
Depth (Km)
Continental Crust
SCLM
Continental Crust
SCLM
Subduction-metasomatized mantle
Delamination
IZANAGI PLATE
Asthenosphere upwelling
Partial melting
Mantle-derived magma (underplating)
Slab rollback
130-110 Ma

Figure 17